

1 **Anthropogenic CO<sub>2</sub>, air-sea CO<sub>2</sub> fluxes and acidification in the Southern**  
2 **Ocean: results from a time-series analysis at station OISO-KERFIX (51°S-**  
3 **68°E).**

4  
5 Nicolas Metzl<sup>1</sup>, Claire Lo Monaco<sup>1</sup>, Coraline Leseurre<sup>1,2</sup>, Céline Ridame<sup>1</sup>, Gilles Reverdin<sup>1</sup>,  
6 Thi Tuyet Trang Chau<sup>3</sup>, Frédéric Chevallier<sup>3</sup>, Marion Gehlen<sup>3</sup>

7  
8 <sup>1</sup> Laboratoire LOCEAN/IPSL, Sorbonne Université-CNRS-IRD-MNHN, Paris, 75005, France

9 <sup>2</sup> Flanders Marine Institute (VLIZ), 8400 Ostend, Belgium

10 <sup>3</sup> Laboratoire LSCE/IPSL, CEA-CNRS-UVSQ, Université Paris-Saclay Gif-sur-Yvette, 91191, France

11  
12 *Correspondence to:* Nicolas Metzl (nicolas.metzl@locean.ipsl.fr)

13  
14  
15 **Abstract:** The temporal variation of the carbonate system, air-sea CO<sub>2</sub> fluxes and pH is analyzed in the Southern  
16 Indian Ocean, south of the Polar Front, based on in-situ data obtained from 1985 to 2021 at a fixed station  
17 (50°40'S-68°25'E) and results from a neural network model that reconstructs the fugacity of CO<sub>2</sub> (fCO<sub>2</sub>) and  
18 fluxes at monthly scale. Anthropogenic CO<sub>2</sub> (C<sub>ant</sub>) is estimated in the water column and is detected down to the  
19 bottom (1600m) in 1985 resulting in an aragonite saturation horizon at 600m that migrated up to 400m in 2021  
20 due to the accumulation of C<sub>ant</sub>. At subsurface, the trend of C<sub>ant</sub> is estimated at +0.53 ± 0.01 μmol.kg<sup>-1</sup>.yr<sup>-1</sup> with a  
21 detectable increase in the trend in recent years. At the surface during austral winter the oceanic fCO<sub>2</sub> increased at  
22 a rate close or slightly lower than in the atmosphere. To the contrary, in summer, we observed contrasting fCO<sub>2</sub>  
23 and dissolved inorganic carbon (C<sub>T</sub>) trends depending on the decade and emphasizing the role of biological  
24 drivers on air-sea CO<sub>2</sub> fluxes and pH inter-annual variability. The regional air-sea CO<sub>2</sub> fluxes evolved from an  
25 annual source to the atmosphere of 0.8 molC.m<sup>-2</sup>.yr<sup>-1</sup> in 1985 to a sink of -0.5 molC.m<sup>-2</sup>.yr<sup>-1</sup> in 2020. Over 1985-  
26 2020, the annual pH trend in surface waters of -0.0165 ± 0.0040.decade<sup>-1</sup> was mainly controlled by the  
27 accumulation of anthropogenic CO<sub>2</sub>, but the summer pH trends were modulated by natural processes that  
28 reduced the acidification rate in the last decade. Using historical data from November 1962 we estimated the  
29 long-term trend for fCO<sub>2</sub>, C<sub>T</sub> and pH confirming that the progressive acidification was driven by the atmospheric  
30 CO<sub>2</sub> increase. In 59 years this led to a diminution of 11% for both aragonite and calcite saturation state. As  
31 atmospheric CO<sub>2</sub> is expected to increase in the future, the pH and carbonate saturation state will decrease at a  
32 faster rate than observed in recent years. A projection of future C<sub>T</sub> concentrations for a high emission scenario  
33 (SSP5-8.5) indicates that the surface pH in 2100 would decrease to 7.32 in winter. This is up to -0.86 lower than  
34 pre-industrial pH and -0.71 lower than pH observed in 2020. The aragonite under-saturation in surface waters  
35 would be reached as soon as 2050 (scenario SSP5-8.5) and 20 years later for a stabilization scenario (SSP2-4.5)  
36 with potential impacts on phytoplankton species and higher trophic levels in the rich ecosystems of the  
37 Kerguelen Island area.

38  
39 **Keywords:** Ocean Carbonate System, Ocean acidification, anthropogenic CO<sub>2</sub>, air-sea CO<sub>2</sub> fluxes, Southern  
40 Ocean, Time-series station

42

## 43 **1 Introduction**

44 The ocean plays an important role in mitigating climate change by taking up a large part of the excess of  
45 heat (Cheng et al., 2020; Fox-Kemper et al., 2021) and of CO<sub>2</sub> released by human activities (Sabine et al., 2004;  
46 Gruber et al., 2019a; Canadell et al., 2021). Since 1750, the global ocean captured 185 ±35 PgC (Petagram of  
47 Carbon) from a total of 700 ±75 PgC of anthropogenic carbon emissions from fossils fuels and land-use changes  
48 (Friedlingstein et al., 2022). The oceanic sink for anthropogenic CO<sub>2</sub> increased progressively from 1.1 ±0.4  
49 PgC.yr<sup>-1</sup> in the 1960s to 2.3 ±0.4 PgC.yr<sup>-1</sup> in the 2000s. Over the decade 2012-2021, the partitioning of the  
50 anthropogenic CO<sub>2</sub> uptake was roughly equal between the ocean (2.9 ± 0.4 PgC.yr<sup>-1</sup>) and the land (3.1 ± 0.6  
51 PgC.yr<sup>-1</sup>) (Friedlingstein et al., 2022). This partitioning has been confirmed for the decade 2013-2022  
52 (Friedlingstein et al., 2023).

53 Ocean observations indicate that the Southern Ocean (SO) south of 45°S has been accumulating each  
54 year about 0.5 PgC.yr<sup>-1</sup> since the 1990s (e.g. Takahashi et al., 2009; Lenton et al., 2013; Rödenbeck et al., 2013;  
55 Long et al., 2021; Fay et al, 2023; Gray, 2024). Results based on BGC-Argo floats (Southern Ocean Carbon and  
56 Climate Observations and Modeling project, SOCCOM) suggest that the CO<sub>2</sub> sink in the SO might be much  
57 lower (0.16 PgC.yr<sup>-1</sup> south of 44°S for the period 2015-2017, Gray et al. 2018; Bushinsky et al., 2019) but there  
58 is an ongoing debate on the size of the carbon sink in this region depending the periods and methods (Long et al.,  
59 2021; Sutton et al., 2021; Hauck et al, 2023b; Gray, 2024). It is also well established that the CO<sub>2</sub> sink in the SO  
60 undergoes substantial decadal variability first documented for the 1990s (Le Quéré et al., 2007; Metzl, 2009;  
61 Lenton et al., 2013) and subsequently identified for the period 1982-2018 (Landschützer et al., 2015; Kepler  
62 and Landschützer, 2019; Mackay et al., 2022; Hauck et al., 2023a, b). However as for the mean state, there are  
63 also uncertainties on both the magnitude and phasing of decadal variability in the SO carbon sink mainly due to  
64 insufficient sampling (Gloege et al, 2021; Hauck et al, 2023a, b). A recent extension of the period to 1957-2020  
65 suggests that the inter-annual to decadal variability of the SO CO<sub>2</sub> sink was most pronounced after the 1980s  
66 (Rödenbeck et al., 2022; Bennington et al., 2022). Whatever the variability of the SO CO<sub>2</sub> sink since the 1960s,  
67 the ocean continuously absorbs atmospheric CO<sub>2</sub> and the distribution of anthropogenic CO<sub>2</sub> (C<sub>ant</sub>) in the SO is  
68 now relatively well documented (e.g. Pardo et al., 2014; Gruber et al., 2019a) thanks to the GLODAP data  
69 synthesis effort for the global ocean (Global Ocean Data Analysis Project, Olsen et al., 2016, 2019, 2020). The  
70 SO takes up about 40% of the total anthropogenic carbon that enters the ocean (Khatiwala et al., 2013; Gruber et  
71 al., 2019a).

72 The anthropogenic CO<sub>2</sub> uptake in the ocean results in lowering carbonate ion concentrations and pH, a  
73 chemical process termed “ocean acidification” (OA) (Caldeira and Wickett 2003; Doney et al., 2009). This  
74 decreases the saturation state with respect to carbonate minerals (aragonite, Ω<sub>ar</sub> and calcite, Ω<sub>ca</sub>), a process most  
75 pronounced in the cold waters at high latitudes where the saturation state is naturally low (Orr et al., 2005;  
76 Takahashi et al., 2014; Jiang et al., 2015). The first estimate of C<sub>ant</sub> distribution in the global ocean (for a  
77 nominal year 1994, Sabine et al., 2004) shows that the accumulation of C<sub>ant</sub> led to an upward migration of the  
78 Ω<sub>ar</sub> and Ω<sub>ca</sub> saturation horizon in all ocean basins (Feely et al., 2004). This change is particularly pronounced  
79 south of the Polar Front (PF) in the SO due to both C<sub>ant</sub> uptake and the enhanced upwelling of carbon-rich deep  
80 waters (e.g. Hauck et al., 2010; Pardo et al., 2017). It has been suggested, through numerical studies, that  
81 depending on future CO<sub>2</sub> emission levels, surface waters in the SO could reach under-saturation state for  
82 aragonite by 2030-2050 (Orr et al., 2005; Gangstø et al., 2008; McNeil and Matear, 2008; Negrete-Garcia et al.,

83 2019). Such a change would have multiple and detrimental impacts on marine ecosystems (Fabry et al., 2008;  
84 Doney et al., 2012; Bopp et al., 2013), in particular calcifying marine organisms, and especially aragonite  
85 producers such as pteropods (Hunt et al., 2008; Gardner et al., 2023), but also calcite producing planktonic  
86 foraminifera (Moy et al., 2009), coccolithophorids (Beaufort et al., 2011), and non-calcifying species such as the  
87 abundant SO diatoms (e.g. Benoiston et al., 2017; Petrou et al., 2019; Weir et al., 2020; Duncan et al., 2022) and  
88 krill (Kawaguchi et al., 2013).

89 Hindcast simulations with Global Ocean Biogeochemical Models (GOBM), as well as projections with  
90 Earth System Models (ESM) have been used to evaluate the ocean carbon cycle over the past decades and future  
91 changes in  $C_{\text{ant}}$  storage, ocean acidification or impacts of global changes on marine ecosystems. However,  
92 current model-based estimates of the contemporary SO  $\text{CO}_2$  sink are subject to relatively large uncertainties (e.g.  
93 Long et al., 2013; Hauck et al., 2020; Gooya et al., 2023; Hauck et al., 2023a, b; Mayot et al., 2023; DeVries et  
94 al, 2023). Difference between GOBM models can reach up to  $0.7 \text{ PgC.yr}^{-1}$  in the SO (Hauck et al., 2020), which  
95 is roughly equivalent to the mean climatological flux of  $0.5 \text{ PgC.yr}^{-1}$  (McNeil et al., 2007; Takahashi et al., 2009;  
96 Lenton et al., 2013). At the high latitudes of the SO ( $> 50^\circ\text{S}$ ) for the 2010s, ESMs from the Coupled Model  
97 Intercomparison Project Phase 6 (CMIP6) simulated either a large sink or a modest source of  $\text{CO}_2$  (McKinley et  
98 al, 2023). This is mainly due to incorrect or missing physical and/or biological processes in the models (e.g.  
99 Pilcher et al., 2015; Kessler and Tjiputra, 2016; Mongwe et al., 2018; Lerner et al., 2021) leading to biases in the  
100 seasonality of temperature, dissolved inorganic carbon  $C_T$ , partial pressure of  $\text{CO}_2$  ( $p\text{CO}_2$ ), air-sea  $\text{CO}_2$  fluxes,  
101 pH or  $\Omega$  (e.g. McNeil and Sasse 2016; Rodgers et al., 2023; Rustogi et al., 2023; Joos et al., 2023). Such model  
102 imperfections should be resolved to gain reliability in future projections of  $\text{CO}_2$  uptake, OA, productivity and the  
103 responses of the marine ecosystems (Frölicher et al., 2015; Hauck et al., 2015; Sasse et al., 2015; Kessler and  
104 Tjiputra, 2016; McNeil and Sasse 2016; Kwiatkowski and Orr, 2018; Negrete-Garcia et al., 2019; Burger et al.,  
105 2020; Terharr et al., 2021; Krumhardt et al., 2022; Jiang et al., 2023; Mongwe et al., 2023). In this context, long-  
106 term biogeochemical observations are particularly valuable to quantify and understand recent past and current  
107 changes, and ultimately evaluate model simulations, as often concluded in modeling studies (e.g. Kessler and  
108 Tjiputra, 2016; Gooya et al., 2023; Wright et al., 2023; Hauck et al., 2023a; Mayot et al., 2023; Rodgers et al.,  
109 2023).

110 Although the SO south of the Polar Front remains much less observed than other oceanic regions,  
111 several observations-based studies have estimated the decrease in pH in surface waters in response to the  
112 increase in oceanic  $\text{CO}_2$  fugacity,  $f\text{CO}_2$  (Mirodikwa et al., 2012; Takahashi et al., 2014; Lauvset et al., 2015;  
113 Munro et al., 2015; Xue et al., 2018; Iida et al., 2021; Leseurre et al., 2022; Brandon et al., 2022). Results  
114 showed a large range in the pH trends from  $-0.008.\text{decade}^{-1}$  to  $-0.035.\text{decade}^{-1}$  depending on the period and the  
115 region of interest. Most of these analyses were based on summer observations (Table 1) and some studies  
116 highlighted contrasting pH trends on a 5-10 years time probably linked to large scale climate variability such as  
117 the Southern Annular Mode (SAM) (e.g. Xue et al., 2018). Given such variability, it is important to continue  
118 monitoring  $f\text{CO}_2$  and pH trends and, if possible, at different seasons as future change in  $\text{CO}_2$  uptake and potential  
119 tipping points of the carbonate saturation state also depend on seasonality (Sasse et al., 2015). The above  
120 observational studies were dedicated to pH changes in surface waters. In contrast to Northern high latitudes (e.g.  
121 Olafsson et al., 2009, 2010; Franco et al., 2021; Skjelvan et al., 2022), few studies in the SO evaluated decadal  
122 changes of carbonate system properties and acidification in the water column based on time-series stations.  
123 These changes in the SO water column were investigated from data collected during cruises generally 3 to 15

124 years apart (e.g., Hauck et al., 2010; Van Heuven et al., 2011; Pardo et al., 2017; Tanhua et al., 2017; Carter et  
 125 al., 2019).

126

127 Table 1: Trends of oceanic  $f\text{CO}_2$  ( $\mu\text{atm.yr}^{-1}$ ) and pH ( $\text{decade}^{-1}$ ) in the Southern Ocean south of the Polar Front  
 128 based on observations. IO: Indian Ocean sector. PO: Pacific Ocean sector. AO: Atlantic Ocean sector. SO SPSS:  
 129 Southern Ocean SubPolar Seasonally Stratified biome (around 50-60°S). PZ: Polar Zone. NR: Not Reported.  
 130 Standard-deviations when available are given in brackets.

131

132

133	134	135	136	137	138	139	140	141	142	143	144	145	146	147	148	149	150	151	152	153	154	155	156	157	158	159	160	161	162
Period	Season	Zone	Trend $f\text{CO}_2$ $\mu\text{atm.yr}^{-1}$	Trend pH $\text{decade}^{-1}$	Reference																								
1991-2000	Summer	IO PZ 55-60°S	2.93	-0.035	Xue et al (2018)																								
2001-2011	Summer	IO PZ 55-60°S	1.41	-0.016	Xue et al (2018)																								
2005-2019	Summer	IO PZ 54-64°S	NR	-0.026(0.003)	Brandon et al (2022)																								
1998-2019	Summer	IO 50°S-68°E	1.9 (0.3)	-0.019 (0.004)	Leseurre et al (2022)																								
1998-2019	Summer	IO 55°S-63°E	2.1 (0.3)	-0.022 (0.003)	Leseurre et al (2022)																								
1998-2007	Summer	IO 55°S-63°E	5.3 (0.4)	-0.050 (0.016)	Leseurre et al (2022)																								
2006-2019	Summer	IO 55°S-63°E	0.3 (0.2)	no trend	Leseurre et al (2022)																								
1969-2003	Summer	PO 55-62°S	1.7 (0.2)	-0.020 (0.003)	Midorikawa (2012)																								
2002-2012	Annual	Drake North	2.21 (0.55)	-0.023 (0.007)	Takahashi (2014)																								
2002-2012	Annual	Drake South	1.50 (0.65)	-0.015 (0.008)	Takahashi (2014)																								
2002-2015	Summer	Drake North	1.95 (0.55)	-0.021 (0.006)	Munro et al (2015)																								
2002-2015	Winter	Drake North	1.92 (0.24)	-0.018 (0.003)	Munro et al (2015)																								
2002-2015	Summer	Drake South	1.30 (0.85)	-0.017 (0.010)	Munro et al (2015)																								
2002-2015	Winter	Drake South	0.67 (0.39)	-0.008 (0.004)	Munro et al (2015)																								
2002-2015	Annual	Drake North	1.74 (0.15)	-0.019 (0.002)	Munro et al (2015)																								
2002-2015	Annual	Drake South	1.16 (0.27)	-0.015 (0.003)	Munro et al (2015)																								
1981-2011	Annual	SO SPSS	1.44 (0.10)	-0.020 (0.002)	Lauvset et al (2015)																								
1991-2011	Annual	SO SPSS	1.46 (0.11)	-0.021 (0.002)	Lauvset et al (2015)																								
1993-2018	Annual	SO 44-75°S	NR	-0.0165 (0.0001)	Iida et al (2021)																								

163

164 The present study complements in time, seasons, and in the water column, the surface  $f\text{CO}_2$  and pH  
 165 trends investigated by Leseurre et al., (2022) in different regions of the Southern Indian Ocean for the period  
 166 1998-2019 during austral summer. South of the PF around 50°S, Leseurre et al. (2022) showed that in summer  
 167 the surface  $f\text{CO}_2$  increase and pH decrease over 20 years were mainly driven by the accumulation of  
 168 anthropogenic  $\text{CO}_2$  by about  $+0.6 \pm 0.2 \mu\text{mol.kg}^{-1}.\text{yr}^{-1}$  and by a small warming of  $+0.03 \pm 0.02 \text{ }^\circ\text{C}.\text{yr}^{-1}$ . In addition  
 169 Leseurre et al. (2022) showed that in the recent decade, 2007-2019, the  $f\text{CO}_2$  trend was low ( $+0.3 \pm 0.2 \mu\text{atm yr}^{-1}$ )  
 170 compared to the previous decade ( $+5.3 \pm 0.4 \mu\text{atm yr}^{-1}$  over 1998-2007), highlighting the sensitivity of the  $f\text{CO}_2$   
 171 and pH trends to the selected time period (especially during summer). In particular, they observed relatively  
 172 stable pH values over 2010-2019 (i.e. no decrease in pH) with no clear explanation on the origin of the slow-  
 173 down of the  $f\text{CO}_2$  and pH trends in surface waters south of the PF in recent years. To complement the analysis  
 174 by Leseurre et al. (2022) based on summer observations over the period 1998-2019 this study focuses on one  
 175 location regularly visited south of the Polar Front (around 50°S-68°E south-west of Kerguelen Island, Figure 1).  
 176 The analysis period is first extended back to 1985 and forward to 2021 to investigate the recent status of  $f\text{CO}_2$   
 177 and pH. We also evaluate the trends during late winter using sparse data in October/November. The combination  
 178 of in situ observations and monthly estimates from a neural network model over the period 1985-2020 (Chau et

179 al., 2022) enables to assess potential changes in seasonality of the surface ocean carbonates system (including  
180  $f\text{CO}_2$ ,  $C_T$ ,  $\text{pH}$ ,  $\Omega$ ) as suggested in recent decades or in future scenarios (Hauck and Völker, 2015; Gallego et al.,  
181 2018; Landschützer et al., 2018; Kwiatkowski and Orr, 2018; Kwiatkowski et al., 2020; Lerner et al., 2021;  
182 Fassbender et al., 2022; Yun et al., 2022; Rodgers et al., 2023; Joos et al., 2023). The changes observed in  
183 surface waters will be related to changes in  $C_{\text{ant}}$  concentrations estimated in the water column and will be  
184 complemented by an analysis of OA at depth between 1985 and 2021. Finally we will explore the long-term  
185 change of surface  $f\text{CO}_2$  and  $\text{pH}$  since the 1960s and potential future changes of the carbonate system at this time-  
186 series site.

187

## 188 **2 Data selection, methods and quality control**

189

### 190 **2.1 Study area and data selection**

191

192 This study focuses on a High Nutrients Low Chlorophyll area (HNLC, Minas and Minas, 1992) in the  
193 Indian sector of the Southern ocean (SO) in the Permanent Open Ocean Zone (POOZ) south of the Polar Front  
194 (PF) and south-west of Kerguelen Islands (around  $50^\circ\text{S}$ - $68^\circ\text{E}$ , Figure 1). The Kerguelen Plateau is an extended  
195 topographic feature that controls part of the Antarctic Circumpolar Current (ACC), generates eddies (Daniault  
196 and Ménard, 1985) and the northward deflection of the PF just east of the Island (Pauthenet et al., 2018). The  
197 Plateau is also a region of relatively high chlorophyll-a (Chl-a) concentration (Moore and Abbott, 2000; Mongin  
198 et al., 2008) and strong  $\text{CO}_2$  uptake during austral spring-summer that contrasts with the weaker sink over the  
199 POOZ/HNLC (Metzl et al., 2006; Jouandet et al., 2008, 2011; Lo Monaco et al., 2014; Leseurre et al., 2022).  
200 The POOZ/HNLC region west (upstream) of the Kerguelen Plateau is characterized by rather stable water mass  
201 properties (temperature, salinity, oxygen or nutrients) over time and low eddy activity compared to the Plateau  
202 (Daniault and Ménard, 1985; Chapman et al., 2015; Dove et al., 2022). In this region, located in the deep  
203 Enderby Basin, the flow is not constrained by topography and there is no local upwelling that would import  $C_T$ -  
204 rich waters to the surface layers as observed on the eastern side of the Kerguelen Plateau (Brady et al., 2021).

205 The Indian sector of the SO is also recognized to host the strongest winds in the SO leading to year-  
206 round high gas transfer coefficients (Wanninkhof and Trinanes 2017). As a result, and in contrast to the Atlantic  
207 sector of the SO, the Indian region south of  $45^\circ\text{S}$  was a periodic annual  $\text{CO}_2$  source, especially in the 1960s to  
208 the 1980s (Rödenbeck et al., 2022; Bennington et al., 2022; Prend et al., 2022; Gray, 2024). In the POOZ-HNLC  
209 region, high winter wind speed (monthly average up to  $16 \text{ m s}^{-1}$ ) and associated heat loss drive deep mixing.  
210 Deep winter mixing entrains subsurface properties to the surface layer, increases surface  $C_T$  concentrations  
211 leading to wintertime outgassing of  $\text{CO}_2$  (Metzl et al., 2006). This combination of characteristics makes the  
212 region an ideal test-bed for 1-D modeling studies investigating the temporal dynamics and drivers of  
213 biogeochemical processes including nutrients, iron, phytoplankton and carbon (Pondaven et al., 1998, 2000;  
214 Louanchi et al., 1999, 2001; Jabaud-Jan et al., 2004; Metzl et al., 2006; Mongin et al., 2006, 2007; Kane et al.,  
215 2011; Pasquer et al., 2015; Demuyneck et al., 2020).

216

217

218

219

220  
221  
222  
223  
224  
225  
226  
227  
228  
229  
230  
231  
232  
233  
234  
235  
236  
237  
238  
239  
240  
241  
242  
243

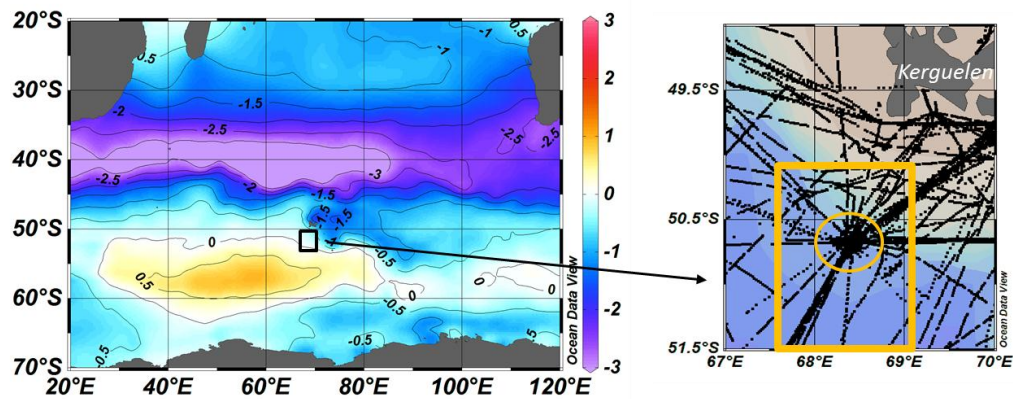


Figure 1: Left: Annual air-sea  $\text{CO}_2$  flux ( $\text{molC.m}^{-2}.\text{yr}^{-1}$ ) in the South Indian Ocean for year 2020 from the FFNN model (negative flux for ocean sink, positive flux for ocean source). The black box identified the location of the study south-west of Kerguelen Islands. Right: Track of cruises with underway  $\text{fCO}_2$  data south-west of Kerguelen Islands. The station at  $50^{\circ}40'S$ - $68^{\circ}25'E$  occupied in 1985, 1992-1993 and 1998-2021 is indicated by a yellow circle. The yellow square is the region selected to calculate the mean values from the underway surface observations and from the FFNN model. Figures produced with ODV (Schlitzer, 2018).

244  
245  
246  
247  
248  
249  
250  
251  
252  
253  
254

Here we used surface and water-column observations around location  $50^{\circ}40'S$ - $68^{\circ}25'E$  (Figure 1, Table S1), historically called KERFIX station (Kerguelen FIXed station) sampled from 1990 to 1995 in the framework of the WOCE/JGOFS programs (Jeandel et al., 1998). The station was first occupied in March 1985 during the INDIGO-1 cruise (Indian Ocean Geochemistry, Poisson, 1985; Poisson et al., 1988) and since 1998 it is regularly visited during the OISO cruises (Océan Indien Service d’Observations, Metzl and Lo Monaco, 1998, <https://doi.org/10.18142/228>). The regular occupation from 1985 to 2021 makes it the longest time-series station in the Southern Ocean POOZ/HNLC area for investigating the inter-annual to decadal trends of carbonate properties in surface waters and across the water-column (0-1600m). Despite the occasional large anomalies in surface waters properties (e.g. lower temperature in December 1998, lower salinity in February 2013) we consider all observations selected for this study both in surface waters and the water-column to be representative of the water masses in this POOZ/HNLC region upstream of the Kerguelen Plateau.

255  
256  
257  
258  
259  
260  
261

Data for the period 1985-2011 were extracted from the GLODAP data-product, version V2.2021 (Lauvset et al., 2021 a, b; Table S1a). Observations collected during OISO cruises from 2012 to 2021 will be included in GLODAP-V3. For the surface water properties, all available underway  $\text{fCO}_2$  data were selected (Figure 1). This includes one cruise in November 1962 (Keeling and Waterman, 1968) and 41 cruises from 1991 to 2021 (Table S1b). All surface temperature, salinity and  $\text{fCO}_2$  data were extracted from the SOCAT data-product version v2022 (Surface Ocean  $\text{CO}_2$  Atlas, Bakker et al., 2016, 2022) and have an accuracy for  $\text{fCO}_2$  between 2 to 5  $\mu\text{atm}$ .

262  
263

## 2.2 Methods

264  
265  
266

The methods for surface underway  $\text{fCO}_2$  and biogeochemical properties (oxygen,  $C_T$ , total alkalinity  $A_T$ , nutrients) in the water-column for the INDIGO-1, KERFIX and OISO cruises were described in previous studies

267 (e.g. Poisson et al., 1993; Louanchi et al., 2001; Metzl et al., 2006; Metzl, 2009; Mahieu et al., 2020; Leseurre et  
268 al., 2022). Here we briefly recall the methods for underway  $f\text{CO}_2$  and water-column observations.

269

### 270 **2.2.1 Surface $f\text{CO}_2$ data**

271

272 For  $f\text{CO}_2$  measurements in 1991-2021, sea-surface water was continuously equilibrated with a "thin  
273 film" type equilibrator thermostated with surface seawater (Poisson et al., 1993). The  $x\text{CO}_2$  in the dried gas was  
274 measured with a non-dispersive infrared analyser (NDIR, Siemens Ultramat 5F or 6F). Standard gases for  
275 calibration (around 270, 350 and 490 ppm) were measured every 6 hours. To correct  $x\text{CO}_2$  dry measurements to  
276  $f\text{CO}_2$  *in situ* data, we used polynomials from Weiss and Price (1980) for vapour pressure and from Copin-  
277 Montégut (1988, 1989) for temperature. Note that when incorporated in the SOCAT data-base, the original  $f\text{CO}_2$   
278 data are recomputed (Pfeil et al., 2013) using temperature correction from Takahashi et al. (1993). Given the  
279 small difference between equilibrium temperature and sea surface temperature ( $+0.56 \pm 0.30$  °C on average for  
280 the cruises in 1998-2021), the  $f\text{CO}_2$  data from SOCAT used in this analysis (Bakker et al., 2022) are almost  
281 identical (within 1  $\mu\text{atm}$ ) to the original  $f\text{CO}_2$  values from our cruises ([www.ncei.noaa.gov/access/ocean-carbon-](http://www.ncei.noaa.gov/access/ocean-carbon-data-system/oceans/VOS_Program/OISO.html)  
282 [data-system/oceans/VOS\\_Program/OISO.html](http://www.ncei.noaa.gov/access/ocean-carbon-data-system/oceans/VOS_Program/OISO.html)).

283

### 284 **2.2.2 Water column data**

285

286 Over the period 1990-1995, water samples were collected during the KERFIX program on the ship *La*  
287 *Curieuse* at standard depths using 8 L Niskin bottles mounted on a stainless steel cable and equipped with  
288 reversing SIS pressure and temperature probes. Methods and accuracy for the geochemical measurements used  
289 in this analysis ( $A_T$ ,  $C_T$ , oxygen, nutrients) are detailed by Jeandel et al. (1998) and by Louanchi et al. (2001).  
290 From 1998 onwards, the station was occupied within the framework of the OISO long-term monitoring program  
291 onboard the *R.V. Marion-Dufresne*. We used Conductivity-Temperature-Depth (CTD) sensors mounted on a 24  
292 bottles rosette equipped with 12 L Niskin bottles. Temperature and salinity measurements have an accuracy of  
293 0.002 °C and 0.005 respectively (Mahieu et al., 2020). Samples for  $A_T$  and  $C_T$  were filled in 500 mL glass bottles  
294 and poisoned with 300  $\mu\text{L}$  of saturated mercuric chloride solution to halt biological activity. Discrete  $C_T$  and  $A_T$   
295 samples were analyzed onboard by potentiometric titration derived from the method developed by Edmond  
296 (1970) using a closed cell. Based on replicate samples from the surface or depth, the repeatability for  $A_T$  and  $C_T$   
297 varies from 1 to 3.5  $\mu\text{mol.kg}^{-1}$  depending on the cruise. The accuracy of  $\pm 3$   $\mu\text{mol.kg}^{-1}$  was ensured by daily  
298 analyses of Certified Reference Materials (CRMs) provided by Andrew Dickson's laboratory (Scripps Institute  
299 of Oceanography).

300 Dissolved oxygen ( $\text{O}_2$ ) concentration was determined by a sensor fixed on the rosette and values were  
301 adjusted based on discrete measurements (Winkler method, Carpenter, 1965) using a potentiometric titration  
302 system. Accuracy for  $\text{O}_2$  is  $\pm 2$   $\mu\text{mol.kg}^{-1}$  (Mahieu et al., 2020). Although long-term deoxygenation in the  
303 Southern ocean has been suggested (Ito et al., 2017; Schmidtke et al., 2017; Oschlies et al., 2018), no significant  
304 trend in  $\text{O}_2$  was identified over 1985-2021 at this station around 50°S in both the surface and the subsurface layer  
305 (at the depth of the temperature minimum representing winter water, a layer used for  $C_{\text{ant}}$  calculations as  
306 described later). However, in the station data a small  $\text{O}_2$  decrease was detected around 800m in the  $\text{O}_2$  minimum  
307 layer over 36 years ( $-0.22 \pm 0.07$   $\mu\text{mol.kg}^{-1}.\text{yr}^{-1}$ ). As this has no impact on the interpretation for pH and  $\Omega$  trends

308 for this analysis, the observed change of O<sub>2</sub> at depth will not be discussed further. Here the O<sub>2</sub> data are mainly  
309 used for the calculation of anthropogenic CO<sub>2</sub> concentrations and the observed O<sub>2</sub> change at depth is too small to  
310 have an impact on temporal variations of C<sub>ant</sub> concentrations given the uncertainty of the calculation.

311 Nitrate (NO<sub>3</sub>) and silicate (DSi) were analyzed on board or at LOCEAN/Paris by colorimetry following  
312 the methods described by Tréguer and Le Corre (1975) for 1998-2008 or from Coverly et al. (2009) for 2009-  
313 2021. The uncertainty of NO<sub>3</sub> and DSi measurements is ±0.1 μmol.kg<sup>-1</sup>. Based on replicate measurements on  
314 deep samples, we estimate an error of about 0.3 % for both nutrients. Phosphate (PO<sub>4</sub>) samples were analyzed  
315 from a few cruises following the method of Murphy and Riley (1962) revised by Strickland and Parsons (1972)  
316 with an uncertainty of ±0.02 μmol.kg<sup>-1</sup>. When nutrients data are not available for a cruise, we used  
317 climatological values based on the seasonal nutrients cycles inferred from data from 1990 to 2021. This method  
318 has a very small impact on the carbonate system calculations and the trend analysis as we did not detect any  
319 significant trends in nutrients in surface or at depth since 1985 (not shown) as opposed to what has been  
320 observed at higher latitudes of the SO (Iida et al., 2013; Hoppema et al., 2015). However, we will see in section  
321 3.1 that the inter-annual variability of nutrients (especially DSi in the HNLC region) might inform on potential  
322 changes in biological processes.

323 Samples were collected in the top layers (0-150m) for chlorophyll-a (Chl-a). For that, one to two liters  
324 of seawater were filtered onto 0.7 μm glass microfiber filters (GF/F, Whatman) and filters were stored at -80°C  
325 onboard. Back at the LOCEAN/Paris laboratory, samples were extracted in 90% acetone (Strickland and  
326 Parsons, 1972) and the fluorescence of Chl-a was measured on a Turner Type 450 fluorometer for the period  
327 1998-2007 and since 2009 at 670 nm on a Hitachi F-4500 spectrofluorometer (Neveux and Lantoiné, 1993).

328

### 329 **2.2.3 Data quality-control and data consistency**

330

331 When exploring the trends of ocean properties based on different cruises more than 35 years apart, it is  
332 important to first verify the consistency of the data and to correct for any bias or drift. The INDIGO data from  
333 1985 (i.e. prior to CRM available for A<sub>T</sub> and C<sub>T</sub>) were first controlled prior to their incorporation into the  
334 original GLODAP product (Sabine et al., 1999; Key et al., 2004) and corrections for A<sub>T</sub> and C<sub>T</sub> were revisited  
335 within the framework of the CARINA project (CARbon IN the Atlantic, Lo Monaco et al., 2010) and the  
336 GLODAPv2 synthesis (Olsen et al, 2016). A secondary quality control was performed on the data from the  
337 OISO cruises collected between 1998 and 2011 within the CARINA and GLODAP-v2 initiatives (Lo Monaco et  
338 al., 2010; Olsen et al., 2016). Significant off-sets were identified for A<sub>T</sub> and C<sub>T</sub> in samples from the KERFIX  
339 cruises (1990-1993) compared to INDIGO and OISO data and it was proposed to correct the original values by -  
340 35 μmol.kg<sup>-1</sup> for C<sub>T</sub> and -49 μmol.kg<sup>-1</sup> for A<sub>T</sub> (Metzl et al., 2006). These corrections were applied in GLODAP  
341 version v2.2019 (Olsen et al., 2019) and resulted in coherent A<sub>T</sub> and C<sub>T</sub> concentrations for KERFIX in the deep  
342 layers compared to other cruises (Supp. Mat., Table S2, Figure S1). The same data quality control protocol as for  
343 GLODAP-v2 was applied to data from OISO cruises for the period 2012-2021 (Mahieu et al., 2020). Given the  
344 accuracy of the data no systematic bias (except in 2014) was found for the properties measured in 2012-2021.  
345 The time-series of A<sub>T</sub> and C<sub>T</sub> at depths below 1450 m for all cruises in 1985-2021 show some variability but no  
346 trend over 36 years as expected in the bottom waters in this region (Supp. Mat., Figure S1). However, we  
347 identified a small bias for C<sub>T</sub> in 2014 (cruise OISO-23) where C<sub>T</sub> concentrations in the deep water appeared  
348 slightly lower (2228-2234 μmol.kg<sup>-1</sup> in 2014 compared to the mean value of 2240.7 ±3.7 μmol.kg<sup>-1</sup>, Table S2,



349 Figure S1). When compared to  $f\text{CO}_2$  in surface waters, we also suspect the  $C_T$  data in the mixed-layer in 2014 to  
350 be too low by about  $10 \mu\text{mol.kg}^{-1}$  (Figures S2, S3). Therefore we applied a WOCE/GLODAP flag 3 for  $C_T$  data  
351 of this cruise and will not use the station data in 2014 for the  $C_{\text{ant}}$  calculations and the trend analysis described in  
352 this study.

353

#### 354 2.2.4 CMEMS-LSCE-FFNN model

355

356 As most of the cruises took place during austral summer and data are not available each year, we  
357 completed the observations with the results from an ensemble of feed-forward neural network models (CMEMS-  
358 LSCE-FFNN or FFNN for simplicity here, Chau et al., 2022). The FFNN model allows mapping at global scale  
359 monthly surface  $f\text{CO}_2$  from the SOCAT gridded datasets and ancillary variables. The reconstructed  $f\text{CO}_2$  is then  
360 used to derive monthly surface  $C_T$  and pH fields as well as air-sea  $\text{CO}_2$  fluxes. This data product is used to  
361 investigate the trends for different seasons and to derive estimates of annual air-sea  $\text{CO}_2$  fluxes to interpret the  
362 change in  $\text{CO}_2$  uptake, if any. For a full description of the model, access to the data and a statistical evaluation of  
363  $f\text{CO}_2$  reconstructions please refer to Chau et al. (2022). Within this study, we compared the FFNN  $f\text{CO}_2$  with  
364 observations from 35 cruises for the years between 1991 and 2020 (Table S3, Figure S2a). Excepted for a few  
365 periods (January 1993 and January 2002), model-data differences are generally within  $\pm 10 \mu\text{atm}$  with a mean  
366 difference of  $2.1 \pm 7 \mu\text{atm}$  for the 35 co-located periods. Note that, as opposed to sea surface  $f\text{CO}_2$ , no temporal  
367 trend was identified for the differences between the observed and reconstructed  $f\text{CO}_2$  (Figure S2b), i.e. the trends  
368 of sea surface  $f\text{CO}_2$  derived from the observations and from the FFNN model should be the same. Aside from the  
369  $f\text{CO}_2$  reconstructions, surface ocean alkalinity ( $A_T$ ) fields are also provided by using the multivariate linear  
370 regression model LIAR (Carter et al., 2016; 2018) based on sea surface temperature, salinity, and nutrients  
371 concentration.

372

#### 373 2.2.5 Calculations of carbonate properties

374

375 Based on the data available for each cruise ( $f\text{CO}_2$ , or  $A_T$  and  $C_T$ ) or from the FFNN model ( $f\text{CO}_2$  and  
376  $A_T$ ), other carbonate system properties (pH,  $[\text{H}^+]$ ,  $[\text{CO}_3^{2-}]$  and  $\Omega$ ) were calculated using the CO2sys program  
377 (version CO2sys\_v2.5, Orr et al., 2018) developed by Lewis and Wallace (1998) and adapted by Pierrot et al.  
378 (2006) with K1 and K2 dissociation constants from Lueker et al. (2000) as recommended (Dickson et al., 2007;  
379 Orr et al., 2015; Wanninkhof et al., 2015). The total boron concentration was calculated according to Uppström  
380 (1974) and  $\text{KSO}_4$  from Dickson (1990). To calculate the properties with the underway surface  $f\text{CO}_2$  dataset, we  
381 used the  $A_T/S$  relationship based on  $A_T$  and  $C_T$  data from the OISO cruises over the period 1998-2019 in the  
382 South Indian sector as described by Leseurre et al. (2022):

383

$$384 A_T = 64.341 \times S + 106.764 \text{ (rmse} = 7.5 \mu\text{mol.kg}^{-1}, n = 4775) \text{ (Eq. 1)}$$

385

386 The use of other  $A_T/S$  relationships (e.g. Millero et al., 1998; Jabaud-Jan et al., 2004; Lee et al., 2006;  
387 Carter et al., 2018) would change slightly the  $A_T$  concentrations but neither the  $A_T$  trend nor the interpretation of  
388 the  $C_T$ , pH or  $\Omega$  trends. However, as salinity is an important predictor in the calculation of  $A_T$ ,  $C_T$  or pH from  
389  $f\text{CO}_2$  data, we have assessed the original underway salinity data and found biases for a few cruises in 1992, 1993

390 and 1995 (Table S1b). For these cruises or when salinity was not measured we used the salinity from the World  
391 Ocean Atlas, WOA (Antonov et al., 2006) in the SOCAT data-sets (Pfeil et al., 2013, identified “WOA” in Table  
392 S1b). Monthly  $f\text{CO}_2$  and  $A_T$  data extracted from the CMEMS-LSCE-FFNN datasets at the station location  
393 ( $50.5^\circ\text{S}$ - $68.5^\circ\text{E}$ ) over 1985-2020 were used to calculate the carbonate properties in the same way as from  
394 observations.

395

## 396 **2.2.6 Comparisons of different datasets and the FFNN model**

397

398 To validate the properties calculated using the  $f\text{CO}_2$  data for 1991-2021 or from the FFNN model over  
399 1985-2020 we compared the calculated values ( $A_T$ ,  $C_T$ , pH,  $[\text{H}^+]$ ,  $[\text{CO}_3^{2-}]$ ,  $\Omega$ ) with those calculated from  $A_T$  and  
400  $C_T$  data measured in the mixed-layer at the KERFIX/OISO station occupied in 1985 and between 1993 and 2021.  
401 For this comparison, we averaged the continuous underway  $f\text{CO}_2$  data selected in a box around the station  
402 location ( $50^\circ\text{S}$ - $51.5^\circ\text{S}$ / $67.5^\circ\text{E}$ - $69^\circ\text{E}$ , yellow box in Figure 1). Results of the comparisons between various datasets  
403 are detailed in the Supplementary Material (Tables S3 and S4). During the period 1993-2021, there are 22 station  
404 occupations with co-located underway  $f\text{CO}_2$  data for different seasons (but mainly in summer). Since we found a  
405 close agreement between measured  $f\text{CO}_2$  and the FFNN model (Table S3, Figure S2), mismatches in all  
406 calculated carbonate system properties between the underway  $f\text{CO}_2$  dataset and the FFNN model are small,  
407 falling within the range of the errors associated with the calculations (Orr et al., 2018). For example, for 35 co-  
408 located periods, the mean differences in calculated  $C_T$  of  $1.5 \pm 5 \mu\text{mol.kg}^{-1}$  or pH of  $-0.002 \pm 0.008$  are in the  
409 range of the theoretical error of about  $5 \mu\text{mol.kg}^{-1}$  and 0.007 respectively when taking into account  
410 measurements errors on salinity, temperature, nutrients,  $f\text{CO}_2$  and  $A_T$  (Orr et al., 2018). On the other hand,  
411 compared to the station data in the mixed-layer (Table S4), the calculated  $A_T$  using Equation 1 is slightly higher  
412 by about  $5 \mu\text{mol.kg}^{-1}$ . This explains the relatively high differences for  $C_T$  (mean difference around  $8 \mu\text{mol.kg}^{-1}$ )  
413 and for pH (mean difference around 0.008) calculated with  $f\text{CO}_2$  and the  $A_T/S$  relationship. The differences of  
414 calculated values with observations are, on average, in the range of uncertainties of the carbonate system  
415 calculations using  $A_T$ - $C_T$  pairs (error for  $f\text{CO}_2$  around  $13 \mu\text{atm}$  and for pH around 0.0144). Importantly, there is  
416 no temporal trend for the differences between calculated and observed properties (Figure S3b). We are thus  
417 confident using the selected  $f\text{CO}_2$  data for the trend analysis presented in this study. The independent comparison  
418 with  $A_T$  and  $C_T$  measurements in the mixed-layer also indicates that the FFNN model results for  $A_T$  and  $C_T$ , are  
419 close to the observations (Table S4, Table S5, Figure S4) as well as for calculated pH,  $[\text{H}^+]$ ,  $[\text{CO}_3^{2-}]$ ,  $\Omega_{\text{Ca}}$  and  
420  $\Omega_{\text{Ar}}$ . This somehow validates the use of the FFNN data for the trend analysis over the period 1985-2020 and for  
421 different seasons, although the FFNN model was not constrained by in-situ  $f\text{CO}_2$  before 1991, few data in austral  
422 winter since 1991, and no Chl-a satellite data available before 1998. Nevertheless, the model shows a good  
423 agreement with observations collected in March 1985 (Table S5, Figure S4).

424

## 425 **3 Results and discussion**

426

### 427 **3.1 Variability and trend of sea surface $f\text{CO}_2$ and air-sea $\text{CO}_2$ fluxes: 1985-2021**

428

429 The  $f\text{CO}_2$  observations around  $50^\circ\text{S}$ - $68^\circ\text{E}$  and their mean values for each cruise are shown in Figure 2a.  
430  $f\text{CO}_2$  measurements are available for different seasons since 1991, though most of them stem from austral  
431 summer (January-February). During austral summer, the ocean  $f\text{CO}_2$  was generally lower than in the atmosphere  
432 (i.e. the ocean was a  $\text{CO}_2$  sink) whereas from July to October it was near equilibrium. The same seasonal change  
433 is obtained from the FFNN model for the period 1991-2020 (Figure 2a). The model also indicates that between  
434 in 1985 and the mid-1990s the  $f\text{CO}_2$  during austral winter (May-September) was always higher than the  
435 atmospheric  $f\text{CO}_2$  leading to an annual  $\text{CO}_2$  source during this period (Figure 3). In 1985 the oceanic  $f\text{CO}_2$  from  
436 the FFNN model was higher than in the atmosphere from March to October (Figure S4) resulting in an annual  
437  $\text{CO}_2$  source of  $+0.8 \text{ molC.m}^{-2}.\text{yr}^{-1}$ . The model estimates a decrease of the annual  $\text{CO}_2$  source until the end of the  
438 1990's followed by an increase of the source over the following decade (Figure 3). Around the year 2010, the  
439 annual  $\text{CO}_2$  flux was around  $+0.5 \text{ molC.m}^{-2}.\text{yr}^{-1}$  and then decreased over the last decade to change into an annual  
440  $\text{CO}_2$  sink that increased to reach  $-0.5 \text{ molC.m}^{-2}.\text{yr}^{-1}$  in 2020. For this reason and given the data available since  
441 1991, we evaluated the summer and winter trends in  $f\text{CO}_2$ ,  $\text{C}_\text{T}$  and  $\text{pH}$  from the FFNN model over 3 periods  
442 1991-2001, 2001-2010, 2010-2020 and compared the summer trends with those deduced from observations  
443 (Table 2). The analysis of trends and their associated drivers for different seasons and periods will allow to  
444 explore links with the variability of primary production and/or the Southern Annual Mode (SAM). Shifts from a  
445 negative to a positive SAM index (Figure 3) may have strengthened the upwelling of deep waters and could  
446 therefore impact ocean properties throughout the water column including  $\text{C}_\text{T}$ , nutrients, primary production or  
447  $\text{pH}$  (e.g. Lovenduski and Gruber, 2005; Lenton et al., 2009; Hauck et al., 2013; Hoppema et al., 2015; Pardo et  
448 al., 2017).

449 From the first underway measurements obtained at the OISO-KERFIX site in February 2021 to the last  
450 measurements used in this study in February 1991, the average oceanic  $f\text{CO}_2$  increased by  $+50.5 \mu\text{atm}$  (from  
451  $344.4 \pm 1.5 \mu\text{atm}$  to  $394.9 \pm 1.5 \mu\text{atm}$ , Figure 2a). During the same period, the atmospheric  $\text{CO}_2$  increased by  $57$   
452  $\mu\text{atm}$  in this region (recorded at Crozet Island, Dlugokencky and Tans, 2022). This first comparison of two  
453 cruises 30 years apart indicates that the oceanic  $f\text{CO}_2$  increase was close to that of the atmosphere. During the  
454 same period, we observed small variations in  $A_\text{T}$  (average  $A_\text{T} = 2276.5 \pm 4.5 \mu\text{mol.kg}^{-1}$ ) and a clear increase in  $\text{C}_\text{T}$   
455 (Figure 4a and S5). This suggests that most of the change observed in oceanic  $f\text{CO}_2$  and  $\text{C}_\text{T}$  over the last 30 years  
456 is due to the uptake of anthropogenic  $\text{CO}_2$ . However, the evolution of air-sea  $\text{CO}_2$  fluxes (Figure 3) suggests that  
457 other mechanisms were at play over shorter periods, and changes in the air-sea  $f\text{CO}_2$  disequilibrium (Figure 2a)  
458 suggests that different drivers may be involved in summer and in winter.

459

460  
461  
462  
463  
464  
465  
466  
467  
468  
469  
470  
471  
472  
473  
474  
475  
476  
477  
478  
479  
480  
481  
482  
483  
484  
485  
486  
487  
488  
489  
490  
491  
492  
493  
494  
495  
496  
497  
498  
499  
500  
501  
502  
503  
504  
505  
506  
507  
508  
509

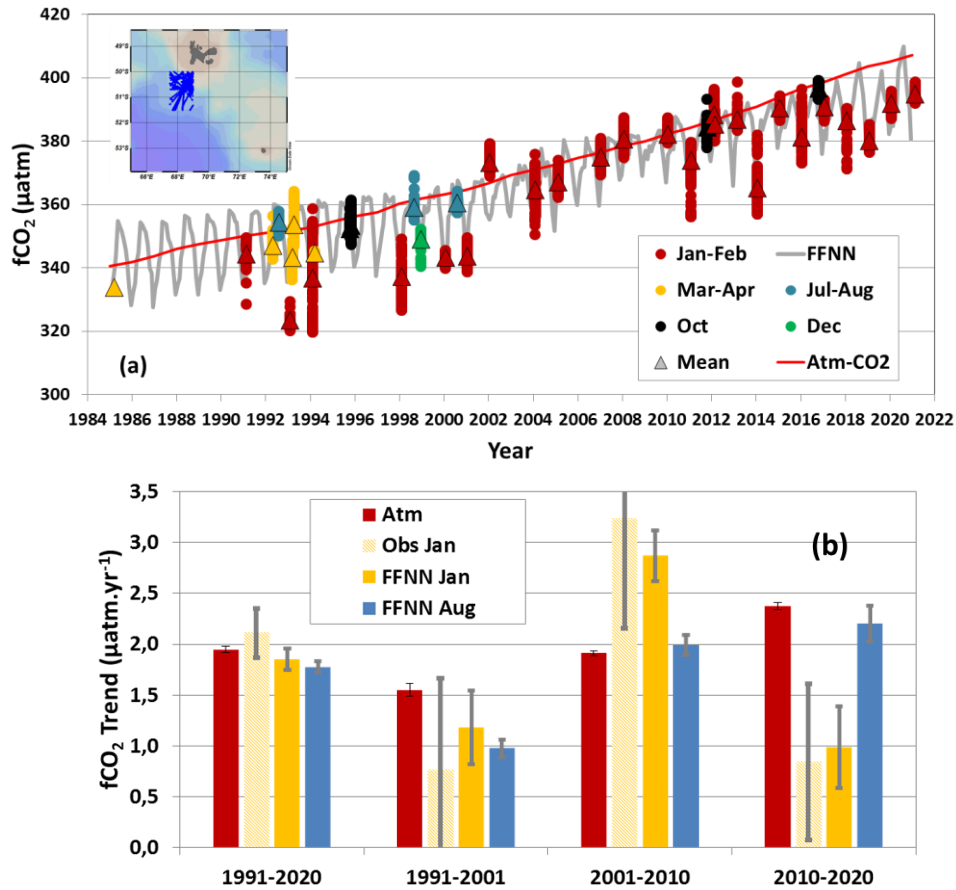


Figure 2: (a): Time-series of sea surface fCO<sub>2</sub> observations (µatm) south-west of Kerguelen Islands in 1985-2021 (insert map shows the location of observations selected around station OISO-KERFIX at 50°40'S-68°25'E). The color dots correspond to 5 periods of the year (January-February, March-April, July-August, October and December) and triangles show the average for each month. The monthly sea surface fCO<sub>2</sub> from the FFNN model is presented for the period 1985-2020 (grey line) and the atmospheric fCO<sub>2</sub> is represented by the red line. In March 1985 there was no underway fCO<sub>2</sub> observation and the triangle corresponds to fCO<sub>2</sub> calculated with A<sub>T</sub> and C<sub>T</sub> measured in the mixed-layer. (b): Trends of atmospheric and oceanic fCO<sub>2</sub> (µatm.yr<sup>-1</sup>) in summer and winter over four different periods based on observations (January) and the FFNN model (January and August).

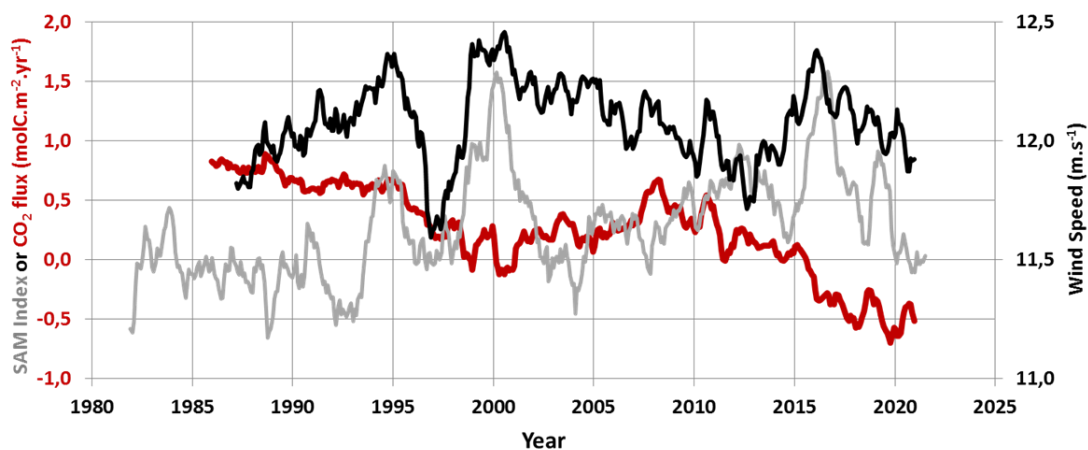


Figure 3: Time series of the SAM index in the Southern Ocean (in grey), wind-speed (in black, m.s<sup>-1</sup>) and air-sea CO<sub>2</sub> flux (molC.m<sup>-2</sup>.yr<sup>-1</sup>) from the FFNN model (in red) at location 50.5°S-68.5°E. A positive (negative) flux represents a CO<sub>2</sub> source (sink). Wind-speed and SAM are presented for 24-months running mean based on monthly values. Note the positive SAM (> 0.5) in 1998-2002 and 2010-2019. SAM data from Marshall (2003), <http://www.nerc-bas.ac.uk/icd/gjma/sam.html>, last access 14/8/2021. Wind speed data from ERA5 (Hersbach et al., 2020).

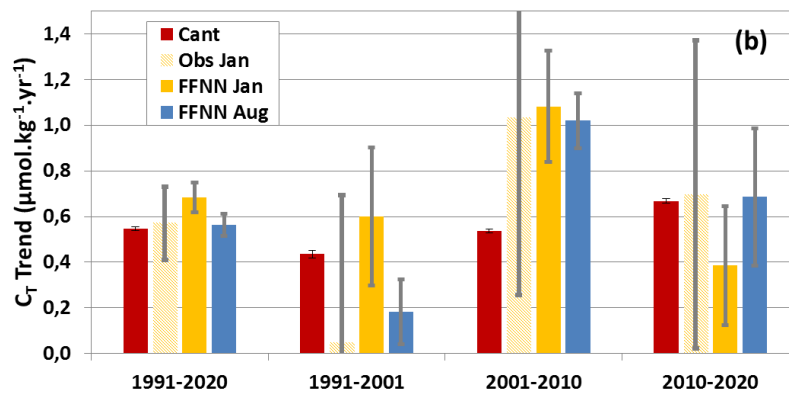
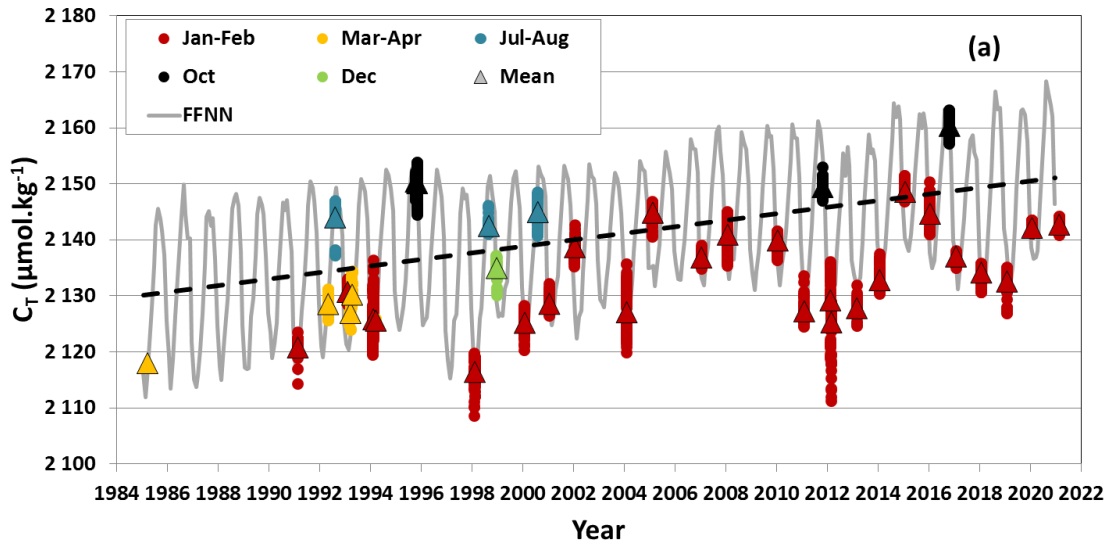


Figure 4: (a): Time-series of surface  $C_T$  ( $\mu\text{mol.kg}^{-1}$ ) around station OISO/KERFIX at  $50^{\circ}40'S-68^{\circ}25'E$  calculated from  $f\text{CO}_2$  data (Figure 2) using the  $A_T/S$  relation (see Sect 2.2.5). The color dots correspond to 5 periods of the year (January-February, March-April, July-August, October and December) and triangles show the average for each month. The monthly sea surface  $C_T$  from the FFNN model is presented for the period 1985-2020 (grey line). The annual  $C_T$  trend of  $+0.58 \pm 0.05 \mu\text{mol.kg}^{-1}.\text{yr}^{-1}$  (dashed line) is derived from the FFNN monthly data. In March 1985 the triangle corresponds to the observed  $C_T$  in the mixed-layer. (b): Trends of sea surface  $C_T$  ( $\mu\text{mol.kg}^{-1}.\text{yr}^{-1}$ ) in summer and winter over four different periods based on observations (for January) and the FFNN model (for January and August). The trend for  $C_{\text{ant}}$  ( $\mu\text{mol.kg}^{-1}.\text{yr}^{-1}$ ) is also shown (red bars) based on estimates in the Winter Water.

Summer data are characterized by a strong inter-annual variability in both  $f\text{CO}_2$  and  $C_T$  (Figures 2a and 4a) with the ocean being a  $\text{CO}_2$  source in January 2002, but a strong sink in January 1993, 1998, 2014, 2016 and 2019. In January 1998, when the surface ocean experienced a warm anomaly (Jabaud-Jan et al., 2004), the low  $f\text{CO}_2$  of  $337 \mu\text{atm}$  and the low  $C_T$  of  $2110 \mu\text{mol.kg}^{-1}$  (Figure 4a and S5) co-occurred with intense primary production (Figure 5), probably supported by diatoms as suggested by very low DSi concentrations ( $< 2 \mu\text{mol.kg}^{-1}$  down to 100m, Figure S6). In January 2014 and 2016, mixed-layer DSi concentrations were also remarkably small ( $< 5 \mu\text{mol.kg}^{-1}$  down to 75m, Figure S6). In 2014 low DSi coincided with Chl-a levels that started to increase in mid-November 2013 and stayed at high level until February 2014 (Surface Chl-a  $> 0.3 \text{ mg.m}^{-3}$ , Figures 5 and S7). The intense primary production contributed to the low  $f\text{CO}_2$  of  $365 \mu\text{atm}$  reached by mid-January 2014, a value as low as 10 years earlier (Figure 2a). To the contrary, in 2002 relatively low Chl-a (mean Chl-a  $< 0.2 \text{ mg.m}^{-3}$ , Figure 5) was associated with higher levels of  $f\text{CO}_2$  ( $373 \mu\text{atm}$ ),  $C_T$  ( $2128 \mu\text{mol.kg}^{-1}$ , Figure 4a, Figure S5a) and DSi (Figure S6). This was also associated with higher salinity indicative of

557 entrainment that might be related to storm events that would have occurred few days before the measurements  
 558 leading to brief positive  $f\text{CO}_2$  anomaly as recently observed from Glider data in the subpolar South Atlantic  
 559 (Nicholson et al., 2022). As opposed to the other periods the ocean was a source of  $\text{CO}_2$  in summer 2002 (this  
 560 particular year was not well reconstructed by the FFNN model, Figure 2a and Figure S2b). The important inter-  
 561 annual variability observed in summer indicates that in this region historically referred to as HNLC (Minas and  
 562 Minas, 1992), primary production could significantly impact  $f\text{CO}_2$  level in summer (Jabaud-Jan et al., 2004;  
 563 Pasquer et al., 2015; Gregor et al., 2018), a result that needs to be taken into account when evaluating drivers of  
 564 inter-annual variability (Rustogi et al., 2023) and the decadal trends of  $f\text{CO}_2$  or pH.

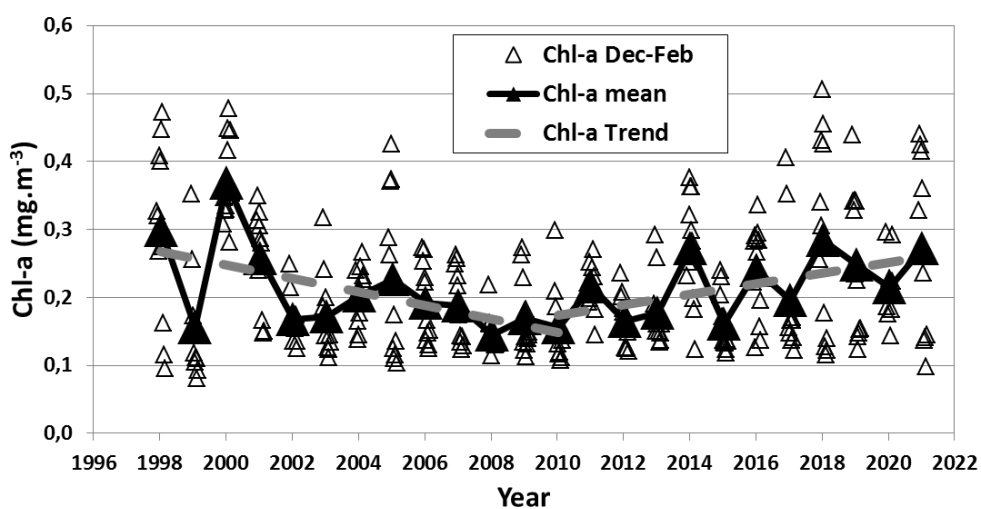
565  
 566 Table 2: Trends of oceanic  $f\text{CO}_2$  ( $\mu\text{atm.yr}^{-1}$ ), pH ( $\text{TS.decade}^{-1}$ ) and  $C_T$  ( $\mu\text{mol.kg}^{-1}.\text{yr}^{-1}$ ) at the OISO-KERFIX location  
 567 ( $50^\circ40'S$ - $68^\circ25'E$ ) in the Southern Indian Ocean for different periods based on observations (Obs.) and the FFNN model  
 568 (FFNN). Standard-deviations are given in brackets.  
 569

570	571	572	573	574	575	576
Period	Season	Trend $f\text{CO}_2$ $\mu\text{atm.yr}^{-1}$	Trend pH $\text{TS.decade}^{-1}$	Trend $C_T$ $\mu\text{mol.kg}^{-1}.\text{yr}^{-1}$		
1962-2016	November	1.31 (0.32)	-0.014 (0.002)	0.47 (0.01)	Obs.	
1991-2021	Summer	2.10 (0.22)	-0.022 (0.002)	0.57 (0.16)	Obs.	
1991-2001	Summer	0.76 (0.90)	-0.009 (0.010)	0.05 (0.64)	Obs.	
2001-2010	Summer	3.23 (1.07)	-0.035 (0.011)	1.03 (0.77)	Obs.	
2010-2020	Summer	0.84 (0.77)	-0.008 (0.008)	0.70 (0.68)	Obs.	
1985-2020	Summer	1.71 (0.08)	-0.018 (0.001)	0.68 (0.05)	FFNN	
1991-2020	Summer	1.85 (0.11)	-0.020 (0.001)	0.68 (0.07)	FFNN	
1991-2001	Summer	1.18 (0.26)	-0.013 (0.004)	0.60 (0.30)	FFNN	
2001-2010	Summer	2.87 (0.25)	-0.030 (0.003)	1.08 (0.24)	FFNN	
2010-2020	Summer	0.98 (0.40)	-0.010 (0.004)	0.38 (0.26)	FFNN	
1985-2020	Winter	1.64 (0.05)	-0.017 (0.001)	0.55 (0.04)	FFNN	
1991-2020	Winter	1.78 (0.15)	-0.018 (0.001)	0.56 (0.05)	FFNN	
1991-2001	Winter	0.98 (0.09)	-0.010 (0.001)	0.18 (0.14)	FFNN	
2001-2010	Winter	1.99 (0.10)	-0.021 (0.001)	1.02 (0.12)	FFNN	
2010-2020	Winter	2.21 (0.17)	-0.022 (0.002)	0.69 (0.30)	FFNN	
1985-2020	Annual	1.57 (0.03)	-0.0165(0.0004)	0.58 (0.05)	FFNN	

596 The Chl-a time-series derived from MODIS suggests higher concentrations in recent years compared to  
 597 2002-2013, with Chl-a peaks identified in 2014, 2016, 2018, 2019 and 2021 (Figure 5 and S7) when the oceanic  
 598  $f\text{CO}_2$  in summer was well below the atmospheric level (Figure 2a).

599 The primary production lowers  $C_T$  concentrations and  $f\text{CO}_2$ , i.e. opposite to the  $C_T$  increase from  
 600 anthropogenic  $\text{CO}_2$  uptake. These counteracting processes might explain the relatively stable  $f\text{CO}_2$  previously  
 601 observed in the Indian POOZ in summer 2007-2019 with an annual  $f\text{CO}_2$  rate of increase of only  $+0.3 \pm 0.2$   
 602  $\mu\text{atm.yr}^{-1}$  (Leseurre et al., 2022). This low rate is confirmed here with the recent data obtained in 2020-2021  
 603 (Figure 2b and Figure S8). For the period 2010-2021, the oceanic  $f\text{CO}_2$  trend in summer derived from  
 604 observations and the FFNN model is lower than  $+1 \mu\text{atm.yr}^{-1}$  (Table 2), i.e. much lower than the atmospheric  
 605  $f\text{CO}_2$  rate of  $+2.4 \mu\text{atm.yr}^{-1}$  and the oceanic  $f\text{CO}_2$  trend of  $+2.21 \pm 0.17 \mu\text{atm.yr}^{-1}$  estimated in winter by the  
 606 FFNN model (Table 2, Figure 2b). This rate is also lower compared to the change observed in October ( $+2.9$   
 607  $\mu\text{atm.yr}^{-1}$ ) albeit being only based on 2 cruises in October 2011 and 2016 (Figure 2a). As the low  $f\text{CO}_2$  trend in  
 608 recent years is detected for summer only this is likely linked to an increase in primary production, as suggested

609 by Chl-a records (Figure 5). From 1998 to 2010 the summer Chl-a concentrations decreased at a rate of  $-0.099$   
610  $\pm 0.041 \text{ mg.m}^{-3}.\text{decade}^{-1}$  whereas from 2010 to 2021 Chl-a increased by  $+0.078 \pm 0.032 \text{ mg.m}^{-3}.\text{decade}^{-1}$  (Figure  
611 5). These trends are coherent with previous studies, e.g. the reduced net primary productivity reported in the  
612 Indian Antarctic zone over 1997-2007 (e.g. Arrigo et al., 2008; Takao et al., 2012) and the shift of the Chl-a  
613 trend in 2010 also reported at large scale in the HNLC region of the Southern Ocean (Basterretxea et al., 2023).  
614 As a consequence, after 2010 the difference between oceanic and atmospheric  $f\text{CO}_2$  ( $\Delta f\text{CO}_2 = f\text{CO}_2^{\text{occ}} - f\text{CO}_2^{\text{atm}}$ )  
615 decreased in summer ( $-1.4 \mu\text{atm.yr}^{-1}$ ) and as it remains relatively steady during winter, the annual  $\text{CO}_2$  flux  
616 progressively varied from a source of  $+0.45 \text{ molC.m}^{-2}.\text{yr}^{-1}$  in 2010 to a sink of  $-0.63 \text{ molC.m}^{-2}.\text{yr}^{-1}$  in 2020  
617 (Figure 3). In addition, as the wind speed was stable during this period ( $12.0 \pm 0.9 \text{ m.s}^{-1}$  on average in 2010-2020,  
618 Figure 3), the variation of the air-sea  $\text{CO}_2$  flux was mainly controlled by  $\Delta f\text{CO}_2$  (e.g. Gu et al., 2023) and the  
619 decadal variation of primary production imprinted a significant change on the  $f\text{CO}_2$  trend and air-sea  $\text{CO}_2$  flux in  
620 this HNLC region. In the region investigated here, increasing Chl-a levels co-occurred with shifts of the SAM  
621 index to a positive state (Figure 3), a link previously suggested south of the Polar Front in the SO but for a short  
622 period over 1997-2004 (Lovenduski and Gruber, 2005). Modeling studies also suggest that summertime  
623 biological activity could play an important role for the variability of the  $\text{CO}_2$  sink in the SO in response to the  
624 SAM (Hauck et al, 2013).



636  
637 Figure 5: Time-series (1998-2021) of sea surface Chl-a ( $\text{mg.m}^{-3}$ ) in summer (December-February) from weekly satellite data  
638 (SeaWIFS and MODIS, open triangles) and associated mean (black triangles). The trends in 1998-2010 and 2010-2021 of  
639 respectively  $-0.0099 \pm 0.0041$  and  $+0.0078 \pm 0.0032 \text{ mg.m}^{-3}.\text{yr}^{-1}$  (dashed grey) indicate a decrease or increase of the primary  
640 production. The full Chl-a record is shown in Supp. Mat. Figure S7.

642 Another process to take into account for interpreting  $f\text{CO}_2$  trends is the change in temperature in surface  
643 waters. Previous analysis suggested a progressive warming in the region investigated here (Auger et al., 2021 for  
644 summer 1993-2017). Over 1998-2019 Leseurre et al. (2022) estimated a warming of Indian POOZ surface  
645 waters of  $+0.03 \pm 0.02 \text{ }^\circ\text{C.yr}^{-1}$ . Extending the time-series for the period 1991-2021 (Figure S9a) we note that the  
646 surface temperature presents sub-decadal variability and that the ocean cooled after 2018 with a trend of  $-0.47$   
647  $\pm 0.16 \text{ }^\circ\text{C.yr}^{-1}$  over 2018-2021 based on the monthly sea surface temperature (SST, Figure S9b). The trend  
648 derived from our in-situ observations in summer over this period was  $-0.25 \pm 0.09 \text{ }^\circ\text{C.yr}^{-1}$ .

649 In 2019, the lower temperature and relatively high Chl-a led to low  $f\text{CO}_2$  ( $380 \mu\text{atm}$ , Figure 2a) and low  
650  $C_T$  ( $2128 \mu\text{mol.kg}^{-1}$ ) compared to 2018 ( $f\text{CO}_2 = 386 \mu\text{atm}$ ;  $C_T = 2137 \mu\text{mol.kg}^{-1}$ , Figure 4a). The decrease in  
651 observed  $f\text{CO}_2$  from summer 2018 to 2019, also reconstructed by the FFNN model (Figure 2a), is contrary to the

652 expected  $f\text{CO}_2$  and  $C_T$  increase due to anthropogenic uptake. In 2020, although the temperature was also lower  
 653 than in 2019, the oceanic  $f\text{CO}_2$  was higher ( $392 \mu\text{atm}$ ) probably due to lower primary production as suggested by  
 654 higher  $\text{DSi}$  (Figure S6), as well as from  $C_T$  ( $2135 \mu\text{mol.kg}^{-1}$ , Figure 4a) and  $\text{Chl-a}$  records (Figure 5). In January  
 655 2021 the temperature was close to that in January 2020, and both  $f\text{CO}_2$  and  $C_T$  were slightly higher ( $395 \mu\text{atm}$ ,  
 656  $2139 \mu\text{mol.kg}^{-1}$ ).  $A_T$  concentrations were stable between 2018 and 2021 ( $2278.9 \pm 1.8 \mu\text{mol.kg}^{-1}$ , Figure S5)  
 657 indicating no effect of  $A_T$  on the observed  $f\text{CO}_2$  change in this region as opposed to the areas north of the Polar  
 658 Front in the Indian Ocean where  $A_T$  variations are often linked to coccolithophores blooms (Balch et al., 2016;  
 659 Smith et al., 2017).

660 The inter-annual and pluri-annual variability observed over 1991-2021 highlights the competitive  
 661 processes that drive  $C_T$ ,  $f\text{CO}_2$  or  $\text{pH}$  temporal variations. In order to separate natural and anthropogenic  
 662 contributions, the anthropogenic  $\text{CO}_2$  signal is estimated in the following section.

663

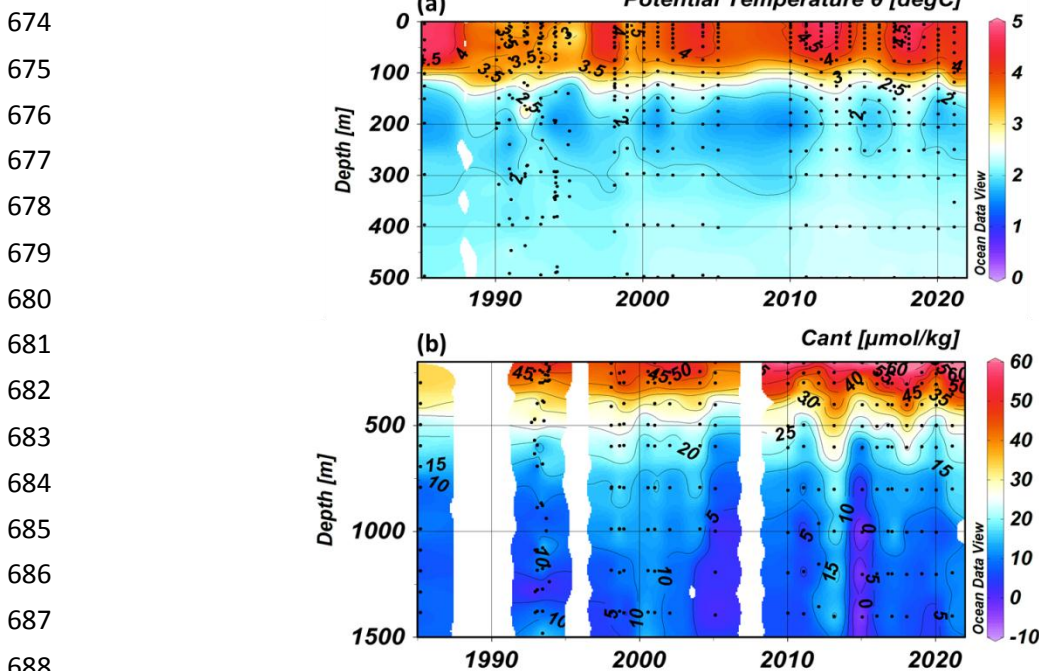
### 664 3.2 Anthropogenic $\text{CO}_2$

#### 665 3.2.1 Anthropogenic $\text{CO}_2$ in the water column

666

667 To calculate anthropogenic  $\text{CO}_2$  concentrations ( $C_{\text{ant}}$ ), we used the TrOCA method developed by  
 668 Touratier et al. (2007) and previously applied in the southern Indian Ocean (Mahieu et al., 2020; Leseurre et al.,  
 669 2022). Such an indirect method is not suitable for evaluating  $C_{\text{ant}}$  concentrations in surface waters due to  
 670 biological activity and gas exchange and we restrict the  $C_{\text{ant}}$  calculations below the productive layer around  
 671 150m. In the region south of the Polar Front, a well-defined subsurface temperature minimum is observed each  
 672 year characterizing the Winter Water (WW) at depth range 150-250m (Figure 6a).

673



689 Figure 6: Hovmöller section (Depth-Time) of (a) potential temperature ( $^{\circ}\text{C}$ ) and (b) anthropogenic  $\text{CO}_2$  ( $C_{\text{ant}}$ ,  $\mu\text{mol.kg}^{-1}$ ) over  
 690 1985-2021 at station OISO-KERFIX ( $50^{\circ}40'S$ - $68^{\circ}25'E$ ). The section for temperature is presented in the layer 0-500m and  
 691 for summer to highlight the temperature minimum around 200m (winter water, WW). The section for  $C_{\text{ant}}$  is limited below  
 692 200m. Section produced with ODV (Schlitzer, 2018).

693



694 The  $C_T$  and  $C_{ant}$  concentrations increased over time in the water column, a signal that is most  
695 pronounced in the top layers (200-400m, Figure 6b). In the deep layer, the presence of the Indo-Pacific Deep  
696 Water (IPDW) around 600-800m is identified by a maximum of  $C_T$  ( $C_T > 2250 \mu\text{mol.kg}^{-1}$ ) and a minimum of  $O_2$   
697 ( $O_2$  close to or  $< 180 \mu\text{mol.kg}^{-1}$ , Figure S10) (Talley, 2013; Chen et al., 2022). In the IPDW layer restricted to  
698 the neutral density (ND) range 27.75-27.85  $\text{kg.m}^{-3}$  there is no significant change in  $C_T$  over time (Figure S10). In  
699 that layer the  $C_{ant}$  concentrations in 1985 ( $17.3 \mu\text{mol.kg}^{-1}$ ) were almost identical to those evaluated in 2021 ( $21.2$   
700  $\mu\text{mol.kg}^{-1}$ ), considering the uncertainty in the  $C_{ant}$  calculations ( $\pm 6.5 \mu\text{mol.kg}^{-1}$ , Touratier et al., 2007). Below  
701 800m, the  $C_{ant}$  concentrations were small but not null (Figure 6b). The average  $C_{ant}$  concentration below 800m  
702 for all years and seasons was  $8.0 \pm 5.3 \mu\text{mol.kg}^{-1}$  ( $n=123$ ) with a very small change detected over time ( $C_{ant} = 7.7$   
703  $\pm 1.3 \mu\text{mol.kg}^{-1}$  in 1985 and  $C_{ant} = 10.4 \pm 0.6 \mu\text{mol.kg}^{-1}$  in 2021). As discussed above (section 2.2.3) the  $C_T$  and  $A_T$   
704 concentrations in the bottom layer ( $>1450\text{m}$ ) were stable over 1985-2021 (Table S2, Figure S1).

705

### 706 3.2.2 Anthropogenic $\text{CO}_2$ trend in the Winter Water

707

708 To separate the natural and anthropogenic signals in surface waters for the driver analysis we assume  
709 that  $C_{ant}$  in the WW is representative of  $C_{ant}$  in the mixed-layer (ML). This is confirmed with few stations  
710 occupied during winter showing that  $C_{ant}$  concentrations in the WW in summer are almost equal to  $C_{ant}$  in the  
711 ML during the preceding winter (Figure S11). The evolution of  $C_{ant}$  in the WW from 1985 to 2021 is presented  
712 in Figure 7a for all seasons. In 1985 the  $C_{ant}$  concentration in the WW was  $47.1 \mu\text{mol.kg}^{-1}$  and  $C_{ant}$  reached a  
713 maximum of  $71.7 \mu\text{mol.kg}^{-1}$  in 2021. The data selected at 200m present some inter-annual variability such as the  
714 relatively low  $C_{ant}$  in 1998, 2005 and 2020 probably related to natural variability. In 1998 and in 2020 the  $O_2$   
715 concentrations were slightly lower in the WW ( $< 300 \mu\text{mol.kg}^{-1}$ ) explaining the lower  $C_{ant}$  concentration ( $44.8$   
716  $\mu\text{mol.kg}^{-1}$  in 1998 and  $53.8 \mu\text{mol.kg}^{-1}$  in 2020) but no anomaly was observed for  $C_T$ . This suggests that the  
717 biological contribution may have been overestimated (lower  $O_2$  is interpreted by the TrOCA method as more  
718 organic matter remineralization which should be associated with higher  $C_T$ ). This could be instead related to a  
719 change in mixing or circulation. In 2005 anomalies of  $C_T$ ,  $A_T$  and  $O_2$  concur to explain the lower  $C_{ant}$  ( $43.9$   
720  $\mu\text{mol.kg}^{-1}$ ).

721 From 1985 to 2021, we estimated a  $C_{ant}$  trend in WW of  $+0.49 \pm 0.09 \mu\text{mol.kg}^{-1}.\text{yr}^{-1}$ . When the  $C_{ant}$   
722 anomalies in 1998, 2005 and 2020 were discarded, this  $C_{ant}$  trend was  $+0.53 \pm 0.01 \mu\text{mol.kg}^{-1}.\text{yr}^{-1}$  (Figure 7a). As  
723 expected, the  $C_{ant}$  concentrations in the ocean are positively related to atmospheric  $\text{CO}_2$  (slope  $+0.26 \pm 0.04$   
724  $\mu\text{mol.kg}^{-1}.\mu\text{atm}^{-1}$ , Figure 7b). Interestingly the slope observed south of the PF in the Indian Ocean is close to that  
725 observed in the Antarctic Intermediate waters (AAIW) in the South Atlantic ( $+0.23 \pm 0.05 \mu\text{mol.kg}^{-1}.\mu\text{atm}^{-1}$ ,  
726 Fontela et al., 2021). Gruber et al. (2019 a, b) evaluated  $C_{ant}$  changes between 1994 and 2007 in the global ocean.  
727 In the South Indian sector, they estimated a mean  $C_{ant}$  accumulation at the surface of  $+6.0 \pm 1.1 \mu\text{mol.kg}^{-1}$  in the  
728 band 50-55°S south of the PF. At our station location (50-52°S/68°E) in the layer 0-250m, the  $C_{ant}$  accumulated  
729 from 1994 to 2007 was  $+5.7 \pm 1.5 \mu\text{mol.kg}^{-1}$ . In 13 years, this corresponds to a trend of  $+0.44 \pm 0.11 \mu\text{mol.kg}^{-1}.\text{yr}^{-1}$ .  
730 Gruber et al. (2019 a, b) did not use the data presented here allowing for an independent comparison to the  
731 present study. Estimates of  $C_{ant}$  accumulation by Gruber et al. (2019 a, b) are in agreement with ours for the  
732 period 1994-2007 ( $+0.49 \pm 0.01 \mu\text{mol.kg}^{-1}.\text{yr}^{-1}$ ) but lower than reported here in recent years ( $+0.61 \pm 0.01$   
733  $\mu\text{mol.kg}^{-1}.\text{yr}^{-1}$  over 2008-2021). Indeed our estimates over 3 decades indicate an increase in the uptake of  
734 anthropogenic  $\text{CO}_2$  with time (Figure 4b).

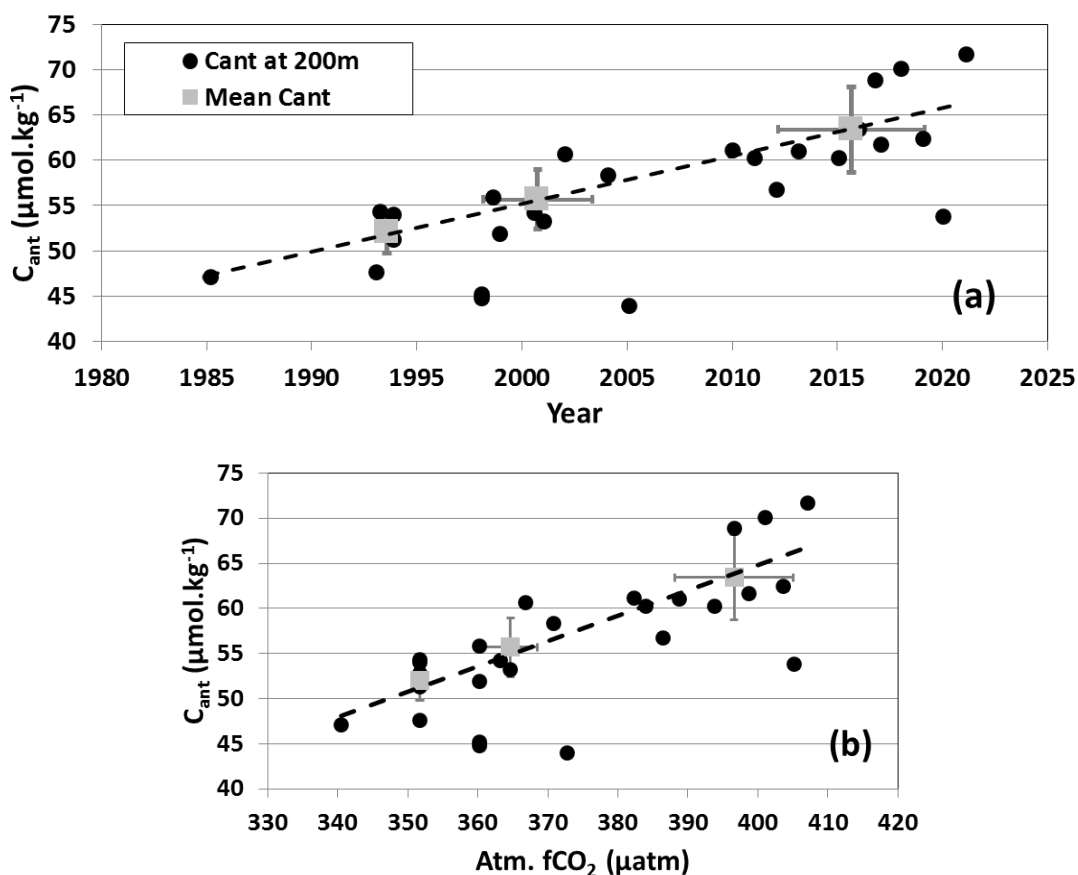


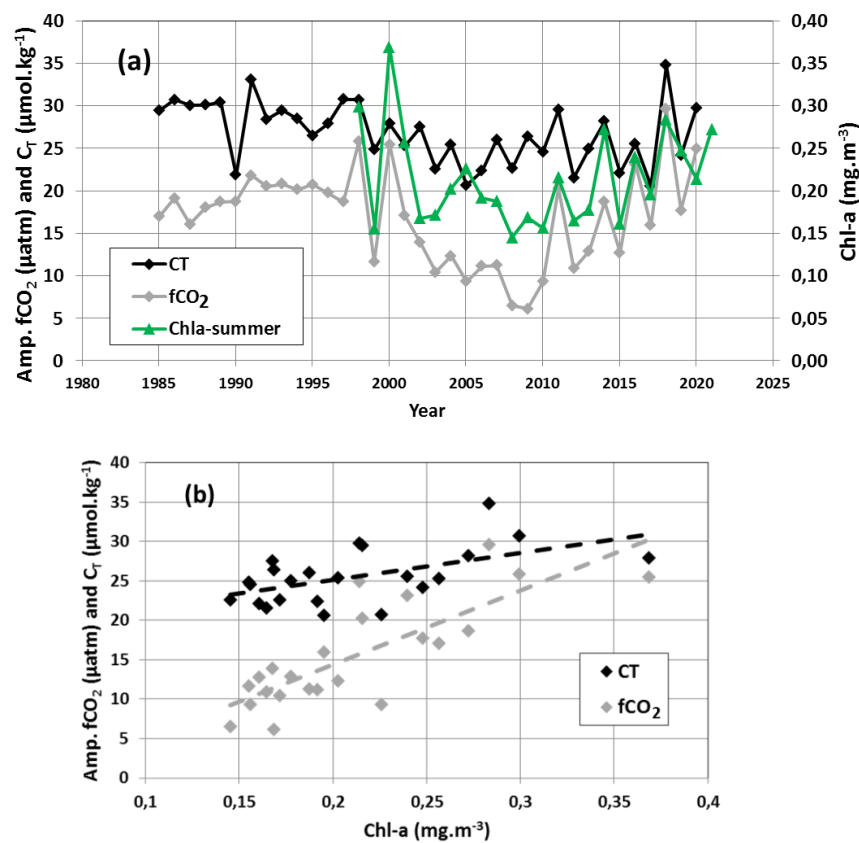
Figure 7: (a): Time-series of anthropogenic CO<sub>2</sub> ( $C_{ant}$   $\mu\text{mol.kg}^{-1}$ ) estimated in the winter water layer (WW around 200m, see figure 6) from 1985 to 2021 at station OISO-KERFIX (50°40'S-68°25'E). Black dots are the individual data in the WW and the grey squares the average for the 1990s, 2000s and 2010s (anomalies in 1998, 2005 and 2020 discarded). The  $C_{ant}$  trend of  $+0.53 \pm 0.01 \mu\text{mol.kg}^{-1}.\text{yr}^{-1}$  is represented (dashed line). (b): same data for  $C_{ant}$  versus atmospheric  $f\text{CO}_2$  (the slope is  $+0.263 \pm 0.042 \mu\text{mol.kg}^{-1}.\mu\text{atm}^{-1}$ ).

### 3.2.3 Anthropogenic and surface $C_T$ seasonal trends

The  $C_{ant}$  trend in the WW over 1985-2021 ( $+0.53 \pm 0.01 \mu\text{mol.kg}^{-1}.\text{yr}^{-1}$ ) is slightly lower than the annual surface  $C_T$  trend derived from the FFNN model for 1985-2020 ( $+0.58 \pm 0.05 \mu\text{mol.kg}^{-1}.\text{yr}^{-1}$  Figure 4a, Table 2) suggesting that anthropogenic CO<sub>2</sub> uptake explains 86% of the  $C_T$  increase in surface waters. Over 1991-2020 the surface  $C_T$  trend appears slightly higher in January than in August (Figure 4b, Table 2). This suggests that in addition to the increase of  $C_T$  due to anthropogenic CO<sub>2</sub> other processes such as the variability of the biological activity, vertical mixing or upwelling contributed to the observed trend. Indeed, as for  $f\text{CO}_2$  (Figures 2b), the  $C_T$  growth rate also depends on seasons and decades (Figure 4b). Over 1991-2001 the  $C_T$  trend from the observations ( $+0.05 \pm 0.64 \mu\text{mol.kg}^{-1}.\text{yr}^{-1}$ , Table 2) is highly uncertain due to few data and the large variability (Figures 4a, b). The FFNN model showed that the  $C_T$  trend in summer was faster than the trend in  $C_{ant}$  (Figure 4b), suggesting that natural processes would have increased  $C_T$ . This could be explained by an increase in vertical mixing due to the increase in wind speed (Figure 3). On the contrary, the winter  $C_T$  trend was lower than the  $C_{ant}$  trend estimated in subsurface waters (Figure 4b).

Over 2001-2010 the  $C_T$  trends were much faster than over the previous decade and they were the same for both seasons (Figure 4b, Table 2). For this decade the summer  $C_T$  trends from the observations and the FFNN

780 model are coherent. They were also twice the  $C_{\text{ant}}$  rate in the WW, which could be explained by enhanced  
 781 upwelling of  $C_T$ -rich deep waters during this period after the SAM reached a high positive index (Figure 3;  
 782 Lenton and Matear, 2007; Le Quéré et al., 2007; Hauck et al., 2013). However, over this period we did not detect  
 783 any clear change at depth for ocean properties (except for  $C_T$  and  $C_{\text{ant}}$ ) that would support this assumption  
 784 (enhanced upwelling). The rapid  $C_T$  (and  $f\text{CO}_2$ ) trend for this decade is probably due to processes occurring at  
 785 the surface (e.g. biological activity, as discussed later) rather than changes in the water column (vertical mixing  
 786 or upwelling). Over the last decade  $C_T$  trends were lower than over the previous one (Figure 4b). For summer,  
 787 this is identified from both observations and the FFNN model. In winter the  $C_T$  trend (from FFNN) is close to  
 788  $C_{\text{ant}}$  indicative of the anthropogenic  $\text{CO}_2$  accumulation. The low  $C_T$  trend at the surface in summer, about half the  
 789  $C_{\text{ant}}$  trend, is likely due to the increase of primary production after 2010 as described above (Figure 5). Thus, it  
 790 appears that the impact of biological activity and its variability in summer could counteract that of anthropogenic  
 791  $\text{CO}_2$  and explain the low temporal change of the carbonate system at the surface in recent years.



813 Figure 8: (a): Time-series of the seasonal amplitude (August minus January) for surface  $C_T$  (black,  $\mu\text{mol.kg}^{-1}$ ) and  $f\text{CO}_2$   
 814 (grey,  $\mu\text{atm}$ ) from the FFNN model at station OISO-KERFIX ( $50^\circ40'S-68^\circ25'E$ ). Also shown are the mean surface Chl-a  
 815 (green,  $\text{mg.m}^{-3}$ ) in summer from 1998 to 2021. (b): Seasonal amplitude of  $f\text{CO}_2$  and  $C_T$  versus summer Chl-a over 1998-  
 816 2020. The dashed lines indicate that the seasonal amplitude (August-January) increases when Chl-a is higher.

819 Given the differences of the  $f\text{CO}_2$  and  $C_T$  trends in summer and winter (Figures 2b and 4b, Table 2) we  
 820 explored the temporal variations of the seasonality. For each year we estimated the differences between August  
 821 and January (Figure 8a). The seasonal amplitude for  $C_T$  was on average  $26.1 \pm 3.4 \mu\text{mol.kg}^{-1}$  and for  $f\text{CO}_2$   $15.1$   
 822  $\pm 5.6 \mu\text{atm}$ . Some large inter-annual variations appear related to the variability of Chl-a in summer (Figure 8a).  
 823 Interestingly the  $f\text{CO}_2$  seasonal amplitude reached a minimum around 2008-2010, then increased over 2010-

824 2020. This signal also appears correlated with the evolution of surface Chl-a in summer (Figure 8). This supports  
825 the conclusion that low phytoplanktonic biomass between 2008 and 2010 reduced the seasonal amplitude of  
826  $f\text{CO}_2$ .

827 The inter-annual variability of the seasonality is clearly identified when comparing  $C_T$  with  $C_T$   
828 calculated due only to  $C_{\text{ant}}$  accumulation (Figure S12). This supports the conclusion that in addition to the  $C_{\text{ant}}$   
829 accumulation, the variations of phytoplanktonic biomass imprinted inter-annual variability on  $C_T$  and  $f\text{CO}_2$  in  
830 summer. This holds for the seasonal amplitude as the results for winter follows the  $C_{\text{ant}}$  trend (Figure 4b, Figure  
831 S12a). The same is true for pH for which reduced seasonal amplitude was found when the production was low  
832 (not shown). However, over 36 years (1985-2020) we did not identify a long-term trend of the seasonal  
833 amplitude for  $C_T$  or for  $f\text{CO}_2$  as suggested by other studies (Landschützer et al., 2018; Rodgers et al., 2023;  
834 Shadwick et al. 2023). Our results highlight a variability over 5-10 years (Figure 8a) and suggest a potential  
835 change in seasonality and annual  $\text{CO}_2$  sink if primary production changes in the future (e.g. Bopp et al., 2013;  
836 Leung et al., 2015; Fu et al., 2016; Kwiatkowski et al., 2020; Krumhardt et al., 2022; Seifert et al., 2023).

837

### 838 **3.3 Anthropogenic $\text{CO}_2$ drives acidification in surface waters and in the water column**

839

#### 840 **3.3.1 Surface pH trend**

841

842 To explore the temporal change of pH in surface waters we used the  $f\text{CO}_2$  observations and the monthly  
843 results from the FFNN model. For both data-sets pH was calculated from  $f\text{CO}_2$  and  $A_T$  reconstructed as  
844 described in section 2.2.5. Figure 9a presents the time-series of pH at the surface (the same time-series for  $[\text{H}^+]$   
845 concentrations is shown in Figure S13). For the full period, 1985-2020, the annual pH trend derived from the  
846 FFNN model is  $-0.0165 \pm 0.0004.\text{decade}^{-1}$  (Table 2) exactly the same as derived at large scale in the Southern  
847 Ocean (south of  $44^\circ\text{S}$ ) for the period 1993-2018 (Iida et al., 2021, Table 1) but when restricted to this period,  
848 1993-2018, the trend from the FFNN model appears slightly faster ( $-0.0182 \pm 0.0006.\text{decade}^{-1}$ ). This is less than  
849 the pH trend derived from  $p\text{CO}_2$  data in the SO SubPolar Seasonally Stratified biome around  $40\text{-}50^\circ\text{S}$  (SO-  
850 SPSS) for 1981-2011 ( $-0.020 \pm 0.002.\text{decade}^{-1}$ , Table 1, Lauvset et al., 2015) and close to the pH trend based on  
851 OceanSODA-ETH reconstructed fields in the SO-SPSS for the period 1982-2021 ( $-0.0189 \pm 0.0010.\text{decade}^{-1}$ , Ma  
852 et al., 2023). However, as for  $f\text{CO}_2$  and  $C_T$ , we estimated different pH trends in summer and winter, as well as  
853 depending on the periods (Figure 9b, Table 2).

854 The winter pH decrease estimated over the last two decades was twice as fast as estimated during the  
855 previous one, mirroring the winter  $f\text{CO}_2$  trends (Table 2). In summer, the pH trend presents a large variability at  
856 decadal scale as it was three times faster over 2001-2010 than during the previous and following decades (Figure  
857 9b, Table 2). Although the trends based on the observations are less robust because the cruises were not  
858 conducted each year, the reduced pH trend in summer after 2010 is confirmed from in-situ data (Figure 9b, Table  
859 2).

860

861

862  
863  
864  
865  
866  
867  
868  
869  
870  
871  
872  
873  
874  
875  
876  
877  
878  
879  
880  
881  
882  
883  
884  
885  
886  
887  
888  
889  
890  
891  
892  
893  
894  
895  
896  
897  
898  
899  
900  
901  
902  
903  
904  
905  
906  
907  
908  
909  
910  
911  
912  
913  
914

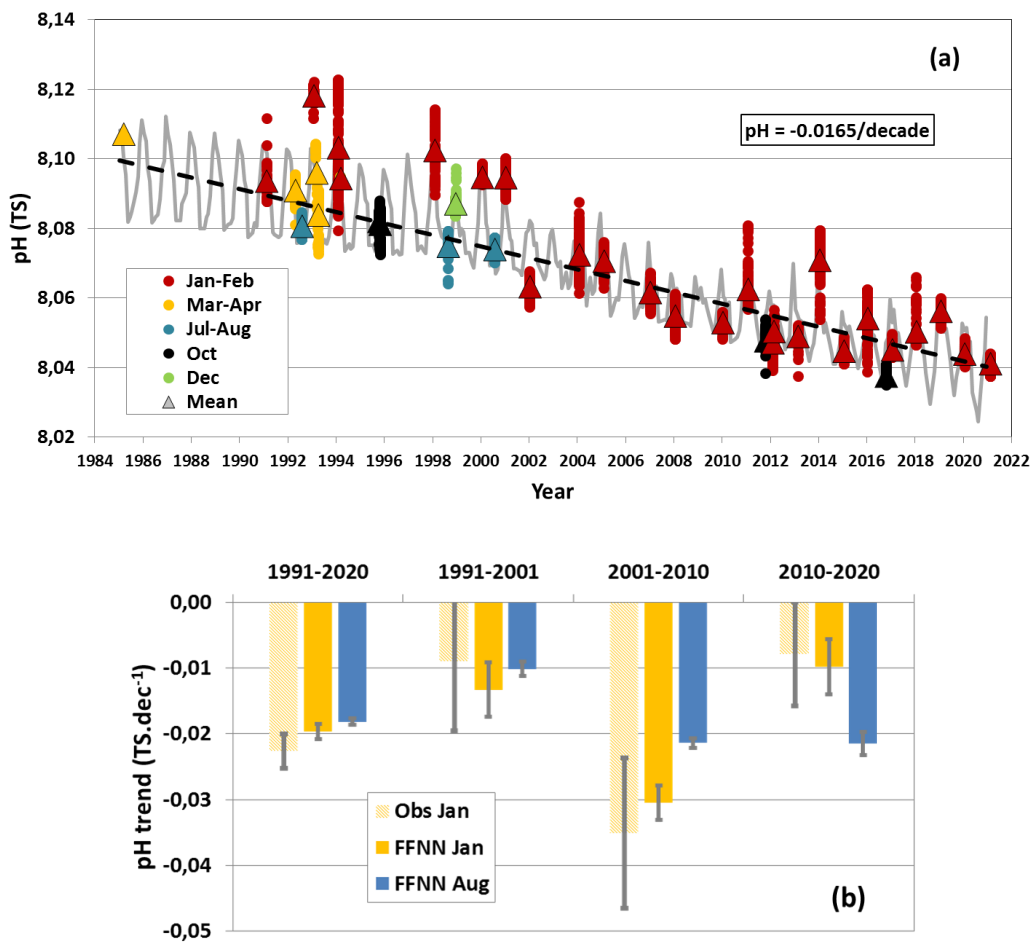
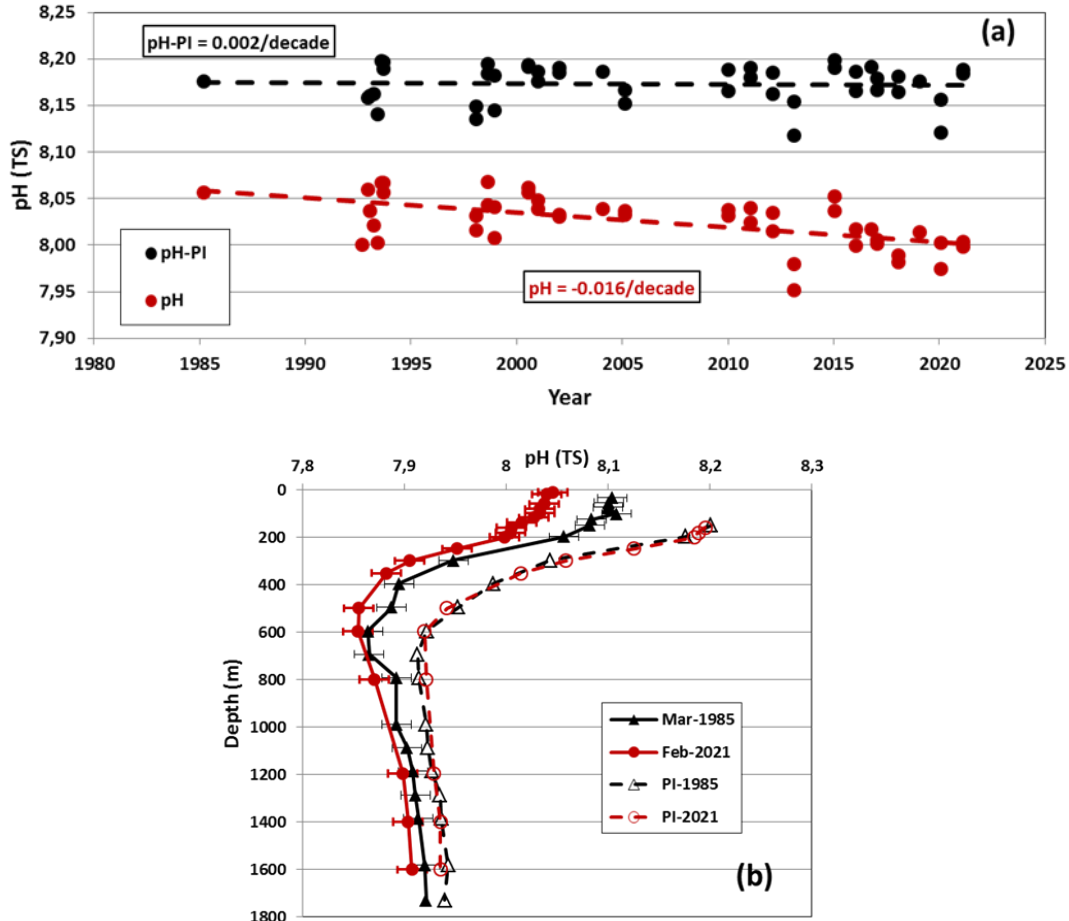


Figure 9: (a): Time-series of surface pH (Total Scale, TS) around station OISO-KERFIX (50°40'S-68°25'E) calculated from  $f\text{CO}_2$  data (Figure 2) using the  $A_T/S$  relation (see Sect.2.2.5). The color dots correspond to 5 periods of the year (January-February, March-April, July-August, October and December) and triangles show the average for each month. The monthly sea surface pH from the FFNN model is presented for the period 1985-2020 (grey line). The annual pH trend in 1985-2020 of  $-0.0165 \pm 0.0004 \text{ decade}^{-1}$  (dashed line) is derived from the FFNN monthly data (the same figure for  $[\text{H}^+]$  concentrations is presented in Supp. Mat. Figure S13). (b): Trends of pH (TS.decade<sup>-1</sup>) in summer and winter four over different periods based on observations (January) and the FFNN model (January and August).

Our results show that the pH trend varied significantly from decade to decade and that part of the variations could be explained by the evolution of phytoplanktonic biomass, but overall the decrease of pH since 1985 was mainly driven by the accumulation of anthropogenic  $\text{CO}_2$ . This is revealed in the Winter Water when comparing pH and pre-industrial pH (Figure 10a). Here, the pre-industrial pH (pH-PI) was calculated after subtracting  $C_{\text{ant}}$  values from the observed  $C_T$  concentrations for each sample in the WW layer. Interestingly the pH trend in the WW of  $-0.0161 \pm 0.0033 \text{ decade}^{-1}$  (here deduced from the station  $A_T$  and  $C_T$  data over 1985-2021) is very close to the annual trend at the surface deduced from the FFNN model over 1985-2020 ( $-0.0165 \pm 0.0004 \text{ decade}^{-1}$ ). This trend is slightly faster than the pH trends of  $-0.0134 \pm 0.001 \text{ decade}^{-1}$  recently estimated in subsurface waters (100-210m) of the Southern Ocean south of the PF and derived for years 1994-2017 from historical data and BGC-Argo floats (Mazloff et al., 2023). For the same period, 1994-2017, at the OISO-KERFIX station we estimated a pH trend in the WW of  $-0.0168 \pm 0.0043 \text{ decade}^{-1}$  and of  $-0.0186 \pm 0.0006 \text{ decade}^{-1}$  in surface waters from the FFNN model.

915  
 916  
 917  
 918  
 919  
 920  
 921  
 922  
 923  
 924  
 925  
 926  
 927  
 928  
 929  
 930  
 931  
 932  
 933  
 934  
 935  
 936  
 937  
 938  
 939  
 940  
 941  
 942  
 943  
 944  
 945  
 946  
 947  
 948  
 949  
 950  
 951



952  
 953  
 954  
 955  
 956  
 957  
 958  
 959  
 960  
 961  
 962  
 963  
 964

Figure 10: (a): Time-series of pH (red dots) and pre-industrial pH (pH-PI, black dots) estimated in the Winter Water layer (WW around 200m, see figure 6) over 1985-2021 at station OISO-KERFIX (50°40'S-68°25'E). pH-PI for each sample was calculated after subtracting  $C_{ant}$  to  $C_T$ . The pH trend from the present days is  $-0.0161 \pm 0.0033 \cdot \text{decade}^{-1}$  (red dashed line). No trend is observed for pH-PI (black dashed). The mean pH-PI in the WW is  $8.173 \pm 0.020$  ( $n=45$ ). (b): Profiles of pH and pH-PI evaluated from March 1985 (black symbols) and February 2021 data (red symbols). The profiles for pH-PI are shown below 150m only as  $C_{ant}$  estimates are not available in the surface layer. Note that the pH-PI profiles are the same either using either the 1985 or 2021 data.

As for other properties ( $A_T$ ,  $O_2$ , temperature, salinity and nutrients), the pre-industrial pH (pH-PI) does not change over time in the WW (mean pH-PI =  $8.173 \pm 0.020$ ,  $n=45$ , Figure 10a). The pH-PI in the WW is in the range of the pre-industrial surface pH value in the Southern Ocean (8.2 for year 1750 and 8.18 for year 1850) derived from Earth system Models (Jiang et al., 2023, their Table S9). In the WW at our location the modern pH (1985-2021) was on average  $-0.147 \pm 0.021$  lower than pre-industrial pH. In 1985 pH in the WW was  $-0.119$  lower than pH-PI and in 2021 it was  $-0.184$  lower than pH-PI (Figure 10a). The progressive decrease of pH was clearly linked to  $C_{ant}$  concentrations in the WW layer and the pH decrease identified below that layer in the water column (Figure 10b).

**3.3.2 Temporal change in the water column**

From 1985 to 2021, signals of decreasing pH and increasing  $C_T$  in surface waters are propagated in the water column down to about 500m. As mentioned above the data in 1985 (first occupation of the station) reveal

965 significant  $C_{\text{ant}}$  levels across the water column (Figure 6b). Therefore the pH down to the bottom was already  
 966 lower in 1985 than at pre-industrial times (Figure 10b). However, the largest  $C_{\text{ant}}$  increases were found in the top  
 967 layers and changes in pH from 1985 to 2021 were small below 500m (Figure 10b, Figure S14). While  
 968 observations for all years fall on a common linear relationship between  $C_{\text{ant}}$  and  $\text{pH}_{\text{ant}}$  for depths greater than 500  
 969 m, the change in pH for a given level of  $C_{\text{ant}}$  increases with time for layers shallower than 500 m (Figure 11).

970

971

972

973

974

975

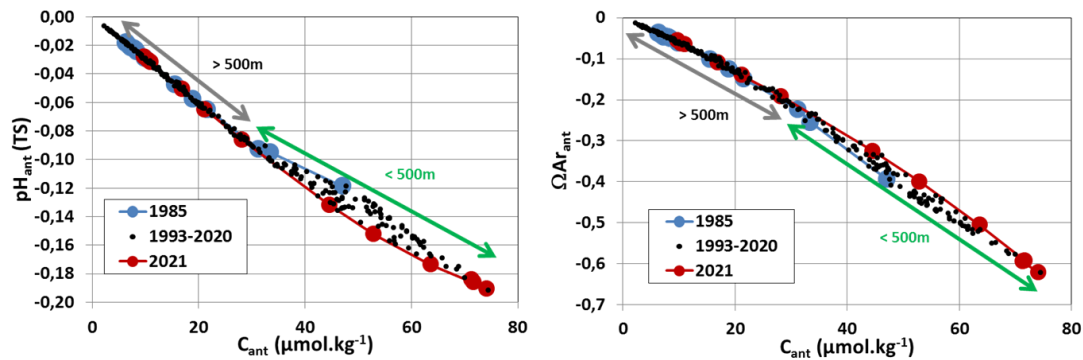
976

977

978

979

980



981

982

983

984

985

Figure 11: Anthropogenic pH ( $\text{pH}_{\text{ant}}$ ) and anthropogenic  $\Omega_{\text{ar}}$  ( $\Omega_{\text{ar,ant}}$ ) versus anthropogenic  $\text{CO}_2$  concentrations ( $C_{\text{ant}}$ ,  $\mu\text{mol.kg}^{-1}$ ) at station OISO-KERFIX ( $50^{\circ}40'S-68^{\circ}25'E$ ). The data are selected in the layer 150-1600m for the periods 1985 (blue), 1993-2020 (black) and 2021 (red). The green arrow identifies the data in the layer 150-500m (for  $C_{\text{ant}} > 30 \mu\text{mol.kg}^{-1}$ ). Below 500m (brown arrow) no change of  $C_{\text{ant}}$  was observed from 1985 to 2021 and thus for  $\text{pH}_{\text{ant}}$  and  $\Omega_{\text{ar,ant}}$ .

986

987

988

989

990

991

992

993

994

995

996

997

998

999

1000

The increase in  $C_{\text{ant}}$  concentrations over time (Figure 6b) also leads to a decrease of carbonate ion concentrations [ $\text{CO}_3^{2-}$ ] and of  $\Omega_{\text{ar}}$  and  $\Omega_{\text{ca}}$  (Figure S14, S15). These decreases are well identified since the pre-industrial era in the whole water column but in the last 36 years, observations do not show any appreciable changes below 500m (Figure 11). The aragonite saturation horizon ( $\Omega_{\text{ar}}=1$ ) was found around 600m in 1985 and around 400m in recent years (2015-2021, Figures S14, S15). Moreover, during the period covered by observations (1985-2021), we did not detect abrupt change of the aragonite saturation horizon from one year to the next (nor between winter and summer, Figure S16). This contrasts with previous regional studies in the SO and most notably with results from the layers close to the deep minimum of carbonate ion concentrations (Hauri et al., 2015; Negrete-Garcia et al., 2019). At our station the [ $\text{CO}_3^{2-}$ ] minimum lies around 500-600m (Figure S14, S15) and, along with the superimposed  $C_{\text{ant}}$  accumulation, explains the upward shift of the aragonite and calcite saturation horizon between the pre-industrial and modern periods (Figure S15). At pre-industrial time under-saturation with regard to aragonite ( $\Omega_{\text{ar}} < 1$ ) was found at the bottom only (1600m) whereas between 1985 and 2021 it was found in the water column below 600 m or 400 m (Figure S15). The subsurface pre-industrial  $\Omega_{\text{ar}}$  value was around 1.9-2 (Figure S15) and in the range of  $\Omega_{\text{ar}}$  value in the Southern Ocean at pre-industrial time from ESM models (Jiang et al., 2023, their Figure 4).

1001

1002

1003

1004

1005

1006

The aragonite under-saturation already occurred in 1985 at 600-700m, a layer corresponding to the [ $\text{CO}_3^{2-}$ ] minimum (Figure S15) and a small increase of  $C_{\text{T}}$  just above this layer (via  $C_{\text{ant}}$  accumulation) would rapidly shift the aragonite saturation horizon above 600m. This might have already occurred and could explain that  $\Omega_{\text{ar}}$  value was 1.02 at 350m in 2021 (Figure S15). These results suggest that for pelagic calcifiers living in subsurface waters (150m or deeper) such as pteropods and foraminifera (e.g. Hunt et al., 2008; Meilland et al., 2018) the impact of acidification might occur sooner than at the surface.

1007 For the interpretation of the trend analysis based on observations, only data below 150m could be used  
1008 as  $C_{\text{ant}}$  was not evaluated in the surface layer. At 200m, based on  $A_T$  and  $C_T$  data, we estimated a decrease in pH  
1009 from 1985 to 2021 by -0.059 (Figure 10b), corresponding to an increase by +1.1  $\text{nmol.kg}^{-1}$  in  $[\text{H}^+]$  (Figure S13),  
1010 and a decrease by -0.16 in  $\Omega_{\text{ar}}$  (Figure S15). Over 36 years, this represents about 30% of the total change since  
1011 the pre-industrial era for pH (-0.184),  $[\text{H}^+]$  (+3.5  $\text{nmol.kg}^{-1}$ ) and  $\Omega_{\text{ar}}$  (-0.6). This is mainly linked to the  $C_{\text{ant}}$   
1012 change that also represents over 36 years 30% of the total accumulation (+24.6  $\mu\text{mol.kg}^{-1}$  from 1985 to 2021 for  
1013 a total concentration of +71.7  $\mu\text{mol.kg}^{-1}$  at 200m in 2021, Figure 7). We conclude that the accumulation of  
1014 anthropogenic  $\text{CO}_2$  drives the change of the carbonate system in subsurface waters and probably also in surface  
1015 waters.

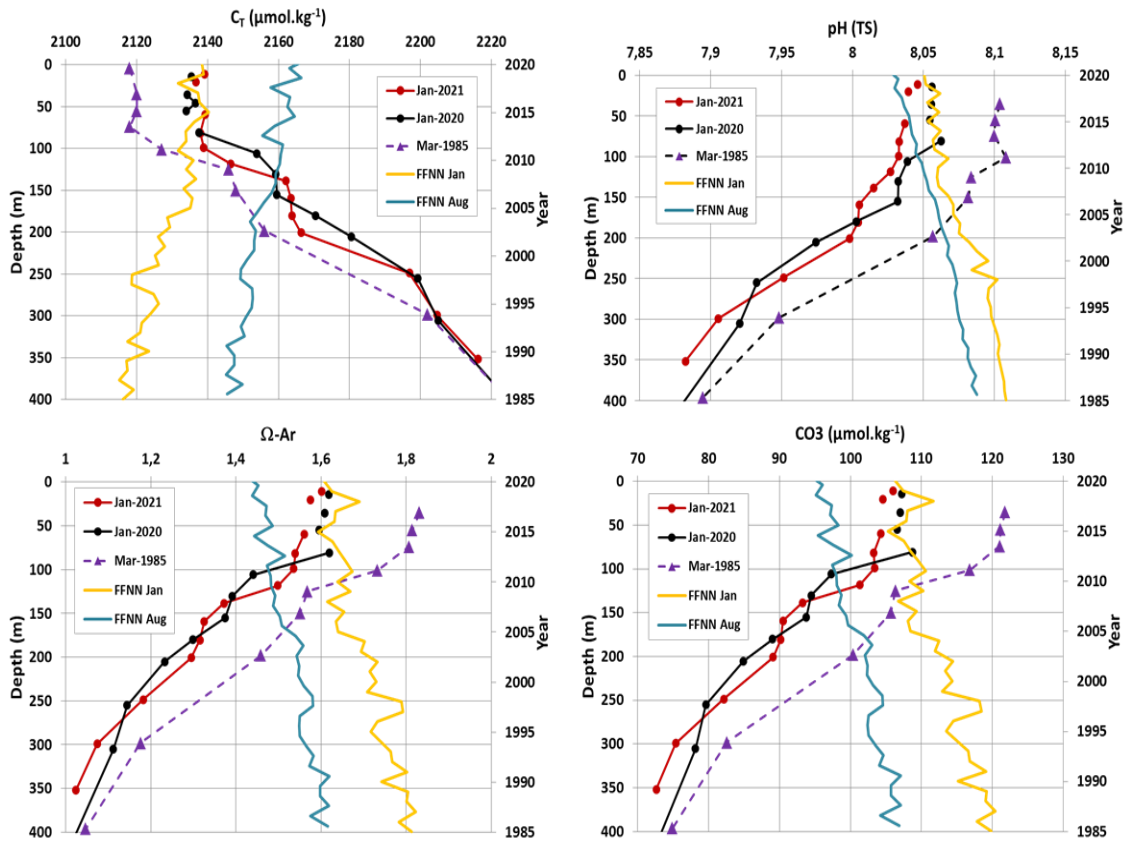
1016 In order to quantify the propagation of surface trends to depth, the temporal variations of carbonate  
1017 system properties at the surface for both summer and winter derived from the FFNN model are compared to the  
1018 changes observed across the water column (Figure 12). The comparison shows that the seasonal amplitude of  
1019 surface waters properties was of a similar magnitude to the observed changes in the mixed layer between 1985  
1020 and 2021. For example, the  $C_T$  and  $\Omega_{\text{ar}}$  seasonal amplitude, respectively around 20  $\mu\text{mol.kg}^{-1}$  and 0.2,  
1021 corresponds to the  $C_T$  increase and  $\Omega_{\text{ar}}$  decrease from 1985 to 2021. The comparisons also highlight that in  
1022 summer the FFNN results were close to observations in the mixed-layer (e.g.  $C_T$  was 2120  $\mu\text{mol.kg}^{-1}$  in 1985 and  
1023 2140  $\mu\text{mol.kg}^{-1}$  in 2021). In winter, at the surface,  $C_T$  was higher and pH,  $[\text{CO}_3^{2-}]$ ,  $\Omega_{\text{ar}}$  were lower (from the  
1024 FFNN model, blue line in Figure 12). The winter surface values in 1985 and 2020/2021 are in good agreement  
1025 with observations at depth in the winter water (150-200m). As an example, in 1985 surface  $C_T$  in winter was  
1026 2145.5  $\mu\text{mol.kg}^{-1}$ , which corresponds to the concentration measured at 150m during summer (purple line in  
1027 Figure 12). In 2020, the winter  $C_T$  at the surface (2168.3  $\mu\text{mol.kg}^{-1}$ ) is equal to  $C_T$  concentrations observed at  
1028 150-180 m in January 2020 or in 2021. For  $\Omega_{\text{ar}}$ , the surface value derived from the FFNN model in winter 1985  
1029 (1.6) was equal to the  $\Omega_{\text{ar}}$  observed at 125 m in March 1985. In 2020, the surface winter estimate of  $\Omega_{\text{ar}}$  (1.42)  
1030 was equal to  $\Omega_{\text{ar}}$  observed at 100-150 m in January 2020 or 2021. The same correspondences between winter  
1031 surface and WW data were identified for pH and  $[\text{CO}_3^{2-}]$  (Figure 12). This supports the use of winter and  
1032 summer surface data from the FFNN model to investigate the seasonal  $\Omega_{\text{ar}}$  trends and their projection in the  
1033 future.

1034 The surface water  $\Omega_{\text{ar}}$  ( $\Omega_{\text{ca}}$ ) trend from the FFNN model in summer of  $-0.0059.\text{yr}^{-1}$  ( $-0.0094.\text{yr}^{-1}$ ) was  
1035 stronger than the winter of  $-0.0050.\text{yr}^{-1}$  ( $-0.0079.\text{yr}^{-1}$ ) and also higher than the trend derived from observations in  
1036 the WW ( $-0.0043.\text{yr}^{-1}$  for  $\Omega_{\text{ar}}$  and  $-0.0069.\text{yr}^{-1}$  for  $\Omega_{\text{ca}}$ ). Our results indicate that the change of carbonate  
1037 properties in the years 1985-2021 were mainly driven by  $C_{\text{ant}}$  accumulation in surface waters and across the  
1038 water column. However, a potential increase in primary productivity after 2010 mitigated the effects of  
1039 increasing  $C_{\text{ant}}$  accumulation in response to increasing atmospheric  $\text{CO}_2$  leading to relatively stable summer  $C_T$   
1040 and  $f\text{CO}_2$  and to a stronger  $\text{CO}_2$  sink (Figure 3). Consequently, when restricted to the period 2010-2020, the  
1041 trend of  $\Omega_{\text{ar}}$  in surface waters in summer was much smaller,  $-0.024 \pm 0.027 \text{ decade}^{-1}$  than during the preceding  
1042 period. This was much smaller than derived from all the data over 1985-2021 ( $-0.048.\text{decade}^{-1}$ ) or estimated  
1043 from reconstructed fields in the SO-SPSS over 1982-2021 ( $-0.0616.\text{decade}^{-1}$ , Ma et al., 2023). It underscores the  
1044 uncertainty in extrapolating time-series to the future depending on the selection of data and periods.

1045



1046  
1047  
1048  
1049  
1050  
1051  
1052  
1053  
1054  
1055  
1056  
1057  
1058  
1059  
1060  
1061  
1062  
1063  
1064  
1065  
1066  
1067  
1068  
1069  
1070  
1071



1072  
1073  
1074  
1075  
1076  
1077  
1078

Figure 12: Profiles (0-400m left axis) of observed and calculated properties ( $C_T$ , pH,  $\Omega\text{-Ar}$ ,  $[\text{CO}_3^{2-}]$ ) at station OISO-KERFIX ( $50^\circ 40'S$ - $68^\circ 25'E$ ) in March 1985, January 2020 and January 2021 along with surface time-series in 1985-2020 (right axis) of the same properties in January (yellow line) and August (blue line) from the FFNN model. The FFNN values in January 2020 are coherent with January 2020 or January 2021 observations in the mixed-layer and in January 1985 are close to the observations in March 1985. Note that the differences of properties between 2020-21 and 1985 have a similar magnitude as the seasonal amplitude (illustrated by the FFNN values for January and August).

1079

### 3.4 Long-term change in surface water, from the sixties to the future.

1080

1081

The data described above allowed evaluating the temporal variations of the properties of the carbonate system and  $C_{\text{ant}}$  over 1985-2021 along with a comparison to the pre-industrial state in the water column. The results over 36 years informed on the recent changes, inter-annual variations and trends, but the time-series appears somehow short to extrapolate the trends over time. What was the change of the carbonate system in surface waters before 1985 and what will be its future evolution ?

1086

1087

#### 3.4.1 Back to the sixties: observed trends since 1962.

1088

1089

To explore the long-term change, we start by comparing our recent data with observations from the LUSIAD cruise conducted in 1962-1963 (Keeling and Waterman, 1968). Some data from this cruise were obtained in mid-November 1962 south of the Polar Front, in the region south-west off Kerguelen Islands. Because of the seasonality, we compared the November 1962 data with our observations obtained in October-November in 1995, 2011 and 2016, and with the FFNN model results for November (Figure 13). The  $C_T$

1093

1094 concentration, pH,  $\Omega_{ar}$  and  $\Omega_{ca}$  for 1962 were calculated using  $fCO_2$  data and  $A_T$  (from the  $A_T/S$  relationship Eq.  
 1095 1) with salinity from the World Ocean Atlas (Antonov et al, 2006).

1096

1097

1098

1099

1100

1101

1102

1103

1104

1105

1106

1107

1108

1109

1110

1111

1112

1113

1114

1115

1116

1117

1118

1119

1120

1121

1122

1123

1124

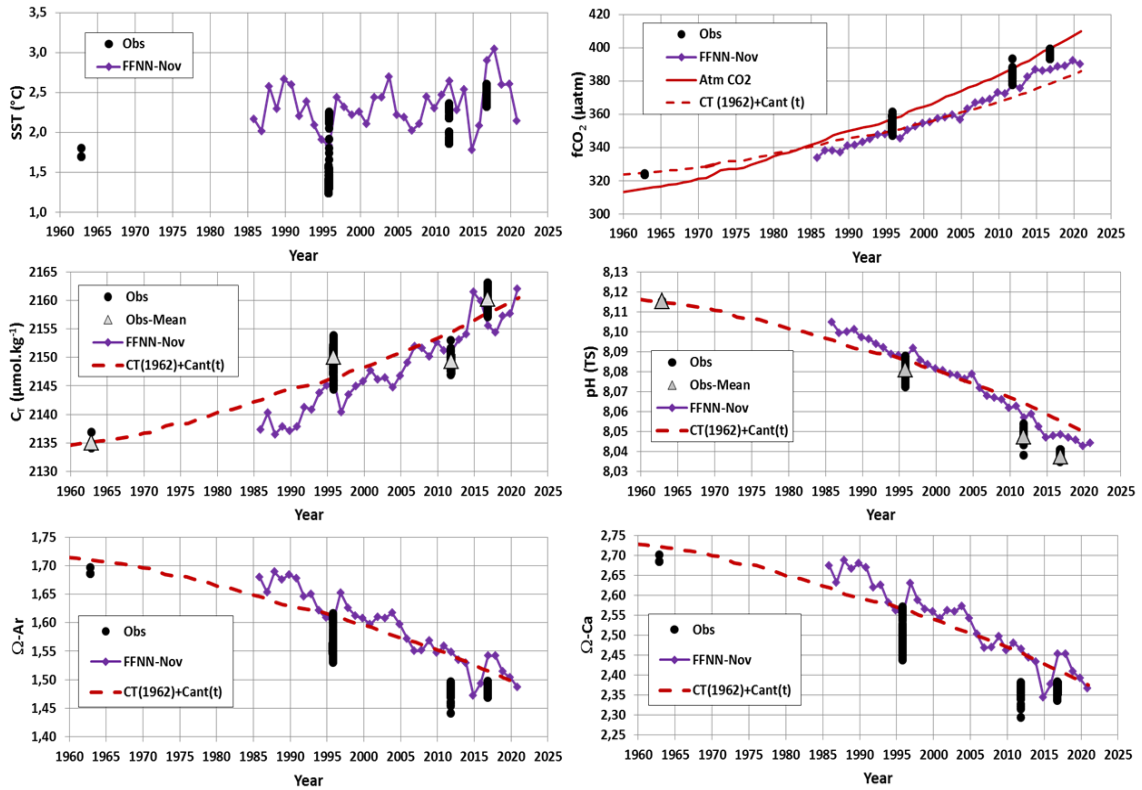


Figure 13: Observed (black dots) sea surface temperature ( $^{\circ}\text{C}$ ),  $fCO_2$  ( $\mu\text{atm}$ ),  $C_T$  ( $\mu\text{mol.kg}^{-1}$ ), pH (TS),  $\Omega_{-ar}$  and  $\Omega_{-ca}$  around station OISO-KERFIX at  $50^{\circ}40'S-68^{\circ}25'E$  for October-November. Also shown are the results for the FFNN model for November in 1985-2020 (Purple). The  $C_T$  concentrations, pH,  $\Omega_{-ar}$  and  $\Omega_{-ca}$  were calculated from  $fCO_2$  data using the  $A_T/S$  relation (Eq. 1). The red line is the atmospheric  $fCO_2$  and red dashed-lines in each plot are the evolution of properties since 1960 corrected for  $C_{ant}$  where  $fCO_2$ , pH,  $\Omega_{-ar}$  and  $\Omega_{-ca}$  were recalculated using  $C_T+C_{ant}$ ,  $A_T$  constant at  $2290 \mu\text{mol.kg}^{-1}$  and SST at  $2^{\circ}\text{C}$ . Grey triangles identify the mean values for  $C_T$  and pH.

1125 First, we note that the measured SST in November 1962 ( $1.7^{\circ}\text{C}$ ) was slightly lower compared to recent  
 1126 years (on average by about  $-0.6^{\circ}\text{C}$ ), but SST as low as  $1.8^{\circ}\text{C}$  for this season was also found in other years (e.g.  
 1127 November 1995, 2014). The change in SST is unlikely to explain the long-term increase in  $fCO_2$  or decrease in  
 1128 pH since 1962 (Figure 13). In 1962, the oceanic  $fCO_2$  was  $324 \mu\text{atm}$ , which is slightly higher than in the  
 1129 atmosphere ( $\Delta fCO_2=+8 \mu\text{atm}$ , a small source), whereas in November 1985-2020 the ocean was a small  $CO_2$  sink  
 1130 on average ( $\Delta fCO_2= -3.3 \pm 4.5 \mu\text{atm}$ ). The  $C_T$  concentration in 1962 ( $2135 \mu\text{mol.kg}^{-1}$ ) was much lower than  
 1131 observed since 1995 and the pH (8.115) was much higher than in the last three decades (Figure 13). Compared to  
 1132 1962, pH in 2016 was  $-0.078$  lower, i.e. representing 70% of the pH decrease of  $-0.11$  in the global ocean since  
 1133 the beginning of the industrial era (Jiang et al, 2019). In November 1962, surface  $C_T$  was lower by  $-15.1$   
 1134  $\mu\text{mol.kg}^{-1}$  compared to the data in October 1995, i.e. a trend of  $+0.46 \mu\text{mol.kg}^{-1}.\text{yr}^{-1}$  over 33 years close to the  
 1135  $C_{ant}$  trend observed in the WW over 1985-2021 as described above ( $+0.53 \pm 0.01 \mu\text{mol.kg}^{-1}.\text{yr}^{-1}$ ). Having the  $C_T$   
 1136 value in 1962, we can project the  $C_T$  in time by adding the  $C_{ant}$  concentration based on the relationship observed  
 1137 between  $C_{ant}$  and atmospheric  $CO_2$  (Figure 7b) assuming that the anthropogenic  $CO_2$  uptake since the sixties is  
 1138 representative of the  $C_T$  change (i.e. the change of  $C_T$  due to natural variability was small). This projection is  
 1139 shown for all properties (red dashed-lines in Figure 13) and confirms that the progressive  $C_{ant}$  accumulation

1140 explained most of the  $C_T$  and  $fCO_2$  increase in surface waters since 1962. We note that the  $C_T$  derived from the  
1141 FFNN model suggests slightly lower  $C_T$  compared to the  $C_{ant}$  projection especially before 2006. The difference  
1142 of projected  $C_T$  and the FFNN model (on average  $-2.2 \pm 2.7 \mu\text{mol.kg}^{-1}$ ) is within the uncertainty of  $C_T$   
1143 calculations (error is  $\pm 5 \mu\text{mol.kg}^{-1}$  when using the  $A_T/fCO_2$  pairs) and the trend of the difference over 1985-2020  
1144 ( $-0.15 \mu\text{mol.kg}^{-1}.\text{yr}^{-1}$ ) is too small to be related with confidence to changes associated with natural processes. On  
1145 the other hand, the oceanic  $fCO_2$  recalculated with the projected  $C_{ant}$  trend suggested that for this season  
1146 (November) the ocean moved from a  $CO_2$  source in 1962-1985 ( $\Delta fCO_2 > 0$ ) to a sink in 1986-2021 ( $\Delta fCO_2 < 0$ )  
1147 in line with results from the FFNN model. The recalculated  $fCO_2$  with  $C_{ant}$  (dashed red line in Figure 13) was  
1148 close to that observed in 1995 or from the FFNN model in 1985-2014 (mean difference over 1985-2014 is  $-1.2$   
1149  $\pm 5.2 \mu\text{atm}$ ). After 2016, the recalculated  $fCO_2$  suggest a stronger sink and the difference with observations in  
1150 2011 and 2016 or the FFNN model is slightly higher (mean difference over 2016-2020 is  $-8.8 \pm 1.5 \mu\text{atm}$ ).  
1151 Although the differences are in the range of the error in  $fCO_2$  calculation using  $A_T-C_T$  pairs ( $\pm 13 \mu\text{atm}$ ), this  
1152 might indicate that after 2016 a process could contribute to increase  $fCO_2$  faster than the effect of  $C_{ant}$  only. This  
1153 difference could be due to the warming that occurred after 2016 when SST was higher than  $2^\circ\text{C}$  and up to  $3^\circ\text{C}$  in  
1154 November 2017 (Figures 13 and S9). The same could be applied for pH that was slightly lower than the pH  
1155 recalculated from  $C_{ant}$  trend after 2015 (the mean difference between recalculated pH and FFNN-pH over 1985-  
1156 2020 is only  $0.002 \pm 0.006$ ). Therefore, we conclude that for November the pH decrease since 1962 was mainly  
1157 driven by the accumulation of anthropogenic  $CO_2$ . Aragonite and calcite saturation states also show a clear  
1158 decrease since 1962 (Figure 13), a diminution of 11% over 59 years for both  $\Omega_{ar}$  and  $\Omega_{ca}$ . Based on these results  
1159 over almost 60 years that confirm the conclusions from the observations in 1985-2021, we now evaluate the  
1160 long-term change of the carbonate system in surface waters in the future.

1161

### 1162 3.4.2 Projecting the observed trends in the future

1163

1164 The trends of the properties based on observations in 1962-2021 and the FFNN model in 1985-2020  
1165 indicate relatively linear trends linked to  $C_{ant}$  uptake albeit with some decadal variability in summer (Figure 4). A  
1166 simple linear extrapolation of the trends in the future suggests that aragonite under-saturation in surface waters  
1167 would be reached in year 2110 for the winter season and 2120 for summer (Figure S17) whereas the subsurface  
1168 trend suggests under-saturation in 2090. In year 2100, surface pH and  $[H^+]$  would be around 7.9 and  $12 \text{ nmol.kg}^{-1}$   
1169 (Figure S17). However, ESM CMIP6 models suggest that under a high emission scenario (SSP5-8.5), pH in  
1170 2100 in the Southern Ocean near  $50^\circ\text{S}$  would be around 7.65 and  $[H^+]$  around  $22 \text{ nmol.kg}^{-1}$  (Jiang et al., 2023,  
1171 their figure 4). This shows that the simple linear extrapolation based on recent observed trends (Figure S17)  
1172 underestimated the future change of the carbonate system for a high emission scenario as previously shown in  
1173 the South-Eastern Indian Ocean based on summer trends derived from observations in 1969-2003 (Midorikawa  
1174 et al., 2012, their figure 4).

1175 To better investigate the changes for the next decades, we assumed that the  $C_{ant}$  trend for the modern  
1176 period (Figure 7) that experienced a “business as usual” scenario after the sixties is representative of the future  
1177 changes in the surface ocean carbonate system. For this analysis, we used two emissions scenarios (Shared  
1178 Socioeconomic Pathways, SSP, Meinshausen et al., 2020) with atmospheric  $xCO_2$  reaching 1135 ppm in 2100 (a  
1179 “high” emission scenario SSP5-8.5) or  $xCO_2$  reaching 603 ppm in 2100 after a stabilization around 2080  
1180 (scenario SSP2-4.5). This enables to simulate future  $C_T$  concentrations for summer or winter (Figure 14) and to

1181 calculate other carbonate properties using  $C_T$  and  $A_T$  (Figure 15, Table 3) in response to approximated future  
1182 changes in physical and geochemical properties excluding impacts of changes in atmospheric and oceanic  
1183 circulation. As the calculated properties are sensitive to  $A_T$  values, we used a fixed  $A_T$  of  $2280 \mu\text{mol.kg}^{-1}$  or  
1184 applied a correction based on the long-term change of sea surface salinity observed in the last 6 decades (1960-  
1185 2017), i.e. a freshening in the Southern Ocean of around  $-0.01$  to  $-0.02.\text{decade}^{-1}$  (Durack and Wijffels, 2010;  
1186 Cheng et al., 2020b). The decrease in salinity in the South Indian Ocean ( $-0.02 \pm 0.01 \text{decade}^{-1}$ ) was recently  
1187 analyzed by Akhoudas et al. (2023) who showed that in the years 1993-2021 the freshening was mainly due to  
1188 an increase in precipitations linked to the acceleration of the atmospheric hydrological cycle. From our data in  
1189 the mixed-layer over 1985-2021, we estimated a trend in salinity of  $-0.021 \pm 0.004 \text{decade}^{-1}$ . For the  $A_T$   
1190 sensitivity test we thus selected a salinity trend of  $-0.01.\text{decade}^{-1}$  in 1962-1985 and  $-0.02.\text{decade}^{-1}$  after 1985 and  
1191 applied these trends to simulate  $A_T$  over 1960-2100 using the  $A_T$ /Salinity relationship (Equation 1). This leads to  
1192 a salinity of 33.650 and  $A_T$  of  $2272 \mu\text{mol.kg}^{-1}$  in the year 2100, about  $8 \mu\text{mol.kg}^{-1}$  lower than observed in 2021  
1193 ( $2280 \mu\text{mol.kg}^{-1}$ ). Compared to the  $C_T$  change from 2021 to 2100 ( $+50$  and  $+193 \mu\text{mol.kg}^{-1}$  for the “low” and  
1194 “high” emissions scenario, Figure 14), the impact of the  $A_T$  decrease has a minor effect on the future change for  
1195 pH,  $[\text{CO}_3^{2-}]$  and  $\Omega$  (Table 3). For example, in winter for the SSP5-8.5 scenario, when the  $A_T$  decrease is taken  
1196 into account, pH in 2100 is 7.316 and  $\Omega_{Ar}$  is 0.33 against 7.372 and 0.34 when  $A_T$  is constant (Table 3). In both  
1197 cases, the surface aragonite under-saturation ( $\Omega_{Ar}=1$ ) in winter occurred in 2055, whereas in summer it is  
1198 identified in 2070. The effect of lower  $A_T$  in the future appeared also small compared to the seasonal differences  
1199 of pH and  $\Omega$  in 2100.

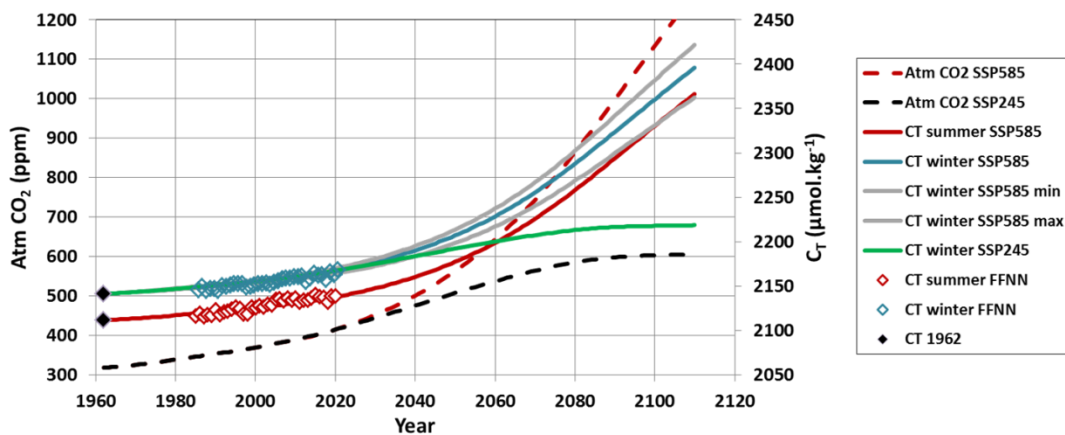
1200 As noted above, the Southern Ocean experienced a warming in recent decades (e.g. Auger et al., 2021)  
1201 and it is projected that warming will continue in the future (IPCC, 2022). Therefore, to test the sensitivity of  
1202 calculated properties to warming we applied a warming of  $+0.0125^\circ\text{C.yr}^{-1}$  in 1985-2020 and  $+0.025^\circ\text{C.yr}^{-1}$  after  
1203 2020 (Azarian et al, 2023). As for  $A_T$ , these results are compared for winter using constant SST (Table 3  $\oplus$ ). The  
1204 effect of the long-term warming does mainly impact the projection of  $[\text{H}^+]$  and pH (Table 3).

1205 These sensitivity tests for temperature and  $A_T$  showed that as for the observed period 1962-2021 (Figure  
1206 13), the projection in the future depends mainly on the anthropogenic  $\text{CO}_2$  accumulation. Here, the  $C_T$   
1207 concentrations were calculated using the  $C_{ant}$  versus atmospheric  $\text{CO}_2$  relationship (Figure 7b). We thus tested  
1208 the results for winter based on the error associated with this relationship (Figure S18). This leads to either higher  
1209 or lower  $C_T$  compared to the original calculation (Figure 14). For the SSP5-8.5 scenario, the winter  $C_T$   
1210 concentrations in 2100 range between  $2328$  and  $2378 \mu\text{mol.kg}^{-1}$ , higher than simulated in the ESM CMIP6  
1211 models around  $50^\circ\text{S}$  ( $2300 \mu\text{mol.kg}^{-1}$ , Jiang et al., 2023). As in the ESM models, the projected  $C_T$  concentration  
1212 in 2100 at our location for the SSP2-4.5 scenario is much lower  $2217 \mu\text{mol.kg}^{-1}$  (Figure 14). The future change  
1213 of the carbonate system is not significantly different using low or high  $C_{ant}$  accumulation (Figure S18) but this  
1214 test gives a range of years to reach aragonite and calcite under-saturation. In winter (SSP5-8.5 scenario),  
1215 aragonite (calcite) would reach under-saturation between year 2050 and 2060 (between year 2070 and 2080).  
1216 Note that for summer we derived under-saturation for  $\Omega_{Ar}$  in year 2065 and for  $\Omega_{Ca}$  in year 2085. For the SSP2-  
1217 4.5 scenario, where  $C_T$  is  $143 \mu\text{mol.kg}^{-1}$  lower in 2100 compared to SSP5-8.5, aragonite under-saturation would  
1218 not be reached before 2070 (Figure 15).

1219

1221 Table 3: Results of the simulated properties for year 2020, 2050 and 2100 for two emission scenarios (SSP5-8.5 and SSP2-  
 1222 4.5). For 2020 the results based on observations in January (Obs) and the FFNN model in January and August also listed.  
 1223 Sensitivity tests: “SSP85 W-T” is for winter with constant temperature and “SSP85 W-A-T” is for winter with constant  $A_T$   
 1224 and temperature.  
 1225

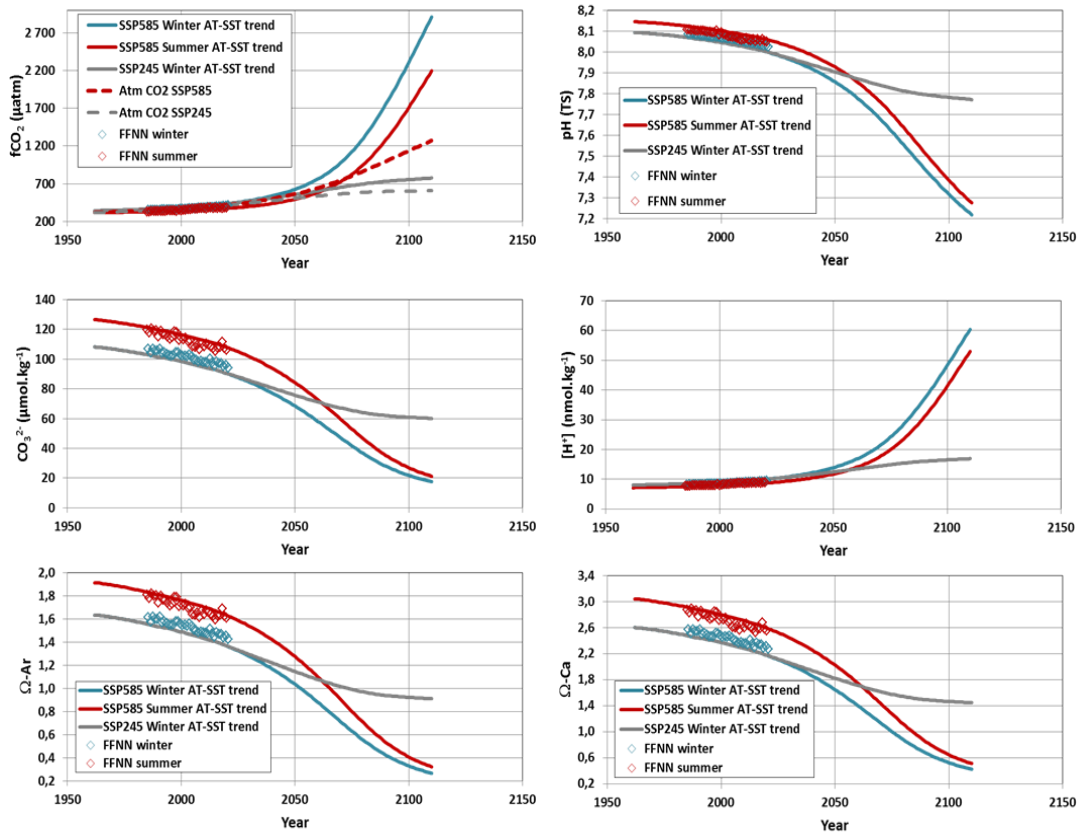
Method	Year	Atm-CO <sub>2</sub> ppm	fCO <sub>2</sub> µatm	C <sub>T</sub> µmol.kg <sup>-1</sup>	A <sub>T</sub> µmol.kg <sup>-1</sup>	pH TS	[H <sup>+</sup> ] nmol.kg <sup>-1</sup>	[CO <sub>3</sub> <sup>2-</sup> ] µmol.kg <sup>-1</sup>	Ω <sub>ca</sub>	Ω <sub>ar</sub>
Obs Jan	2020	410.6	391.9	2142.2	2281.8	8.044	9.04	105.2	2.53	1.59
Std obs.			(2.0)	(0.7)	(0.3)	(0.002)	(0.04)	(0.5)	(0.01)	(0.01)
FFNN Jan	2020	410.6	385.1	2138.5	2280.1	8.051	8.90	106.3	2.55	1.61
SSP Summer	2020	414.9	375.4	2137.5	2282.1	8.061	8.70	108.0	2.60	1.63
FFNN Aug	2020	410.6	410.0	2168.3	2289.8	8.024	9.45	94.2	2.27	1.42
SSP Winter	2020	414.9	434.5	2167.3	2282.1	8.001	9.98	90.4	2.18	1.37
SSP585 Summer	2050	562.8	526.5	2177.2	2278.3	7.928	11.79	84.2	2.02	1.28
SSP585 Winter	2050	562.8	624.7	2207.0	2278.3	7.857	13.91	68.5	1.65	1.04
SSP585 W-A-T	2050	562.8	585.7	2207.0	2280.0	7.880	13.17	69.0	1.66	1.04
SSP585 W-T	2050	562.8	592.7	2207.0	2278.3	7.875	13.32	68.1	1.64	1.03
SSP245 Winter	2050	506.9	554.8	2192.0	2278.3	7.905	12.46	75.8	1.92	1.15
SSP585 Summer	2100	1135.2	1986.9	2330.6	2271.8	7.394	41.31	26.9	0.65	0.41
SSP585 Winter	2100	1135.2	2306.3	2360.4	2271.8	7.316	48.26	21.8	0.52	0.33
SSP585 W-A-T	2100	1135.2	1993.1	2360.4	2280.0	7.372	42.44	22.6	0.54	0.34
SSP585 W-T	2100	1135.2	2097.0	2360.4	2271.8	7.349	44.74	21.3	0.51	0.32
SSP245 Winter	2100	602.8	753.9	2217.7	2271.8	7.782	16.51	60.9	1.47	0.92



1267 Figure 14: Evolution of atmospheric CO<sub>2</sub> (ppm) and sea surface C<sub>T</sub> (µmol.kg<sup>-1</sup>) between 1960 and 2110 evaluated for 2  
 1268 scenarios (SSP2-4.5 black dashed and SSP5-8.5 red dashed), for summer (red line for SSP5-8.5) and winter (blue line for  
 1269 SSP5-8.5 and green line for SSP2-4.5). Grey lines are the high and low C<sub>T</sub> for winter SSP5-8.5 based on the error in the  
 1270 C<sub>ant</sub>/fCO<sub>2</sub> relationship (figure 7b). Also shown are the results for the FFNN model in 1985-2020 for summer (red diamonds)  
 1271 and winter (blue diamonds) and C<sub>T</sub> in 1962 (black diamonds). The C<sub>T</sub> values for different seasons and scenarios were used to  
 1272 calculate the carbonate properties in the future (Figure 15).  
 1273

1274  
 1275  
 1276  
 1277  
 1278

1279  
 1280  
 1281  
 1282  
 1283  
 1284  
 1285  
 1286  
 1287  
 1288  
 1289  
 1290  
 1291  
 1292  
 1293  
 1294  
 1295  
 1296  
 1297  
 1298  
 1299  
 1300  
 1301  
 1302  
 1303  
 1304



1305 Figure 15: Evolution of sea surface  $f\text{CO}_2$  ( $\mu\text{atm}$ ), pH (TS),  $[\text{CO}_3^{2-}]$  ( $\mu\text{mol.kg}^{-1}$ ),  $[\text{H}^+]$  ( $\text{nmol.kg}^{-1}$ ),  $\Omega\text{-Ar}$  and  $\Omega\text{-Ca}$  between  
 1306 1960 and 2110 evaluated for the SSP5-8.5 scenario for winter (blue line) and summer (red line) taking into account both  $A_T$   
 1307 and SST future trends. For winter the results are also presented using the SSP2-4.5 scenario (grey lines). Also shown are the  
 1308 results for the FFNN model in 1985-2020 for summer (red diamonds) and winter (blue diamonds). Atmospheric  $f\text{CO}_2$  is also  
 1309 shown for SSP5-8.5 (red dashed) and SSP2-4.5 (grey dashed). Values in 2020, 2050 and 2100 for different sensitivity tests  
 1310 are listed in Table 3.  
 1311

1312 **4 Summary and concluding remarks**

1313  
 1314 The times-series of high quality observations collected between 1985 and 2021 and the results from the  
 1315 FFNN model at one location, south of the Polar Front in the Southern Indian Ocean ( $50^\circ\text{S}$ - $68^\circ\text{E}$ ) presented in  
 1316 this analysis offered new results on the inter-annual variability, decadal to long-term trends of the carbonate  
 1317 system in surface waters, air-sea  $\text{CO}_2$  fluxes and associated drivers. The evaluation of anthropogenic  $\text{CO}_2$   
 1318 concentrations in the water column indicated that the trends of the carbonate species are mainly driven by the  
 1319 anthropogenic  $\text{CO}_2$  uptake leading to a progressive acidification in surface waters and at depth.

1320 In 1985, the  $C_{\text{ant}}$  concentrations were approaching  $50 \mu\text{mol.kg}^{-1}$  at 200 m and  $C_{\text{ant}}$  was detected in the  
 1321 water column down to the bottom (1600m). This explains why aragonite under-saturation was observed at 600-  
 1322 700m in 1985, where  $[\text{CO}_3^{2-}]$  concentration was at its minimum, whereas for the pre-industrial era the whole  
 1323 water column was super-saturated (this study Figure S15; Lauvset et al., 2020, their Figure S15). 36 years later,  
 1324 because of the anthropogenic  $\text{CO}_2$  accumulation, we observed an upward migration of the aragonite saturation  
 1325 horizon that was found around 400 m in 2021 (a shoaling rate of around  $-6 \text{ m.yr}^{-1}$ ).

1326 At subsurface, in the Winter Water layer, the  $C_{\text{ant}}$  trend is estimated at  $+0.53 \pm 0.01 \mu\text{mol.kg}^{-1}.\text{yr}^{-1}$  over  
 1327 1985-2021 with a detectable increase of the trend in recent years. The  $C_{\text{ant}}$  concentrations in the ocean are closely

1328 related to the atmospheric CO<sub>2</sub> concentrations and the slope we observed south of the PF in the Indian sector of  
1329 +0.263 ±0.042 μmol.kg<sup>-1</sup>.μatm<sup>-1</sup> is close to that observed in the AAIW in the South Atlantic (Fontela et al.,  
1330 2021). This suggests that local observations in the South Indian POOZ captured the link between C<sub>ant</sub> and  
1331 atmospheric CO<sub>2</sub> at larger scale.

1332 In surface waters, over 1991-2020 the oceanic fCO<sub>2</sub> increased at a rate close or slightly lower than in  
1333 the atmosphere (Figure 2b) and the C<sub>T</sub> trend followed the C<sub>ant</sub> accumulation (Figure 4b, S12a). However in the  
1334 last decade both observations and the FFNN model showed low fCO<sub>2</sub> trends in summer (less than 1 μatm.yr<sup>-1</sup>).  
1335 The change in summer trend appears related to primary production as revealed by a decrease of Chl-a in 1998-  
1336 2010 followed by an increase after 2010. Biological activity counteracts the C<sub>T</sub> increase due to C<sub>ant</sub>, resulting in  
1337 rather stable C<sub>T</sub> and fCO<sub>2</sub> in summer during the last decade. As a result, the region moved from an annual source  
1338 of +0.8 molC.m<sup>-2</sup>.yr<sup>-1</sup> in 1985 to a sink of -0.5 molC.m<sup>-2</sup>.yr<sup>-1</sup> in 2020. Adding historical data from November  
1339 1962 that indicate an annual source of 2.2 molC.m<sup>-2</sup>.yr<sup>-1</sup>, and extrapolating to the entire South Indian POOZ (50-  
1340 58°S/20-120°E, 6.5 Mkm<sup>2</sup>), suggest that this region changed from a CO<sub>2</sub> source of 0.17 PgC.yr<sup>-1</sup> in 1962,  
1341 reduced to 0.06 PgC.yr<sup>-1</sup> in 1985 and a CO<sub>2</sub> sink of -0.04 PgC.yr<sup>-1</sup> in 2020. This can be compared with  
1342 reconstructed fluxes from a data-based model that produced a CO<sub>2</sub> source around 0.10 PgC.yr<sup>-1</sup> in 1960-1990  
1343 and a sink around -0.05 PgC.yr<sup>-1</sup> in 2020 in the south Indian sector (Rödenbeck et al., 2022, their Figure 6).  
1344 Based on the FFNN reconstructions, the increase of the ocean CO<sub>2</sub> sink was particularly pronounced after 2011  
1345 (Figure 3) when phytoplankton biomass was increasing in this HNLC region and occurred when the SAM index  
1346 was in a positive state. Although observations in the water column do not suggest enhanced upwelling, we  
1347 cannot eliminate the possibility that the SAM influenced changes in primary production.

1348 For October/November, the estimated increase in C<sub>T</sub> concentration in surface waters over 54 years (+21  
1349 μmol.kg<sup>-1</sup>) was almost equal to the increase of C<sub>ant</sub> (+22.3 μmol.kg<sup>-1</sup>). As a result, surface ocean pH dropped  
1350 from 8.11 in 1962 to 8.044 in 2020. Over a multi-decadal time scale (30 years or more), acidification in the  
1351 South Indian POOZ was mainly controlled by the uptake of anthropogenic CO<sub>2</sub>. However, our data also indicate  
1352 a modulation of the summer pH trend by natural processes. After 2010, a very small pH trend was estimated in  
1353 summer (-0.0098.decade<sup>-1</sup> ±0.0042) when the region experienced in increase in primary productivity. On the  
1354 opposite, in winter, the pH trends continuously increased with time. At the subsurface (Winter Water layer), the  
1355 trend of pH based on A<sub>T</sub> and C<sub>T</sub> data over 1985-2021 (-0.0161 ±0.0033.decade<sup>-1</sup>) is also almost equal to the  
1356 annual surface trend from the FFNN model. A simple extrapolation of the trends in the WW indicated that  
1357 under-saturation (Ω<1) would be reached at year 2090 for aragonite and year 2180 for calcite. However, as  
1358 atmospheric CO<sub>2</sub> is expected to increase and ocean C<sub>T</sub> will increase in the future, pH and Ω will decrease at a  
1359 faster rate than observed in the last decades. A projection of future C<sub>T</sub> concentrations based on two emission  
1360 scenarios, excluding changes in ocean circulation, indicated that the winter surface pH in 2100 would decrease to  
1361 7.32 for a high emission scenario (SSP5-8.5) or to 7.782 for a low emission scenario (SSP2-4.5). This is up to -  
1362 0.86 lower than pre-industrial pH and -0.71 lower than pH observed in 2020. For the winter season the aragonite  
1363 under-saturation in surface would be reached around 2050 for a high emissions scenario and 2070 for a low  
1364 emission scenario.

1365 The time-series presented here for the Southern Ocean, along with other historical time-series of A<sub>T</sub> and  
1366 C<sub>T</sub> in the water-column (BATS, HOT, ESTOC, KNOT, Iceland or Irminger seas; Bates et al., 2014; Lange et al.,  
1367 2023) or the recent BGC-Argo floats in the Southern Ocean (Mazloff et al., 2023) offer useful data for the  
1368 evaluation of biogeochemical and Earth system models, especially for the physical and biological drivers of the

1369 carbonate system not well represented in current models at seasonal to decadal scales in the Southern Ocean (e.g.  
1370 Hauck et al., 2023a; Rodgers et al., 2023; Joos et al., 2023). Observing the decadal changes of the carbonate  
1371 system in the water column is also an important step to extend the evaluation of biogeochemical and ESM  
1372 models below the surface (Jiang et al., 2023). It is important to maintain such time-series for monitoring the  
1373 future evolution of the ocean CO<sub>2</sub> sink, of the acidification and its impact on phytoplankton species and higher  
1374 trophic levels. This is especially the case in Marine Protected Area such as the French Sub-Antarctic islands  
1375 including the Kerguelen Archipelago which was listed as a UNESCO World Heritage site in 2019.

1376

1377 **Data availability:**

1378 Data used in this study are available in SOCAT ([www.socat.info](http://www.socat.info)) for fCO<sub>2</sub> surface data, in GLODAP  
1379 ([www.glodap.info](http://www.glodap.info)) for water-column data and at NCEI/OCADS ([www.ncei.noaa.gov/access/ocean-carbon-data-  
1380 system/oceans/VOS\\_Program/OISO.html](http://www.ncei.noaa.gov/access/ocean-carbon-data-system/oceans/VOS_Program/OISO.html)). The CMEMS-LSCE-FFNN model data are available at E.U.  
1381 Copernicus Marine Service Information (<https://resources.marine.copernicus.eu/products>).

1382

1383 **Authors contributions:**

1384 CLM and NM are co-I of the ongoing OISO project. CLM, NM, CL and CR participated to OISO cruises.  
1385 Underway fCO<sub>2</sub> was measured by CLM, NM, CL, and qualified by CLM and NM. Nutrients data were measured  
1386 and qualified by CLM and CL. Chl-a data were measured and qualified by CR. Water column data were  
1387 qualified by CLM, NM, CL, CR and GR. MG, FC and TTTC developed the CMEMS-LSCE-FFNN model and  
1388 provided the model results. NM started the analysis, wrote the draft of the manuscript and prepared the figures  
1389 All authors contributed to revising the draft manuscript.

1390

1391 **Competing interest:** The authors declare that they have no conflict of interest.

1392

1393 **Acknowledgments:** The OISO program was supported by the French institutes INSU (Institut National des  
1394 Sciences de l'Univers) and IPEV (Institut Polaire Paul-Emile Victor), OSU Ecce-Terra (at Sorbonne Université),  
1395 the French programs SOERE/Great-Gases and ICOS-France. We thank the French Oceanographic Fleet for  
1396 financial and logistic support for the OISO program (<https://campagnes.flotteoceanographique.fr/series/228/>).  
1397 We thank the captains and crew of *R.R.V. Marion Dufresne* and the staff at IFREMER, GENAVIR and IPEV.  
1398 We also thank Jonathan Fin and Claude Mignon for their help during the OISO cruises. The development of the  
1399 neural network model benefited from funding by the French INSU-GMMC project "PPR-Green-Grog (grant no  
1400 5-DS-PPR-GGREOG), the EU H2020 project AtlantOS (grant no 633211), as well as through the Copernicus  
1401 Marine Environment Monitoring Service (project 83-CMEMS-TAC-MOB). We thank all colleagues that  
1402 contributed to the quality control of ocean data made available through CARINA and GLODAP  
1403 ([www.glodap.info](http://www.glodap.info)). The Surface Ocean CO<sub>2</sub> Atlas (SOCAT, [www.socat.info](http://www.socat.info)) is an international effort, endorsed  
1404 by the International Ocean Carbon Coordination Project (IOCCP), the Surface Ocean Lower Atmosphere Study  
1405 (SOLAS) and the Integrated Marine Biogeochemistry and Ecosystem Research program (IMBER), to deliver a  
1406 uniformly quality-controlled surface ocean CO<sub>2</sub> database. We thank the associate editor, Ismael Hernández-  
1407 Carrasco, and two anonymous reviewers for their detailed comments and supportive reviews.

1408

1409 **References**

1410



1411 Akhoudas, C. H., Sallée, J.-B., Reverdin, G., Haumann, F. A., Pauthenet, E., Chapman, C. C., Margirier, F., Lo  
1412 Monaco, C., Metzl, N., Meilland, J., and Stranne, C.: Isotopic evidence for an intensified hydrological cycle in  
1413 the Indian sector of the Southern Ocean. *Nat Commun* 14, 2763. <https://doi.org/10.1038/s41467-023-38425-5>,  
1414 2023

1415

1416 Aminot, A., and Kérouel, R.: *Hydrologie des écosystèmes marins: paramètres et analyses*. Ed. Ifremer, 336 p.,  
1417 2004

1418

1419 Antonov, J. I., Locarnini, R. A., Boyer, T. P., Mishonov, A. V., and Garcia, H. E.: World Ocean Atlas 2005, in:  
1420 Volume 2: Salinity, edited by: Levitus, S., NOAA Atlas NESDIS 62, US Government Printing Office,  
1421 Washington, DC, 182 pp., <https://repository.library.noaa.gov/view/noaa/1127>, 2006.

1422

1423 Arrigo, K. R., van Dijken, G. L., and Bushinsky, S.: Primary production in the Southern Ocean, 1997–2006, *J.*  
1424 *Geophys. Res.-Oceans*, 113, C08004, doi:doi:10.1029/2007jc004551, 2008.

1425

1426 Auger, M., Morrow, R., Kestenare, E., Sallée, J.-B., and Cowley, R.: Southern Ocean in-situ temperature trends  
1427 over 25 years emerge from interannual variability, *Nat. Commun.*, 12, 514,  
1428 <https://doi.org/10.1038/s41467-020-20781-1>, 2021

1429

1430 Azarian, C., Bopp, L., Pietri, A., Sallée, J.-B., and d'Ovidio, F.: Current and projected patterns of warming and  
1431 marine heatwaves in the Southern Indian Ocean, *Progress in Oceanography*,  
1432 doi:<https://doi.org/10.1016/j.pocean.2023.103036>, 2023

1433

1434 Bakker, D. C. E., Pfeil, B., Landa, C. S., Metzl, N., O'Brien, K. M., Olsen, A., Smith, K., Cosca, C., Harasawa,  
1435 S., Jones, S. D., Nakaoka, S.-I., Nojiri, Y., Schuster, U., Steinhoff, T., Sweeney, C., Takahashi, T., Tilbrook, B.,  
1436 Wada, C., Wanninkhof, R., Alin, S. R., Balestrini, C. F., Barbero, L., Bates, N. R., Bianchi, A. A., Bonou, F.,  
1437 Boutin, J., Bozec, Y., Burger, E. F., Cai, W.-J., Castle, R. D., Chen, L., Chierici, M., Currie, K., Evans, W.,  
1438 Featherstone, C., Feely, R. A., Fransson, A., Goyet, C., Greenwood, N., Gregor, L., Hankin, S., Hardman-  
1439 Mountford, N. J., Harlay, J., Hauck, J., Hoppema, M., Humphreys, M. P., Hunt, C. W., Huss, B., Ibánhez, J. S.  
1440 P., Johannessen, T., Keeling, R., Kitidis, V., Körtzinger, A., Kozyr, A., Krasakopoulou, E., Kuwata, A.,  
1441 Landschützer, P., Lauvset, S. K., Lefèvre, N., Lo Monaco, C., Manke, A., Mathis, J. T., Merlivat, L., Millero, F.  
1442 J., Monteiro, P. M. S., Munro, D. R., Murata, A., Newberger, T., Omar, A. M., Ono, T., Paterson, K., Pearce, D.,  
1443 Pierrot, D., Robbins, L. L., Saito, S., Salisbury, J., Schlitzer, R., Schneider, B., Schweitzer, R., Sieger, R.,  
1444 Skjelvan, I., Sullivan, K. F., Sutherland, S. C., Sutton, A. J., Tadokoro, K., Telszewski, M., Tuma, M., Van  
1445 Heuven, S. M. A. C., Vandemark, D., Ward, B., Watson, A. J., and Xu, S. : A multi-decade record of high-  
1446 quality fCO<sub>2</sub> data in version 3 of the Surface Ocean CO<sub>2</sub> Atlas (SOCAT), *Earth Syst. Sci. Data*, 8, 383-413,  
1447 doi:10.5194/essd-8-383-2016, 2016.

1448

1449 Bakker, D. C. E. et al: Surface Ocean CO<sub>2</sub> Atlas Database Version 2022 (SOCATv2022) (NCEI Accession  
1450 0253659). NOAA National Centers for Environmental Information. Dataset. <https://doi.org/10.25921/1h9f-nb73>.  
1451 Last Accessed [21 June 2022], 2022

1452

1453 Balch, W.M., Bates, N.R., Lam, P.J., Twining, B.S., Rosengard, S. Z., Bowler, B.C., Drapeau, D.T., Garley, R.,  
1454 Lubelczyk, L.C., Mitchell, C., and Rauschenberg, S.: Factors regulating the Great Calcite Belt in the Southern  
1455 Ocean and its biogeochemical significance. *Global Biogeochem. Cycles*, 30, doi: 10.1002/2016GB005414, 2016

1456

1457 Basterretxea, G., Font-Muñoz, J. S., Hernández-Carrasco, I., and Sañudo-Wilhelmy, S. A.: Global variability of  
1458 high-nutrient low-chlorophyll regions using neural networks and wavelet coherence analysis, *Ocean Sci.*, 19,  
1459 973–990, <https://doi.org/10.5194/os-19-973-2023>, 2023.

1460

1461 Bates, N., Astor, Y., Church, M., Currie, K., Dore, J., González-Dávila, M., Lorenzoni, L., Muller-Karger, F.,  
1462 Olafsson, J., and Santa-Casiano, M.: A Time-Series View of Changing Ocean Chemistry Due to Ocean Uptake  
1463 of Anthropogenic CO<sub>2</sub> and Ocean Acidification, *Oceanography*, 27, 126–141,

1464 <https://doi.org/10.5670/oceanog.2014.16>, 2014.

1465

1466 Beaufort, L., Probert, I., de Garidel-Thoron, T., Bendif, E.M., Ruiz-Pino, D., Metzl, N., Goyet, C., Buchet, N.,  
1467 Coupel, P., Grelaud, M., Rost, B., Rickaby, R.E.M., and de Vargas C.: Sensitivity of coccolithophores to  
1468 carbonate chemistry and ocean acidification. *Nature*, doi:10.1038/nature10295. 2011

1469

1470 Bennington, V., Gloege, L., and McKinley, G. A.: Variability in the global ocean carbon sink from 1959 to 2020  
1471 by correcting models with observations. *Geophysical Research Letters*, 49, e2022GL098632.  
1472 <https://doi.org/10.1029/2022GL098632>, 2022

1473

1474 Benoiston, A.-S., Ibarbalz, F. M., Bittner, L., Guidi, L., Jahn, O., Dutkiewicz, S., and Bowler, C.: The evolution  
1475 of diatoms and their biogeochemical functions. *Phil. Trans. R. Soc. B* 372: 20160397.  
1476 <http://dx.doi.org/10.1098/rstb.2016.0397>, 2017

1477

1478 Bopp, L., Resplandy, L., Orr, J. C., Doney, S. C., Dunne, J. P., Gehlen, M., Halloran, P., Heinze, C., Ilyina, T.,  
1479 Séférian, R., Tjiputra, J., and Vichi, M.: Multiple stressors of ocean ecosystems in the 21st century: projections  
1480 with CMIP5 models, *Biogeosciences*, 10, 6225–6245, <https://doi.org/10.5194/bg-10-6225-2013>, 2013.

1481

1482 Brady, R. X., Maltrud, M. E., Wolfram, P. J., Drake, H. F., and Lovenduski, N. S.: The influence of ocean  
1483 topography on the upwelling of carbon in the Southern Ocean. *Geophysical Research Letters*, 48,  
1484 e2021GL095088. <https://doi.org/10.1029/2021GL095088>, 2021

1485

1486 Brandon, M., Goyet, C., Touratier, F., Lefèvre, N., Kestenare, E., and Morrow, R.: Spatial and temporal  
1487 variability of the physical, carbonate and CO<sub>2</sub> properties in the Southern Ocean surface waters during austral  
1488 summer (2005–2019), *Deep-Sea Research Part I*, <https://doi.org/10.1016/j.dsr.2022.103836>, 2022

1489

1490 Burger, F. A., John, J. G., and Frölicher, T. L.: Increase in ocean acidity variability and extremes under  
1491 increasing atmospheric CO<sub>2</sub>, *Biogeosciences*, 17, 4633–4662, <https://doi.org/10.5194/bg-17-4633-2020>, 2020

1492

1493 Bushinsky, S. M., Landschützer, P., Rödenbeck, C., Gray, A. R., Baker, D., Mazloff, M. R., Resplandy, L.,  
1494 Johnson, K. S., and Sarmiento, J. L.: Reassessing Southern Ocean air-sea CO<sub>2</sub> flux estimates with the addition of  
1495 biogeochemical float observations. *Global Biogeochemical Cycles*, 33. doi: 10.1029/2019GB006176, 2019

1496

1497 Caldeira, K., and Wickett, M.: Anthropogenic carbon and ocean pH. *Nature*, 425, 365. doi: 10.1038/425365a,  
1498 2003

1499

1500 Canadell, J. G., Monteiro, P. M. S., Costa, M. H., Cotrim da Cunha, L., Cox, P. M., Eliseev, A. V., Henson, S.,  
1501 Ishii, M., Jaccard, S., Koven, C., Lohila, A., Patra, P. K., Piao, S., Rogelj, J., Syampungani, S., Zaehle, S., and  
1502 Zickfeld, K.: Global Carbon and other Biogeochemical Cycles and Feedbacks, in: *Climate Change 2021: The*  
1503 *Physical Science Basis. Contribution of Working Group I to the Sixth Assessment Report of the*  
1504 *Intergovernmental Panel on Climate Change*, edited by: Masson-Delmotte, V., Zhai, P., Pirani, A., Connors, S.  
1505 L., Péan, C., Berger, S., Caud, N., Chen, Y., Goldfarb, L., Gomis, M. I., Huang, M., Leitzell, K., Lonnoy, E.,  
1506 Matthews, J. B. R., Maycock, T. K., Waterfield, T., Yelekçi, O., Yu, R., and Zhou, B., Cambridge University  
1507 Press, Cambridge, United Kingdom and New York, NY, USA, 673–816, doi:10.1017/9781009157896, 2021

1508

1509 Carpenter, J. H.: The Accuracy of the Winkler Method for Dissolved Oxygen Analysis, *Limnol. Oceanogr.*, 10,  
1510 135–140, <https://doi.org/10.4319/lo.1965.10.1.0135>, 1965.

1511

1512 Carter, B. R., Williams, N. L., Gray, A. R., and Feely, R. A.: Locally interpolated alkalinity regression for global  
1513 alkalinity estimation. *Limnol. Oceanogr.: Methods* 14: 268–277. doi:10.1002/lom3.10087, 2016

1514

1515 Carter, B. R., Feely, R. A., Williams, N. L., Dickson, A. G., Fong, M. B., and Takeshita, Y.: Updated methods  
1516 for global locally interpolated estimation of alkalinity, pH, and nitrate. *Limnology and Oceanography: Methods*,  
1517 16: 119-131. doi: 10.1002/lom3.10232, 2018  
1518  
1519 Carter, B. R., Feely, R. A., Wanninkhof, R., Kouketsu, S., Sonnerup, R. E., Pardo, P. C., et al: Pacific  
1520 anthropogenic carbon between 1991 and 2017. *Global Biogeochemical Cycles*, 33, 597–617.  
1521 <https://doi.org/10.1029/2018GB006154>, 2019  
1522  
1523 Chapman, C., Mcc Hogg, A., Kiss, A., and Rintoul, S.: The dynamics of Southern Ocean storm tracks. *Journal of*  
1524 *Physical Oceanography*, 45 (3), pp.884 - 903. 10.1175/JPO-D-14-0075.1, 2015  
1525  
1526 Chau, T. T. T., Gehlen, M., and Chevallier, F.: A seamless ensemble-based reconstruction of surface ocean  $p\text{CO}_2$   
1527 and air–sea  $\text{CO}_2$  fluxes over the global coastal and open oceans, *Biogeosciences*, 19, 1087–1109,  
1528 <https://doi.org/10.5194/bg-19-1087-2022>, 2022.  
1529  
1530 Chen, H., Haumann, F. A., Talley, L. D., Johnson, K. S., and Sarmiento, J. L.: The deep ocean's carbon exhaust.  
1531 *Global Biogeochemical Cycles*. doi: <https://doi.org/10.1002/essoar.10507757.1>, 2022  
1532  
1533 Cheng, L. J., Abraham, J., Zhu, J., Trenberth, K. E., Fasullo, J., Boyer, T., Locarnini, R., Zhang, B., Yu, F. J.,  
1534 Wan, L. Y., Chen, X. R., Song, X. Z., Liu, Y. L., and Mann, M. E.: Record-setting ocean warmth continued in  
1535 2019, *Adv. Atmos. Sci*, 37, 137-142. <https://doi.org/10.1007/s00376-020-9283-7>, 2020a  
1536  
1537 Cheng L., K. E. Trenberth, N. Gruber, J. P. Abraham, J. Fasullo, G. Li, M. E. Mann, X. Zhao, Jiang Zhu:  
1538 Improved estimates of changes in upper ocean salinity and the hydrological cycle. *Journal of Climate*. doi:  
1539 <https://doi.org/10.1175/JCLI-D-20-0366.1>, 2020b  
1540  
1541 Copin-Montégut, C.: A new formula for the effect of temperature on the partial pressure of  $\text{CO}_2$  in seawater.  
1542 *Marine Chemistry*, 25, 29-37. [https://doi.org/10.1016/0304-4203\(88\)90012-6](https://doi.org/10.1016/0304-4203(88)90012-6), 1988.  
1543  
1544 Copin-Montégut, C.: A new formula for the effect of temperature on the partial pressure of  $\text{CO}_2$  in seawater.  
1545 Corrigendum. *Marine Chemistry*, 27, 143-144. [https://doi.org/10.1016/0304-4203\(89\)90034-0](https://doi.org/10.1016/0304-4203(89)90034-0), 1989.  
1546  
1547 Coverly, S. C., Aminot, A., and R. K erouel: Nutrients in Seawater Using Segmented Flow Analysis, In: *Practical*  
1548 *Guidelines for the Analysis of Seawater*, Edited by: Oliver Wurl, CRC Press,  
1549 <https://doi.org/10.1201/9781420073072>, 2009  
1550  
1551 Danialt, N., and M enard, Y.: Eddy kinetic energy distribution in the Southern Ocean from altimetry and FGGE  
1552 drifting buoys, *J. Geophys. Res.*, 90 (C6), 11877–11889, doi:10.1029/JC090iC06p11877, 1985  
1553  
1554 Demuynck, P., Tyrrell, T., Naveira Garabato, A., Moore, M. C., and Martin, A. P.: Spatial variations in silicate-  
1555 to-nitrate ratios in Southern Ocean surface waters are controlled in the short term by physics rather than biology,  
1556 *Biogeosciences*, 17, 2289–2314, <https://doi.org/10.5194/bg-17-2289-2020>, 2020.  
1557  
1558 DeVries, T., Yamamoto, K., Wanninkhof, R., Gruber, N., Hauck, J., M uller, J. D., et al.: Magnitude, trends, and  
1559 variability of the global ocean carbon sink from 1985-2018. *Global Biogeochemical Cycles*, 37,  
1560 e2023GB007780, doi:10.1029/2023GB007780, 2023.  
1561  
1562 Dickson, A. G.: Standard potential of the reaction:  $\text{AgCl(s)} + \frac{1}{2}\text{H}_2\text{(g)} = \text{Ag(s)} + \text{HCl(aq)}$ , and the standard  
1563 acidity constant of the ion  $\text{HSO}_4^-$  in synthetic sea water from 273.15 to 318.15 K. *J. Chem. Thermodyn.* **22**:  
1564 113–127. doi:10.1016/0021-9614(90)90074-Z, 1990  
1565

1566 Dickson, A. G., Sabine, C. L. and Christian, J. R. (Eds.): Guide to Best Practices for Ocean CO<sub>2</sub> Measurements.  
1567 *PICES Special Publication 3*, 191 pp., [https://www.ncei.noaa.gov/access/ocean-carbon-acidification-data-](https://www.ncei.noaa.gov/access/ocean-carbon-acidification-data-system/oceans/Handbook_2007.html)  
1568 [system/oceans/Handbook\\_2007.html](https://www.ncei.noaa.gov/access/ocean-carbon-acidification-data-system/oceans/Handbook_2007.html), 2007  
1569  
1570 Dlugokencky, E. and Tans, P.: Trends in atmospheric carbon dioxide, National Oceanic & Atmospheric  
1571 Administration, Earth System Research Laboratory (NOAA/ESRL), available at: [http://](http://www.esrl.noaa.gov/gmd/ccg/trends/global.html)  
1572 [www.esrl.noaa.gov/gmd/ccg/trends/global.html](http://www.esrl.noaa.gov/gmd/ccg/trends/global.html), (last access: 8 January 2022), 2022  
1573  
1574 Doney, S. C., Fabry, V. J., Feely, R. A., and Kleypas, J. A.: Ocean Acidification: The Other CO<sub>2</sub> Problem,  
1575 *Annu. Rev. Mar. Sci.*, 1, 169–192, <https://doi.org/10.1146/annurev.marine.010908.163834>, 2009.  
1576  
1577 Doney, S. C., Ruckelshaus, M., Duffy, J. E., Barry, J. P., Chan, F., English, C. A., Galindo, H. M., Grebmeier, J.  
1578 M., Hollowed, A. B., Knowlton, N., Polovina, J., Rabalais, N. N., Sydeman, W. J., and Talley, L. D.: Climate  
1579 change impacts on marine ecosystems, *Annu. Rev. Mar. Sci.*, 4, 11–37. [10.1146/annurev-marine-041911-](https://doi.org/10.1146/annurev-marine-041911-111611)  
1580 [111611](https://doi.org/10.1146/annurev-marine-041911-111611), 2012.  
1581  
1582 Dove, L. A., Balwada D., Thompson, A. F., and Gray, A. R.: Enhanced ventilation in energetic regions of the  
1583 Antarctic Circumpolar Current. *Geophys. Res. Lett.* 49(13):e2021GL097574,  
1584 <https://doi.org/10.1029/2021GL097574>. 2022.  
1585  
1586 Duncan, R.J., Nielsen, D.A., Sheehan, C.E., Deppeler, S., Hancock, A.M., Schulz, K.G., Davidson, A.T. and  
1587 Petrou, K.: Ocean acidification alters the nutritional value of Antarctic diatoms. *New Phytol*, 233: 1813-1827.  
1588 <https://doi-org.insu.bib.cnrs.fr/10.1111/nph.17868>, 2022  
1589  
1590 Durack, P. J. and Wijffels, S. E.: Fifty-year trends in global ocean salinities and their relationship to broad-scale  
1591 warming. *J. Climate*, 23, 4342–4362, <https://doi.org/10.1175/2010JCLI3377.1>, 2010  
1592  
1593 Fabry, V. J., Seibel, B. A., Feely, R. A., and Orr, J. C.: Impacts of ocean acidification on marine fauna and  
1594 ecosystem processes. – *ICES Journal of Marine Science*, 65: 414–432, doi: [10.1093/icesjms/fsn048](https://doi.org/10.1093/icesjms/fsn048), 2008  
1595  
1596 Fassbender, A. J., Schlunegger, S., Rodgers, K. B., and Dunne, J. P.: Quantifying the role of seasonality in the  
1597 marine carbon cycle feedback: An ESM2M case study. *Global Biogeochemical Cycles*, 36, e2021GB007018.  
1598 doi:[10.1029/2021GB007018](https://doi.org/10.1029/2021GB007018), 2022  
1599  
1600 Fay, A. R., Munro, D. R., McKinley, G. A., Pierrot, D., Sutherland, S. C., Sweeney, C., and Wanninkhof, R.:  
1601 Updated climatological mean delta fCO<sub>2</sub> and net sea–air CO<sub>2</sub> flux over the global open ocean regions, *Earth*  
1602 *Syst. Sci. Data Discuss.* [preprint], <https://doi.org/10.5194/essd-2023-429>, in review, 2023.  
1603  
1604 Fox-Kemper, B., Hewitt, H. T. , Xiao, C., Adalgeirsdottir, G., Drijfhout, S. S., Edwards, T. L., Golledge, N. R.,  
1605 Hemer, M., Kopp, R. E., Krinner, G., Mix, A., Notz, D., Nowicki, S., Nurhati, I. S., Ruiz, L., Sallée, J.-B.,  
1606 Slangen, A. B. A., and Yu, Y.: *Climate Change 2021: The Physical Science Basis. Contribution of Working*  
1607 *Group I to the Sixth Assessment Report of the Intergovernmental Panel on Climate Change*, chapter Ocean,  
1608 Cryosphere and Sea Level Change, pages 1211-1362. Cambridge University Press, United Kingdom and New  
1609 York, NY, USA, August 2021. doi:[10.1017/9781009157896](https://doi.org/10.1017/9781009157896).  
1610  
1611 Fontela, M., Vélo, A., Gilcoto, M., and Pérez, F.: Anthropogenic CO<sub>2</sub> and Ocean Acidification in Argentine  
1612 Basin Water Masses over Almost Five Decades of Observations. *Science of The Total Environment*, 779.  
1613 <https://doi.org/10.1016/j.scitotenv.2021.146570>, 2021  
1614  
1615 Franco, A. C., Ianson, D., Ross, T., Hamme, R. C., Monahan, A. H., Christian, J. R., et al.: Anthropogenic and  
1616 climatic contributions to observed carbon system trends in the northeast Pacific. *Global Biogeochemical Cycles*,  
1617 35, e2020GB006829. Doi: [10.1029/2020GB006829](https://doi.org/10.1029/2020GB006829), 2021  
1618

1619 Friedlingstein, P., O'Sullivan, M., Jones, M. W., Andrew, R. M., Gregor, L., Hauck, J., Le Quéré, C., Luijkx, I.  
1620 T., Olsen, A., Peters, G. P., Peters, W., Pongratz, J., Schwingshackl, C., Sitch, S., Canadell, J. G., Ciais, P.,  
1621 Jackson, R. B., Alin, S. R., Alkama, R., Arneeth, A., Arora, V. K., Bates, N. R., Becker, M., Bellouin, N., Bittig,  
1622 H. C., Bopp, L., Chevallier, F., Chini, L. P., Cronin, M., Evans, W., Falk, S., Feely, R. A., Gasser, T., Gehlen,  
1623 M., Gkritzalis, T., Gloege, L., Grassi, G., Gruber, N., Gürses, Ö., Harris, I., Hefner, M., Houghton, R. A., Hurtt,  
1624 G. C., Iida, Y., Ilyina, T., Jain, A. K., Jersild, A., Kadono, K., Kato, E., Kennedy, D., Klein Goldewijk, K.,  
1625 Knauer, J., Korsbakken, J. I., Landschützer, P., Lefèvre, N., Lindsay, K., Liu, J., Liu, Z., Marland, G., Mayot, N.,  
1626 McGrath, M. J., Metzl, N., Monacchi, N. M., Munro, D. R., Nakaoka, S.-I., Niwa, Y., O'Brien, K., Ono, T.,  
1627 Palmer, P. I., Pan, N., Pierrot, D., Pocock, K., Poulter, B., Resplandy, L., Robertson, E., Rödenbeck, C.,  
1628 Rodriguez, C., Rosan, T. M., Schwinger, J., Séférian, R., Shutler, J. D., Skjelvan, I., Steinhoff, T., Sun, Q.,  
1629 Sutton, A. J., Sweeney, C., Takao, S., Tanhua, T., Tans, P. P., Tian, X., Tian, H., Tilbrook, B., Tsujino, H.,  
1630 Tubiello, F., van der Werf, G. R., Walker, A. P., Wanninkhof, R., Whitehead, C., Willstrand Wranne, A.,  
1631 Wright, R., Yuan, W., Yue, C., Yue, X., Zaehle, S., Zeng, J., and Zheng, B.: Global Carbon Budget 2022, *Earth*  
1632 *Syst. Sci. Data*, 14, 4811–4900, <https://doi.org/10.5194/essd-14-4811-2022>, 2022.

1633  
1634 Friedlingstein, P., O'Sullivan, M., Jones, M. W., Andrew, R. M., Bakker, D. C. E., Hauck, J., Landschützer, P.,  
1635 Le Quéré, C., Luijkx, I. T., Peters, G. P., Peters, W., Pongratz, J., Schwingshackl, C., Sitch, S., Canadell, J. G.,  
1636 Ciais, P., Jackson, R. B., Alin, S. R., Anthoni, P., Barbero, L., Bates, N. R., Becker, M., Bellouin, N., Decharme,  
1637 B., Bopp, L., Brasika, I. B. M., Cadule, P., Chamberlain, M. A., Chandra, N., Chau, T.-T.-T., Chevallier, F.,  
1638 Chini, L. P., Cronin, M., Dou, X., Enyo, K., Evans, W., Falk, S., Feely, R. A., Feng, L., Ford, D. J., Gasser, T.,  
1639 Ghattas, J., Gkritzalis, T., Grassi, G., Gregor, L., Gruber, N., Gürses, Ö., Harris, I., Hefner, M., Heinke, J.,  
1640 Houghton, R. A., Hurtt, G. C., Iida, Y., Ilyina, T., Jacobson, A. R., Jain, A., Jarníková, T., Jersild, A., Jiang, F.,  
1641 Jin, Z., Joos, F., Kato, E., Keeling, R. F., Kennedy, D., Klein Goldewijk, K., Knauer, J., Korsbakken, J. I.,  
1642 Körtzinger, A., Lan, X., Lefèvre, N., Li, H., Liu, J., Liu, Z., Ma, L., Marland, G., Mayot, N., McGuire, P. C.,  
1643 McKinley, G. A., Meyer, G., Morgan, E. J., Munro, D. R., Nakaoka, S.-I., Niwa, Y., O'Brien, K. M., Olsen, A.,  
1644 Omar, A. M., Ono, T., Paulsen, M., Pierrot, D., Pocock, K., Poulter, B., Powis, C. M., Rehder, G., Resplandy, L.,  
1645 Robertson, E., Rödenbeck, C., Rosan, T. M., Schwinger, J., Séférian, R., Smallman, T. L., Smith, S. M.,  
1646 Sospedra-Alfonso, R., Sun, Q., Sutton, A. J., Sweeney, C., Takao, S., Tans, P. P., Tian, H., Tilbrook, B., Tsujino,  
1647 H., Tubiello, F., van der Werf, G. R., van Ooijen, E., Wanninkhof, R., Watanabe, M., Wimart-Rousseau, C.,  
1648 Yang, D., Yang, X., Yuan, W., Yue, X., Zaehle, S., Zeng, J., and Zheng, B.: Global Carbon Budget 2023, *Earth*  
1649 *Syst. Sci. Data*, 15, 5301–5369, <https://doi.org/10.5194/essd-15-5301-2023>, 2023.

1650  
1651 Frölicher, T. L., Sarmiento, J. L., Paynter, D. J., Dunne, J. P., Krasting, J. P., and Winton, M.: Dominance of the  
1652 southern ocean in anthropogenic carbon and heat uptake in CMIP5 models. *Journal of Climate*, 28(2), 862–886.  
1653 <https://doi.org/10.1175/JCLI-D-14-00117.1>, 2015

1654  
1655 Fu, W., Randerson, J. T., and Moore, J. K.: Climate change impacts on net primary production (NPP) and export  
1656 production (EP) regulated by increasing stratification and phytoplankton community structure in the CMIP5  
1657 models, *Biogeosciences*, 13, 5151–5170, <https://doi.org/10.5194/bg-13-5151-2016>, 2016.

1658  
1659 Gallego, M. A., Timmermann, A., Friedrich, T., and Zeebe, R. E.: Drivers of future seasonal cycle changes in  
1660 oceanic  $p\text{CO}_2$ , *Biogeosciences*, 15, 5315–5327, <https://doi.org/10.5194/bg-15-5315-2018>, 2018.

1661  
1662 Gangstø, R., Gehlen, M., Schneider, B., Bopp, L., Aumont, O., and Joos, F.: Modeling the marine aragonite  
1663 cycle: changes under rising carbon dioxide and its role in shallow water  $\text{CaCO}_3$  dissolution, *Biogeosciences*, 5,  
1664 1057–1072, <https://doi.org/10.5194/bg-5-1057-2008>, 2008.

1665  
1666 Gardner J., Peck, V. L., Bakker, D. C. E., Tarling, G. A. and Manno, C.: Contrasting life cycles of Southern  
1667 Ocean pteropods alter their vulnerability to climate change. *Front. Mar. Sci.* 10:1118570.  
1668 doi: 10.3389/fmars.2023.1118570, 2023

1669

1670 Gloege, L., McKinley, G. A., Landschützer, P., Fay, A. R., Frölicher, T. L., Fyfe, J. C., et al: Quantifying errors  
1671 in observationally based estimates of ocean carbon sink variability. *Global Biogeochemical Cycles*, 35,  
1672 e2020GB006788. <https://doi.org/10.1029/2020GB006788>, 2021.

1673

1674 Gooya, P., Swart, N. C., and Hamme, R. C.: Time-varying changes and uncertainties in the CMIP6 ocean carbon  
1675 sink from global to local scale, *Earth Syst. Dynam.*, 14, 383–398, <https://doi.org/10.5194/esd-14-383-2023>,  
1676 2023.

1677

1678 Gray, A., Johnson, K. S., Bushinsky, S. M., Riser, S. C., Russell, J. L., Talley, L. D., et al.: Autonomous  
1679 biogeochemical floats detect significant carbon dioxide outgassing in the high-latitude Southern Ocean.  
1680 *Geophysical Research Letters*, 45, 9049–9057. <https://doi.org/10.1029/2018GL078013>, 2018.

1681

1682 Gray, A., R.: The Four-Dimensional Carbon Cycle of the Southern Ocean. *Annu. Rev. Mar. Sci.* 16:23.1–23.28.  
1683 <https://doi.org/10.1146/annurev-marine-041923-104057>, 2024.

1684

1685 Gregor, L., Kok, S., and Monteiro, P. M. S.: Interannual drivers of the seasonal cycle of CO<sub>2</sub> in the Southern  
1686 Ocean, *Biogeosciences*, 15, 2361-2378, <https://doi.org/10.5194/bg-15-2361-2018>, 2018.

1687

1688 Gruber, N., Clement, D. , Carter, B. R., Feely, R. A., van Heuven, S., Hoppema, M., Ishii, M., Key, R. M.,  
1689 Kozyr, A., Lauvset, S. K., Lo Monaco, C. , Mathis, J. T., Murata, A., Olsen, A., Perez, F. F., Sabine, C. L.,  
1690 Tanhua, T., and Wanninkhof, R.: The oceanic sink for anthropogenic CO<sub>2</sub> from 1994 to 2007, *Science* vol. 363  
1691 (issue 6432), pp. 1193-1199. DOI: 10.1126/science.aau5153, 2019a.

1692

1693 Gruber, N., Clement, D., Carter, B. R., Feely, R. A., Heuven, S., van, Hoppema, M., Ishii, M., Key, R. M.,  
1694 Kozyr, A., Lauvset, S. K., Lo Monaco, C., Mathis, J. T., Murata, A., Olsen, A., Perez, F. F., Sabine, C. L.,  
1695 Tanhua, T., and Wanninkhof, R.: The oceanic sink for anthropogenic CO<sub>2</sub> from 1994 to 2007 – the data (NCEI  
1696 Accession 0186034), NOAA National Centers for Environmental Information [data set],  
1697 <https://doi.org/10.25921/wdn2-pt10>, 2019b.

1698

1699 Gruber, N., Landschützer, P., and Lovenduski, N. S.: The Variable Southern Ocean Carbon Sink, *Annu.*  
1700 *Rev. Mar. Sci.*, Vol. 11, doi:10.1146/annurev-marine-121916-063407, 2019c.

1701

1702 Gu, Y., Katul, G. G., & Cassar, N. Multiscale temporal variability of the global air-sea CO<sub>2</sub> flux anomaly.  
1703 *Journal of Geophysical Research: Biogeosciences*, 128, e2022JG006934. <https://doi.org/10.1029/2022JG006934>,  
1704 2023

1705

1706 Hauri, C., Friedrich, T., and Timmermann, A.: Abrupt onset and prolongation of aragonite undersaturation  
1707 events in the Southern Ocean, *Nature Climate Change*, doi:10.1038/nclimate2844, 2015.

1708

1709 Hauck J., Hoppema, M., Bellerby, R. G. J., Völker, C., and Wolf-Gladrow, D.: Data-based estimation of  
1710 anthropogenic carbon and acidification in the Weddell Sea on a decadal timescale. *J. Geophys. Res.* 115,  
1711 C03004. doi:10.1029/2009jc005479, 2010

1712

1713 Hauck, J., Völker, C., Wang, T., Hoppema, M., Losch, M., and Wolf-Gladrow, D. A.: Seasonally different  
1714 carbon flux changes in the Southern Ocean in response to the southern annular mode. *Global Biogeochemical*  
1715 *Cycles*, 27(4), 1236–1245. <https://doi.org/10.1002/2013GB004600>, 2013

1716

1717 Hauck, J. and Völker, C.: Rising atmospheric CO<sub>2</sub> leads to large impact of biology on Southern Ocean CO<sub>2</sub>  
1718 uptake via changes of the Revelle factor, *Geophys. Res. Lett.*, 42, 1459–1464, doi:10.1002/2015GL063070,  
1719 2015

1720

1721 Hauck, J., Volker, C., Wolf-Gladrow, D. A., Laufkotter, C., Vogt, M., Aumont, O., et al.: On the Southern  
1722 Ocean CO<sub>2</sub> uptake and the role of the biological carbon pump in the 21st century. *Global Biogeochemical*  
1723 *Cycles*, 29(9), 1451–1470. <https://doi.org/10.1002/2015GB005140>, 2015  
1724

1725 Hauck, J., Zeising, M., Le Quéré, C., Gruber, N., Bakker, D. C. E., Bopp, L., Chau, T. T., Gürses, Ö., Ilyina, T.,  
1726 Landschützer, P., Lenton, A., Resplandy, L., Rödenbeck, C., Schwinger, J., and Séférian, R.: Consistency and  
1727 challenges in the ocean carbon sink estimate for the Global Carbon Budget. *Front. Mar. Sci.* doi:  
1728 10.3389/fmars.2020.571720, 2020  
1729

1730 Hauck, J., Nissen, C., Landschützer, P., Rödenbeck, C., Bushinsky, S., and Olsen, A.: Sparse observations  
1731 induce large biases in estimates of the global ocean CO<sub>2</sub> sink: an ocean model subsampling experiment. *Phil.*  
1732 *Trans. R. Soc. A* 381: 20220063. <https://doi.org/10.1098/rsta.2022.0063>, 2023a  
1733

1734 Hauck, J., Gregor, L., Nissen, C., Patara, L., Hague, M., Mongwe, P., et al.: The Southern Ocean carbon cycle  
1735 1985–2018: Mean, seasonal cycle, trends, and storage. *Global Biogeochemical Cycles*, 37, e2023GB007848.  
1736 <https://doi.org/10.1029/2023GB007848>, 2023b  
1737

1738 Hersbach, H., Bell, B., Berrisford, P., Hirahara, S., Horányi, A., Muñoz-Sabater, J., Nicolas, J., Peubey, C.,  
1739 Radu, R., Schepers, D., Simmons, A., Soci, C., Abdalla, S., Abellan, X., Balsamo, G., Bechtold, P., Biavati, G.,  
1740 Bidlot, J., Bonavita, M., De Chiara, G., Dahlgren, P., Dee, D., Diamantakis, M., Dragani, R., Flemming, J.,  
1741 Forbes, R., Fuentes, M., Geer, A., Haimberger, L., Healy, S., Hogan, R. J., Hólm, E., Janisková, M., Keeley, S.,  
1742 Laloyaux, P., Lopez, P., Lupu, C., Radnoti, G., de Rosnay, P., Rozum, I., Vamborg, F., Villaume, S., and  
1743 Thépaut, J.-N.: The ERA5 global reanalysis, *Q. J. Roy. Meteor. Soc.*, 146, 1999–2049,  
1744 <https://doi.org/10.1002/qj.3803>, 2020.  
1745

1746 Hoppema, M., Bakker, K., van Heuven, S. M. A. C., van Ooijen, J. C., and de Baar, H. J. W.: Distributions,  
1747 trends and inter-annual variability of nutrients along a repeat section through the Weddell Sea (1996–2011).  
1748 *Marine Chemistry*, 177, 545–553. <https://doi.org/10.1016/j.marchem.2015.08.007>, 2015  
1749

1750 Hunt, B. P. V., Pakhomov, E. A., Hosie, G. W., Siegel, V., Ward, P., and Bernard, K.: Pteropods in Southern  
1751 Ocean ecosystems, *Progress in Oceanography*, Volume 78, Issue 3, Pages 193-221,  
1752 <https://doi.org/10.1016/j.pocean.2008.06.001>, 2008  
1753

1754 Iida, T., Odate, T., and Fukuchi, M.: Long-term trends of nutrients and apparent oxygen utilization south of the  
1755 polar front in Southern Ocean intermediate water from 1965 to 2008. *PLoS One*, 8, e71766.  
1756 <https://doi.org/10.1371/journal.pone.0071766>, 2013  
1757

1758 Iida, Y., Takatani, Y., Kojima, A., and Ishii, M.: Global trends of ocean CO<sub>2</sub> sink and ocean acidification: an  
1759 observation based reconstruction of surface ocean inorganic carbon variables, *J. Oceanogr.*, 77, 323–358,  
1760 <https://doi.org/10.1007/s10872-020-00571-5>, 2021.  
1761

1762 IPCC: Changing Ocean, Marine Ecosystems, and Dependent Communities. in *The Ocean and Cryosphere in a*  
1763 *Changing Climate* 447–588 (Cambridge University Press, 2022). doi:10.1017/9781009157964.007, 2022  
1764

1765 Ito, T., Minobe, S., Long, M. C., Deutsch, C. Upper ocean O<sub>2</sub> trends: 1958–2015. *Geophysical Research Letters*  
1766 44, 4214–4223, <https://doi.org/10.1002/2017GL073613>, 2017.  
1767

1768 Jabaud-Jan, A., Metzl, N., Brunet, C., Poisson, A., and Schauer, B.: Variability of the Carbon Dioxide System in  
1769 the Southern Indian Ocean (20°S-60°S): the impact of a warm anomaly in austral summer 1998. *Global*  
1770 *Biogeochemical Cycles*, Vol. 18, No. 1, GB1042, [10.1029/2002GB002017](https://doi.org/10.1029/2002GB002017), 2004  
1771

1772 Jeandel, C., Ruiz-Pino, D., Gjata, E., Poisson, A., Brunet, C., Charriaud, E., Dehairs, F., Delille, D., Fiala, M.,  
1773 Fravallo, C., Miquel, J. C., Park, Y. H., Pondaven, P., Quéguiner, B., Razouls, S., Schauer, B., and Tréguer, P.:

1774 KERFIX, a time-series station in the Southern Ocean: a presentation. *Journal of Marine Systems*, 17, 1-4, 555-  
1775 569., [https://doi.org/10.1016/S0924-7963\(98\)00064-5](https://doi.org/10.1016/S0924-7963(98)00064-5), 1998  
1776  
1777 Jiang, L.-Q., Feely, R. A., Carter, B. R., Greeley, D. J., Gledhill, D. K., and Arzayus K. M.: Climatological  
1778 distribution of aragonite saturation state in the global oceans, *Global Biogeochem. Cycles*, 29, 1656–1673,  
1779 doi:10.1002/2015GB005198, 2015.  
1780  
1781 Jiang, L.-Q., Carter, B. R., Feely, R. A., Lauvset, S. K., and Olsen, A.: Surface ocean pH and buffer capacity:  
1782 past, present and future. *Sci Rep* 9, 18624, doi:10.1038/s41598-019-55039-4, 2019  
1783  
1784 Jiang, L.-Q., Dunne, J., Carter, B. R., Tjiputra, J. F., Terhaar, J., Sharp, J. D., et al.: Global surface ocean  
1785 acidification indicators from 1750 to 2100. *Journal of Advances in Modeling Earth Systems*, 15,  
1786 e2022MS003563. <https://doi.org/10.1029/2022MS003563>, 2023  
1787  
1788 Joos, F., Hameau, A., Frölicher, T. L., and Stephenson, D. B.: Anthropogenic attribution of the increasing  
1789 seasonal amplitude in surface ocean pCO<sub>2</sub>. *Geophysical Research Letters*, 50, e2023GL102857.  
1790 <https://doi.org/10.1029/2023GL102857>, 2023  
1791  
1792 Jouandet, M.-P., Blain, S., Metzl, N., Brunet, C., Trull, T., and Obernosterer, I.: A seasonal carbon budget for a  
1793 naturally iron fertilized bloom (Kerguelen I. Southern Ocean). *Deep-Sea Res II*, 55, 856-867.  
1794 doi:10.1016/j.dsr2.2007.12.037, 2008  
1795  
1796 Jouandet M.P., Blain, S., Metzl, N., and Mongin, C.: Interannual variability of the net community production and  
1797 air-sea CO<sub>2</sub> flux in a natural iron fertilization region of the Southern Ocean. (Kerguelen plateau), *Antarctic*  
1798 *Science*, doi:10.1017/S0954102011000411, 2011  
1799  
1800 Kane, A., Moulin, C., Thiria, S., Bopp, L., Berrada, M., Tagliabue, A., Crépon, M., Aumont, O., and Badran, F.:  
1801 Improving the parameters of a global ocean biogeochemical model via variational assimilation of in situ data at  
1802 five time series stations, *J. Geophys. Res.*, 116, C06011, doi:10.1029/2009JC006005, 2011  
1803  
1804 Kawaguchi, S., Ishida, A., King, R. et al.: Risk maps for Antarctic krill under projected Southern Ocean  
1805 acidification. *Nature Clim. Change*, 3, 843–847, DOI: 10.1038/NCLIMATE1937, 2013  
1806  
1807 Keeling, C. D., and Waterman, L. S.: Carbon dioxide in surface ocean waters: 3. Measurements on Lusiad  
1808 Expedition 1962–1963, *J. Geophys. Res.*, 73( 14), 4529– 4541, doi:10.1029/JB073i014p04529, 1968  
1809  
1810 Keppler, L. and Landschützer, P.: Regional Wind Variability Modulates the Southern Ocean Carbon Sink, *Sci.*  
1811 *Rep.-UK*, 9, 7384, <https://doi.org/10.1038/s41598-019-43826-y>, 2019.  
1812  
1813 Kessler, A. and Tjiputra, J.: The Southern Ocean as a constraint to reduce uncertainty in future ocean carbon  
1814 sinks, *Earth Syst. Dynam.*, 7, 295-312, doi:10.5194/esd-7-295-2016, 2016.  
1815  
1816 Key, R. M., Kozyr, A., Sabine, C. L., Lee, K., Wanninkhof, R., Bullister, J. L., Feely, R. A., Millero, F. J.,  
1817 Mordy, C., and Peng, T. H.: A global ocean carbon climatology: Results from Global Data Analysis Project  
1818 (GLODAP), *Global Biogeochemical Cycles*, 18, GB4031, <https://doi.org/10.1029/2004GB002247>, 2004.  
1819  
1820 Khatiwala, S., Tanhua, T., Mikaloff Fletcher, S., Gerber, M., Doney, S. C., Graven, H. D., Gruber, N.,  
1821 McKinley, G. A., Murata, A., Ríos, A. F., and Sabine, C. L.: Global ocean storage of anthropogenic carbon,  
1822 *Biogeosciences*, 10, 2169–2191, <https://doi.org/10.5194/bg-10-2169-2013>, 2013.  
1823  
1824 Krumhardt, K. M., Long, M. C., Sylvester, Z. T. and Petrik, C. M.: Climate drivers of Southern Ocean  
1825 phytoplankton community composition and potential impacts on higher trophic levels. *Front. Mar. Sci.*  
1826 9:916140. doi: 10.3389/fmars.2022.916140, 2022



1827  
1828 Kwiatkowski, L., and Orr, J. C.: Diverging seasonal extremes for ocean acidification during the twenty-first  
1829 century. *Nature Climate Change*, 8(2), 141–145. <https://doi.org/10.1038/s41558-017-0054-0>, 2018  
1830  
1831 Kwiatkowski, L., Torres, O., Bopp, L., Aumont, O., Chamberlain, M., Christian, J. R., Dunne, J. P., Gehlen, M.,  
1832 Ilyina, T., John, J. G., Lenton, A., Li, H., Lovenduski, N. S., Orr, J. C., Palmieri, J., Santana-Falcón, Y.,  
1833 Schwinger, J., Séférian, R., Stock, C. A., Tagliabue, A., Takano, Y., Tjiputra, J., Toyama, K., Tsujino, H.,  
1834 Watanabe, M., Yamamoto, A., Yool, A., and Ziehn, T.: Twenty-first century ocean warming, acidification,  
1835 deoxygenation, and upper-ocean nutrient and primary production decline from CMIP6 model projections,  
1836 *Biogeosciences*, 17, 3439–3470, <https://doi.org/10.5194/bg-17-3439-2020>, 2020.  
1837  
1838 Lange, N., Fiedler, B., Álvarez, M., Benoit-Cattin, A., Benway, H., Buttigieg, P. L., Coppola, L., Currie, K.,  
1839 Flecha, S., Honda, M., Huertas, I. E., Lauvset, S. K., Muller-Karger, F., Körtzinger, A., O'Brien, K. M.,  
1840 Ólafsdóttir, S. R., Pacheco, F. C., Rueda-Roa, D., Skjelvan, I., Wakita, M., White, A., and Tanhua, T.: Synthesis  
1841 Product for Ocean Time-Series (SPOTS) – A ship-based biogeochemical pilot, *Earth Syst. Sci. Data Discuss.*  
1842 [preprint], <https://doi.org/10.5194/essd-2023-238>, in review, 2023.  
1843  
1844 Landschützer, P., Gruber, N., Haumann, F. A., Rödenbeck, C., Bakker, D. C. E., Van Heuven, S., Hoppema, M.,  
1845 Metzl, N., Sweeney, C., Takahashi, T., Tilbrook, B., and Wanninkhof, R.: The reinvigoration of the Southern  
1846 Ocean carbon sink, *Science*, 349, 1221–1224, <https://doi.org/10.1126/science.aab2620>, 2015.  
1847  
1848 Landschützer, P., Gruber, N., Bakker, D. C. E., Stemmler, I., and Six, K. D.: Strengthening seasonal marine CO<sub>2</sub>  
1849 variations due to increasing atmospheric CO<sub>2</sub>. *Nature Climate Change*, 8(2), 146–150.  
1850 <https://doi.org/10.1038/s41558-017-0057-x>, 2018  
1851  
1852 Lauvset, S. K., Gruber, N., Landschützer, P., Olsen, A., and Tjiputra, J.: Trends and drivers in global surface  
1853 ocean pH over the past 3 decades. *Biogeosciences*, 12, 1285–1298, doi:10.5194/bg-12-1285-2015, 2015  
1854  
1855 Lauvset, S. K., Carter, B. R., Perez, F. F., Jiang, L.-Q., Feely, R. A., Velo, A., and Olsen, A.: Processes Driving  
1856 Global Interior Ocean pH Distribution, *Global Biogeochem. Cycles*, 34, e2019GB006 229,  
1857 <https://doi.org/10.1029/2019GB006229>, 2020.  
1858  
1859 Lauvset, S. K., Lange, N., Tanhua, T., Bittig, H. C., Olsen, A., Kozyr, A., Álvarez, M., Becker, S., Brown, P. J.,  
1860 Carter, B. R., Cotrim da Cunha, L., Feely, R. A., van Heuven, S., Hoppema, M., Ishii, M., Jeansson, E.,  
1861 Jutterström, S., Jones, S. D., Karlsen, M. K., Lo Monaco, C., Michaelis, P., Murata, A., Pérez, F. F., Pfeil, B.,  
1862 Schirnack, C., Steinfeldt, R., Suzuki, T., Tilbrook, B., Velo, A., Wanninkhof, R., Woosley, R. J., and Key, R. M.:  
1863 An updated version of the global interior ocean biogeochemical data product, GLODAPv2.2021, *Earth Syst. Sci.*  
1864 *Data*, 13, 5565–5589, <https://doi.org/10.5194/essd-13-5565-2021>, 2021a.  
1865  
1866 Lauvset, Siv K.; Lange, Nico; Tanhua, Toste; Bittig, Henry C.; Olsen, Are; Kozyr, Alex; Álvarez, Marta;  
1867 Becker, Susan; Brown, Peter J.; Carter, Brendan R.; Cotrim da Cunha, Leticia; Feely, Richard A.; van Heuven,  
1868 Steven M. A. C.; Hoppema, Mario; Ishii, Masao; Jeansson, Emil; Jutterström, Sara; Jones, Steve D.; Karlsen,  
1869 Maren K.; Lo Monaco, Claire; Michaelis, Patrick; Murata, Akihiko; Pérez, Fiz F.; Pfeil, Benjamin; Schirnack,  
1870 Carsten; Steinfeldt, Reiner; Suzuki, Toru; Tilbrook, Bronte; Velo, Antón; Wanninkhof, Rik; Woosley, Ryan J.;  
1871 Key, Robert M.: Global Ocean Data Analysis Project version 2.2021 (GLODAPv2.2021) (NCEI Accession  
1872 0237935). [subset used GLODAPv2.2021\_Indian\_Ocean.cvs]. NOAA National Centers for Environmental  
1873 Information. Dataset. <https://doi.org/10.25921/ttqg-n825>., Accessed 2/8/2021. 2021b.  
1874  
1875 Lee, K., Tong, L. T., Millero, F. J., Sabine, C. L., Dickson, A. G., Goyet, C., Park, G. H., Wanninkhof, R., Feely,  
1876 R. A., and Key, R. M.: Global relationships of total alkalinity with salinity and temperature in surface waters of  
1877 the world's oceans. *Geophys. Res. Lett.* 33, L19605. doi10.1029/2006GL027207, 2006.  
1878

1879 Lenton, A., Codron, F., Bopp, L., Metzl, N., Cadule, P., Tagliabue, A., and Le Sommer, J.: Stratospheric ozone  
1880 depletion reduces ocean carbon uptake and enhances ocean acidification. *Geophys. Res. Lett.*, 36, L12606, 2009.  
1881 doi:10.1029/2009GL038227, 2009  
1882  
1883 Lenton, A., Tilbrook, B., Law, R. M., Bakker, D., Doney, S. C., Gruber, N., Ishii, M., Hoppema, M.,  
1884 Lovenduski, N. S., Matear, R. J., McNeil, B. I., Metzl, N., Mikaloff Fletcher, S. E., Monteiro, P. M. S.,  
1885 Rödenbeck, C., Sweeney, C., and Takahashi, T.: Sea–air CO<sub>2</sub> fluxes in the Southern Ocean for the period 1990–  
1886 2009, *Biogeosciences*, 10, 4037–4054, <https://doi.org/10.5194/bg-10-4037-2013>, 2013.  
1887  
1888 Le Quéré, C., Rödenbeck, C., Buitenhuis, E. T., Conway, T. J., Langenfelds, R., Gomez, A., Labuschagne, C.,  
1889 Ramonet, M., Nakazawa, T., Metzl, N., Gillett, N., and Heimann, M.: Saturation of the Southern Ocean CO<sub>2</sub>  
1890 Sink Due to Recent Climate Change, *Science*, 316, 1735–1738, <https://doi.org/10.1126/science.1136188>, 2007.  
1891  
1892 Lerner, P., Romanou, A., Kelley, M., Romanski, J., Ruedy, R., and Russell, G.: Drivers of air-sea CO<sub>2</sub> flux  
1893 seasonality and its long-term changes in the NASA-GISS model CMIP6 submission. *Journal of Advances in*  
1894 *Modeling Earth Systems*, 13, e2019MS002028. <https://doi.org/10.1029/2019MS002028>, 2021.  
1895  
1896 Leseurre, C., Lo Monaco, C., Reverdin, G., Metzl, N., Fin, J., Mignon, C., and Benito, L.: Summer trends and  
1897 drivers of sea surface fCO<sub>2</sub> and pH changes observed in the southern Indian Ocean over the last two decades  
1898 (1998–2019), *Biogeosciences*, 19, 2599–2625, <https://doi.org/10.5194/bg-19-2599-2022>, 2022.  
1899  
1900 Leung, S., Cabré, A., and Marinov, I.: A latitudinally banded phytoplankton response to 21st century climate  
1901 change in the Southern Ocean across the CMIP5 model suite, *Biogeosciences*, 12, 5715–5734,  
1902 <https://doi.org/10.5194/bg-12-5715-2015>, 2015.  
1903  
1904 Lewis E., and Wallace, D. W. R.: Program developed for CO<sub>2</sub> system calculations. ORNL/CDIAC-105. Carbon  
1905 Dioxide Information Analysis Center, Oak Ridge National Laboratory, US. Dept. of Energy, Oak Ridge, TN,  
1906 1998.  
1907  
1908 Lo Monaco, C., Goyet, C., Metzl, N., Poisson, A., and Touratier, F.: Distribution and inventory of anthropogenic  
1909 CO<sub>2</sub> in the Southern Ocean: Comparison of three databased methods, *J. Geophys. Res.-Oceans*, 110, C09S02,  
1910 <https://doi.org/10.1029/2004JC002571>, 2005.  
1911  
1912 Lo Monaco, C., Álvarez, M., Key, R. M., Lin, X., Tanhua, T., Tilbrook, B., Bakker, D. C. E., van Heuven, S.,  
1913 Hoppema, M., Metzl, N., Ríos, A. F., Sabine, C. L., and Velo, A.: Assessing the internal consistency of the  
1914 CARINA database in the Indian sector of the Southern Ocean, *Earth Syst. Sci. Data*, 2, 51–70,  
1915 <https://doi.org/10.5194/essd-2-51-2010>, 2010.  
1916  
1917 Lo Monaco, C., Metzl, N., D’Ovidio, F., Llort, J., and Ridame, C.: Rapid establishment of the CO<sub>2</sub> sink  
1918 associated with Kerguelen’s bloom observed during the KEOPS2/OISO20 cruise, *Biogeosciences Discuss.*, 11,  
1919 17543–17578, <https://doi.org/10.5194/bgd-11-17543-2014>, 2014.  
1920  
1921 Long, M. C., Lindsay, K., Peacock, S., Moore, J. K., and Doney, S. C.: Twentieth-Century Oceanic Carbon  
1922 Uptake and Storage in CESM1(BGC), *J. Climate*, 26 (18), 6775–6800, doi:10.1175/JCLI-D-12-00184.1, 2013.  
1923  
1924 Long, M. C., Stephens, B. B., McKain, K., Sweeney, C., Keeling, R. F., Kort, E. A., Morgan, E. J., Bent, J. D.,  
1925 Chandra, N., Chevallier, F., Commane, R., Daube, B. C., Krummel, P. B., Loh, Z., Lujikx, I. T., Munro, D.,  
1926 Patra, P., Peters, W., Ramonet, M., Rödenbeck, C., Stavert, A., Tans, P., and Wofsy, S. C.: Strong Southern  
1927 Ocean carbon uptake evident in airborne observations, *Science*, 374, 1275–1280,  
1928 <https://doi.org/10.1126/science.abi4355>, 2021.  
1929

1930 Louanchi, F., Ruiz-Pino, D., and Poisson, A.: Temporal variations of mixed layer oceanic CO<sub>2</sub> at JGOFS-  
1931 KERFIX time-series station: Physical versus biogeochemical processes. *Journal of Marine Research* 57(1): 165-  
1932 187. <https://doi.org/10.1357/002224099765038607>, 1999.

1933

1934 Louanchi, F., Ruiz-Pino, D. P., Jeandel, C., Brunet, C., Schauer, B., Masson, A., Fiala, M., and Poisson, A.:  
1935 Dissolved inorganic carbon, alkalinity, nutrient and oxygen seasonal and interannual variations at the Antarctic  
1936 Ocean JGOFS-KERFIX site. *Deep Sea Research Part I: Oceanographic Research Papers* 48(7): 1581-1603,  
1937 [https://doi.org/10.1016/S0967-0637\(00\)00086-8](https://doi.org/10.1016/S0967-0637(00)00086-8), 2001.

1938

1939 Lovenduski, N. S., and Gruber, N.: Impact of the Southern Annular Mode on Southern Ocean circulation and  
1940 biology, *Geophys. Res. Lett.*, 32, L11603, doi:10.1029/2005GL022727, 2005.

1941

1942 Lueker, T. J., Dickson, A. G., and Keeling, C. D.: Ocean pCO<sub>2</sub> calculated from dissolved inorganic carbon,  
1943 alkalinity, and equations for K-1 and K-2: validation based on laboratory measurements of CO<sub>2</sub> in gas and  
1944 seawater at equilibrium. *Marine Chemistry* 70, 105-119. [https://doi.org/10.1016/S0304-4203\(00\)00022-0](https://doi.org/10.1016/S0304-4203(00)00022-0), 2000.

1945

1946 Ma, D., Gregor, L., and Gruber, N.: Four decades of trends and drivers of global surface ocean acidification.  
1947 *Global Biogeochemical Cycles*, 37, e2023GB007765. 10.1029/2023GB007765, 2023.

1948

1949 Mackay, N., Watson, A. J., Suntharalingam, P. et al.: Improved winter data coverage of the Southern Ocean CO<sub>2</sub>  
1950 sink from extrapolation of summertime observations. *Commun Earth Environ* 3, 265,  
1951 <https://doi.org/10.1038/s43247-022-00592-6>, 2022.

1952

1953 Mahieu, L., Lo Monaco, C., Metzl, N., Fin, J., and Mignon, C.: Variability and stability of anthropogenic CO<sub>2</sub> in  
1954 Antarctic Bottom Water observed in the Indian sector of the Southern Ocean, 1978–2018, *Ocean Sci.*, 16, 1559–  
1955 1576, <https://doi.org/10.5194/os-16-1559-2020>, 2020.

1956

1957 Marshall, G. J.: Trends in the Southern Annular Mode from observations and reanalyses. *J. Clim.*, 16, 4134-  
1958 4143, doi:10.1175/1520-0442%282003%29016<4134%3ATITSAM>2.0.CO%3B2, 2003.

1959

1960 Mayot, N., Le Quéré, C., Rödenbeck, C., Bernardello, R., Bopp, L., Djeutchouang, L. M., Gehlen, M., Gregor,  
1961 L., Gruber, N., Hauck, J., Iida, Y., Ilyina, T., Keeling, R. F., Landschützer, P., Manning, A. C., Patara, L.,  
1962 Resplandy, L., Schwinger, J., Séférian, R., Watson, A. J., Wright, R. M. and Zeng, J.: Climate-driven variability  
1963 of the Southern Ocean CO<sub>2</sub> sink. *Phil. Trans. R. Soc. A*. 381: 20220055, <http://doi.org/10.1098/rsta.2022.0055>,  
1964 2023

1965

1966 Mazloff, M. R., Verdy, A., Gille, S. T., Johnson, K. S., Cornuelle, B. D., and Sarmiento, J.: Southern Ocean  
1967 acidification revealed by biogeochemical-Argo floats. *Journal of Geophysical Research: Oceans*, 128,  
1968 e2022JC019530. <https://doi.org/10.1029/2022JC019530>, 2023.

1969

1970 McKinley, G. A., Bennington, V. S., Meinshausen, M., and Nicholls, Z.: Modern air-sea flux distributions  
1971 reduce uncertainty in the future ocean carbon sink, *Environmental Research Letters*, 18, doi:10.1088/1748-  
1972 9326/acc195, 2023.

1973

1974 McNeil, B. I. and Matear, R. J.: Southern Ocean acidification: A tipping point at 450-ppm atmospheric  
1975 CO<sub>2</sub>, *P. Natl. Acad. Sci. USA*, 105, 18860–18864, <https://doi.org/10.1073/pnas.0806318105>, 2008.

1976

1977 McNeil, B. I. and Sasse, T. P.: Future ocean hypercapnia driven by anthropogenic amplification of the natural  
1978 CO<sub>2</sub> cycle, *Nature*, 529, 383–386, doi:10.1038/nature16156, 2016

1979

1980 McNeil, B. I., Metzl, N., Key, R. M., Matear, R. J. and Corbiere, A.: An empirical estimate of the Southern  
1981 Ocean air-sea CO<sub>2</sub> flux, *Global Biogeochem. Cycles*, Vol. 21, No. 3, GB3011 10.1029/2007GB002991, 2007.

1982

1983 Meinshausen, M., Nicholls, Z. R. J., Lewis, J., Gidden, M. J., Vogel, E., Freund, M., et al.: The shared  
1984 socioeconomic pathway (SSP) greenhouse gas concentrations and their extensions to 2500. *Geoscientific Model*  
1985 *Development*, 13(8), 3571–3605. <https://doi.org/10.5194/gmd-13-3571-2020>, 2020.

1986

1987 Metzl, N., and Lo Monaco, C.: OISO- Océan Indien Service d'Observation,  
1988 <https://doi.org/10.18142/228>, 1998.

1989

1990 Metzl, N., Brunet, C., Jabaud-Jan, A., Poisson, A., and Schauer, B.: Summer and winter air–sea CO<sub>2</sub> fluxes in  
1991 the Southern Ocean, *Deep-Sea Res.*, 53, 1548–1563, <https://doi.org/10.1016/j.dsr.2006.07.006>, 2006.

1992

1993 Metzl, N.: Decadal increase of oceanic carbon dioxide in Southern Indian Ocean surface waters (1991–2007),  
1994 *Deep-Sea Res. Pt. II*, 56, 607–619, <https://doi.org/10.1016/j.dsr2.2008.12.007>, 2009.

1995

1996 Midorikawa, T., Inoue, H. Y., Ishii, M., Sasano, D., Kosugi, N., Hashida, G., Nakaoka, S., and Suzuki, T.:  
1997 Decreasing pH trend estimated from 35-year time series of carbonate parameters in the Pacific sector of the  
1998 Southern Ocean in summer, *Deep-Sea Res.*, 61, 131–139, <https://doi.org/10.1016/j.dsr.2011.12.003>, 2012.

1999

2000 Millero, F. J., Lee, K., and Roche, M.: Distribution of alkalinity in the surface waters of the major oceans, *Mar.*  
2001 *Chem.*, 60, 111–130, [https://doi.org/10.1016/S0304-4203\(97\)00084-4](https://doi.org/10.1016/S0304-4203(97)00084-4), 1998.

2002

2003 Minas, H. J., and Minas, M.: Net community production in high nutrient-low chlorophyll waters of the tropical  
2004 and Antarctic oceans – grazing vs iron hypothesis, *Oceanol. Acta*, 15, 145–162, 1992.

2005

2006 Mongin, M., Nelson, D. M., Pondaven, P., and Tréguer, P.: Simulation of upper-ocean biogeochemistry with a  
2007 flexible-composition phytoplankton model: C, N and Si cycling and Fe limitation in the Southern Ocean. *Deep*  
2008 *Sea Research Part II: Topical Studies in Oceanography*, Elsevier, 2006, 53 (5-7), pp.601-619.  
2009 [10.1016/j.dsr2.2006.01.021](https://doi.org/10.1016/j.dsr2.2006.01.021), 2006.

2010

2011 Mongin, M., Nelson, D. M., Pondaven P., and Tréguer, P.: Potential phytoplankton responses to iron and  
2012 stratification changes in the Southern Ocean based on a flexible-composition phytoplankton model. *Global*  
2013 *Biogeochemical Cycles* 21 (GB4020), [/http://dx.doi.org/10.1029/2007GB002972S](http://dx.doi.org/10.1029/2007GB002972S), 2007.

2014

2015 Mongin, M., Molina, E., and Trull, T. W.: Seasonality and scale of the Kerguelen plateau phytoplankton bloom:  
2016 A remote sensing and modeling analysis of the influence of natural iron fertilization in the Southern Ocean.  
2017 *Deep Sea Research Part II: Topical Studies in Oceanography*, Vol 55, Issues 5–7, Pages 880-892,  
2018 <https://doi.org/10.1016/j.dsr2.2007.12.039>. 2008.

2019

2020 Mongwe, N. P., Vichi, M., and Monteiro, P. M. S.: The seasonal cycle of pCO<sub>2</sub> and CO<sub>2</sub> fluxes in the Southern  
2021 Ocean: diagnosing anomalies in CMIP5 Earth system models, *Biogeosciences*, 15, 2851–2872,  
2022 <https://doi.org/10.5194/bg-15-2851-2018>, 2018.

2023

2024 Mongwe, P., Gregor, L., Tjiputra, J., Hauck, J., Ito, T., Danek, C., Vichi, M., Thomalla S., and Monteiro, M. S.:  
2025 A shift in the mechanism of CO<sub>2</sub> uptake in the Southern Ocean under high emission-scenario, DOI:  
2026 [10.21203/rs.3.rs-2849464/v1](https://doi.org/10.21203/rs.3.rs-2849464/v1), 2023.

2027

2028 Moore, J. K. and Abbott, M. R.: Phytoplankton chlorophyll distributions and primary production in the Southern  
2029 Ocean, *J. Geophys. Res.-Oceans*, 105, 28709–28722, <https://doi.org/10.1029/1999JC000043>, 2000

2030

2031 Moy, A. D., Palmer, M. R., Howard, W. R., Bijma, J., Cooper, M. J., Calvo, E., Pelejero, C., Gagan M. K. and  
2032 Chalk, T. B.: Reduced calcification in modern Southern Ocean planktonic foraminifera. *Nature Geosci* 2, 276–  
2033 280. <https://doi-org.insu.bib.cnrs.fr/10.1038/ngeo460>, 2009.

2034

2035 Negrete-García, G., Lovenduski, N. S., Hauri, C., Krumhardt, K. M., and Lauvset, S. K.: Sudden  
2036 emergence of a shallow aragonite saturation horizon in the Southern Ocean. *Nature Climate Change*, 1758-  
2037 6798, 10.1038/s41558-019-0418-8, 2019.

2038

2039 Neveux, J., and Lantoiné, F.: Spectrofluorometric assay of chlorophylls and phaeopigments using the least  
2040 squares approximation technique, *Deep-Sea Res. I*, 40(9), 1747-1765, [https://doi.org/10.1016/0967-](https://doi.org/10.1016/0967-0637(93)90030-7)  
2041 [0637\(93\)90030-7](https://doi.org/10.1016/0967-0637(93)90030-7), 1993.

2042

2043 Nicholson S. A., Whitt, D. B., Fer, I., du Plessis, M. D., Lebéhot A. D., et al.: Storms drive outgassing of CO<sub>2</sub> in  
2044 the subpolar Southern Ocean. *Nat. Commun.* 13:158. <https://doi.org/10.1038/s41467-021-27780-w>, 2022

2045

2046 Olafsson, J., Olafsdottir, S. R., Benoit-Cattin, A., Danielsen, M., Arnarson, T. S., and Takahashi, T.: Rate of  
2047 Iceland Sea acidification from time series measurements. *Biogeosciences* 6, 2661–2668.  
2048 <https://doi.org/10.5194/bg-6-2661-2009>, 2009.

2049

2050 Olafsson, J., Olafsdottir, S. R., Benoit-Cattin, A., and Takahashi, T.: The Irminger Sea and the Iceland Sea time  
2051 series measurements of sea water carbon and nutrient chemistry 1983–2006. *Earth Syst. Sci. Data* 2, 99–104.  
2052 <https://doi.org/10.5194/essd-2-99-2010>, 2010.

2053

2054 Olsen, A., Key, R. M., van Heuven, S., Lauvset, S. K., Velo, A., Lin, X., Schirnick, C., Kozyr, A., Tanhua, T.,  
2055 Hoppema, M., Jutterström, S., Steinfeldt, R., Jeansson, E., Ishii, M., Pérez, F. F., and Suzuki, T.: The Global  
2056 Ocean Data Analysis Project version 2 (GLODAPv2) – an internally consistent data product for the world ocean,  
2057 *Earth Syst. Sci. Data*, 8, 297–323, <https://doi.org/10.5194/essd-8-297-2016>, 2016.

2058

2059 Olsen, A., Lange, N., Key, R. M., Tanhua, T., Álvarez, M., Becker, S., Bittig, H. C., Carter, B. R., Cotrim da  
2060 Cunha, L., Feely, R. A., van Heuven, S., Hoppema, M., Ishii, M., Jeansson, E., Jones, S. D., Jutterström, S.,  
2061 Karlsen, M. K., Kozyr, A., Lauvset, S. K., Lo Monaco, C., Murata, A., Pérez, F. F., Pfeil, B., Schirnick, C.,  
2062 Steinfeldt, R., Suzuki, T., Telszewski, M., Tilbrook, B., Velo, A., and Wanninkhof, R.: GLODAPv2.2019 – an  
2063 update of GLODAPv2, *Earth Syst. Sci. Data*, 11, 1437–1461, <https://doi.org/10.5194/essd-11-1437-2019>, 2019.

2064

2065 Olsen, A., Lange, N., Key, R. M., Tanhua, T., Bittig, H. C., Kozyr, A., Álvarez, M., Azetsu-Scott, K., Becker, S.,  
2066 Brown, P. J., Carter, B. R., Cotrim da Cunha, L., Feely, R. A., van Heuven, S., Hoppema, M., Ishii, M.,  
2067 Jeansson, E., Jutterström, S., Landa, C. S., Lauvset, S. K., Michaelis, P., Murata, A., Pérez, F. F., Pfeil, B.,  
2068 Schirnick, C., Steinfeldt, R., Suzuki, T., Tilbrook, B., Velo, A., Wanninkhof, R., and Woosley, R. J.: An updated  
2069 version of the global interior ocean biogeochemical data product, GLODAPv2.2020, *Earth Syst. Sci. Data*, 12,  
2070 3653–3678, <https://doi.org/10.5194/essd-12-3653-2020>, 2020.

2071

2072 Orr, J. C., Fabry, V. J., Aumont, O., Bopp, L., Doney, S. C., Feely, R. A., Gnanadesikan, A., Gruber, N., Ishida,  
2073 A., Joos, F., Key, R. M., Lindsay, K., Maier-Reimer, E., Matear, R., Monfray, P., Mouchet, A., Najjar, R. G.,  
2074 Plattner, G.-K., Rodgers, K. B., Sabine, C. L., Sarmiento, J. L., Schlitzer, R., Slater, R. D., Totterdell, I. J.,  
2075 Weirig, M.-F., Yamanaka, Y., and Yool, A.: Anthropogenic ocean acidification over the twenty-first century and  
2076 its impact on calcifying organisms, *Nature*, 437, 681–686, <https://doi.org/10.1038/nature04095>, 2005.

2077

2078 Orr, J. C., Epitalon, J.-M., and Gattuso, J.-P.: Comparison of ten packages that compute ocean carbonate  
2079 chemistry, *Biogeosciences*, 12(5), 1483–1510, doi:10.5194/bg-12-1483-2015, 2015.

2080

2081 Orr, J. C., Epitalon, J.-M., Dickson, A. G., and Gattuso, J.-P.: Routine uncertainty propagation for the marine  
2082 carbon dioxide system, *Marine Chemistry*, Vol. 207, 84-107, doi:10.1016/j.marchem.2018.10.006., 2018.

2083

2084 Oeschlies, A., Brandt, P., Stramma, L., and Schmidtko, S.: Drivers and mechanisms of ocean deoxygenation. *Nat.*  
2085 *Geosci.* 11, 467–473. doi: 10.1038/s41561-018-0152-2, 2018.

2086

2087 Pardo, P. C., Pérez, F. F., Khatiwala, S., and Ríos, A. F.: Anthropogenic CO<sub>2</sub> estimates in the Southern Ocean:  
2088 Storage partitioning in the different water masses, *Prog. Oceanogr.*, 120, 230–242,  
2089 <https://doi.org/10.1016/j.pocean.2013.09.005>, 2014.  
2090

2091 Pardo, P. C., Tilbrook, B., Langlais, C., Trull, T. W., and Rintoul, S. R.: Carbon uptake and biogeochemical  
2092 change in the Southern Ocean, south of Tasmania. *Biogeosciences*, 14(22), 5217–5237.  
2093 <https://doi.org/10.5194/bg-14-5217-2017>, 2017.  
2094

2095 Pasquer, B., Metzl, N., Goosse, H., and Lancelot, C.: What drives the seasonality of air-sea CO<sub>2</sub> fluxes in the  
2096 ice-free zone of the Southern Ocean: A 1D coupled physical-biogeochemical model approach. *Marine*  
2097 *Chemistry*, 177 (3): 554-565. [doi:10.1016/j.marchem.2015.08.008](https://doi.org/10.1016/j.marchem.2015.08.008), 2015.  
2098

2099 Pauthenet, E., Roquet, F., Madec, G., Guinet, C., Hindell, M., McMahon, C. R., Harcourt, R., and Nerini, D.:  
2100 Seasonal Meandering of the Polar Front Upstream of the Kerguelen Plateau, *Geophys. Res. Lett.*, 45, 9774–  
2101 9781, <https://doi.org/10.1029/2018GL079614>, 2018.  
2102

2103 Petrou, K., Baker, K. G., Nielsen, D. A., Hancock, A. M., Schulz, K. G. and Davidson, A. T.: Acidification  
2104 diminishes diatom silica production in the Southern Ocean. *Nature Climate Change*, 9, 781-786,  
2105 <https://doi.org/10.1038/s41558-019-0557-y>, 2019.  
2106

2107 Pierrot, D., Lewis, E., and Wallace, D. W. R.: MS Excel Program Developed for CO<sub>2</sub> System Calculations  
2108 ORNL/CDIAC-105, Carbon Dioxide Inf. Anal. Cent., Oak Ridge Natl. Lab., U. S. Dept. of Energy, Oak Ridge,  
2109 Tenn., [https://cdiac.ess-dive.lbl.gov/ftp/co2sys/CO2SYS\\_calc\\_XLS\\_v2.1/](https://cdiac.ess-dive.lbl.gov/ftp/co2sys/CO2SYS_calc_XLS_v2.1/) (last access: 3 March 2022), 2006.  
2110

2111 Pilcher, D. J., Brody, S. R., Johnson, L., and Bronselaer, B.: Assessing the abilities of CMIP5 models to  
2112 represent the seasonal cycle of surface ocean pCO<sub>2</sub>, *J. Geophys. Res. Oceans*, 120, 4625–4637,  
2113 [doi:10.1002/2015JC010759](https://doi.org/10.1002/2015JC010759), 2015.  
2114

2115 Pfeil, B., Olsen, A., Bakker, D. C. E., Hankin, S., Koyuk, H., Kozyr, A., Malczyk, J., Manke, A., Metzl, N.,  
2116 Sabine, C. L., Akl, J., Alin, S. R., Bates, N., Bellerby, R. G. J., Borges, A., Boutin, J., Brown, P. J., Cai, W.-J.,  
2117 Chavez, F. P., Chen, A., Cosca, C., Fassbender, A. J., Feely, R. A., González-Dávila, M., Goyet, C., Hales,  
2118 B., Hardman-Mountford, N., Heinze, C., Hood, M., Hoppema, M., Hunt, C. W., Hydes, D., Ishii, M.,  
2119 Johannessen, T., Jones, S. D., Key, R. M., Körtzinger, A., Landschützer, P., Lauvset, S. K., Lefèvre, N.,  
2120 Lenton, A., Lourantou, A., Merlivat, L., Midorikawa, T., Mintrop, L., Miyazaki, C., Murata, A., Nakadate, A.,  
2121 Nakano, Y., Nakaoka, S., Nojiri, Y., Omar, A. M., Padin, X. A., Park, G.-H., Paterson, K., Perez, F. F., Pierrot,  
2122 D., Poisson, A., Ríos, A. F., Santana-Casiano, J. M., Salisbury, J., Sarma, V. V. S. S., Schlitzer, R.,  
2123 Schneider, B., Schuster, U., Sieger, R., Skjelvan, I., Steinhoff, T., Suzuki, T., Takahashi, T., Tedesco, K.,  
2124 Telszewski, M., Thomas, H., Tilbrook, B., Tjiputra, J., Vandemark, D., Veness, T., Wanninkhof, R., Watson,  
2125 A. J., Weiss, R., Wong, C. S., and Yoshikawa-Inoue, H.: A uniform, quality controlled Surface Ocean CO<sub>2</sub> Atlas  
2126 (SOCAT), *Earth Syst. Sci. Data*, 5, 125-143, [doi:10.5194/essd-5-125-2013](https://doi.org/10.5194/essd-5-125-2013), 2013.  
2127

2128 Poisson, A.: INDIGO 1 - MD 43 cruise, RV Marion Dufresne, <https://doi.org/10.17600/85000111>, 1985.  
2129

2130 Poisson, A., Schauer, B., and Brunet, C. : MD43/INDIGO 1, Cruise report; Les rapports des campagnes à la mer,  
2131 85(06). Les publications de la Mission de Recherche des Terres Australes et Antarctiques Françaises, Paris, 267  
2132 pp., 1988.  
2133

2134 Poisson, A., Metzl, N., Brunet, C., Schauer, B., Bres, B., Ruiz-Pino, D., and Louanchi, F.: Variability of sources  
2135 and sinks of CO<sub>2</sub> in the western Indian and southern oceans during the year 1991, *J. Geophys. Res. Oceans*, 98,  
2136 22759–22778, <https://doi.org/10.1029/93JC02501>, 1993.  
2137

2138 Pondaven, P., Fravallo, C., Ruiz-Pino, D., Tréguer, P., Quéguiner, B., and Jeandel, C.: Modelling the silica pump  
2139 in the Permanently Open Ocean Zone of the Southern Ocean, *J. Mar. Syst.*, 17, 1-4, 587–619,  
2140 [https://doi.org/10.1016/S0924-7963\(98\)00066-9](https://doi.org/10.1016/S0924-7963(98)00066-9), 1998.  
2141  
2142 Pondaven, P., Ruiz-Pino, D., Fravallo, C., Tréguer, P., and Jeandel, C.: Interannual variability of Si and N cycles  
2143 at the time-series station KERFIX between 1990 and 1995 – a 1-D modelling study, *Deep-Sea Res. Pt. I*, 47, 2,  
2144 223–257, [https://doi.org/10.1016/S0967-0637\(99\)00053-9](https://doi.org/10.1016/S0967-0637(99)00053-9), 2000.  
2145  
2146 Prend, C. J., Gray, A. R., Talley, L. D., Gille, S. T., Haumann, F. A., Johnson, K. S., et al.: Indo-Pacific sector  
2147 dominates Southern Ocean carbon outgassing. *Global Biogeochemical Cycles*, 36, e2021GB007226.  
2148 <https://doi.org/10.1029/2021GB007226>, 2022.  
2149  
2150 Racapé, V., Lo Monaco, C., Metzl, N., and Pierre, C.: Summer and winter distribution of  $\delta^{13}\text{C}_{\text{DIC}}$  in surface  
2151 waters of the South Indian Ocean (20°S–60°S). *Tellus-B*, DOI: 10.1111/j.1600-0889.2010.00504, 2010.  
2152  
2153 Reynolds, R. W., Rayner, N. A., Smith, T. M., Stokes, D. C., and Wang, W.: An improved in situ and satellite  
2154 SST analysis for climate. *J. Clim.* 15, 1609–1625. [https://doi.org/10.1175/1520-0442\(2002\)015<1609:AIISAS>2.0.CO;2](https://doi.org/10.1175/1520-0442(2002)015<1609:AIISAS>2.0.CO;2), 2002.  
2155  
2156 Rödenbeck, C., Keeling, R. F., Bakker, D. C. E., Metzl, N., Olsen, A., Sabine, C., and Heimann, M.: Global  
2157 surface-ocean pCO<sub>2</sub> and sea–air CO<sub>2</sub> flux variability from an observation-driven ocean mixed-layer scheme,  
2158 *Ocean Sci.*, 9, 193–216, <https://doi.org/10.5194/os-9-193-2013>, 2013.  
2159  
2160 Rödenbeck, C., DeVries, T., Hauck, J., Le Quéré, C., and Keeling, R. F.: Data-based estimates of  
2161 interannual sea–air CO<sub>2</sub> flux variations 1957–2020 and their relation to environmental drivers,  
2162 *Biogeosciences*, 19, 2627–2652, <https://doi.org/10.5194/bg-19-2627-2022>, 2022.  
2163  
2164 Rodgers, K. B., Schwinger, J., Fassbender, A. J., Landschützer, P., Yamaguchi, R., Frenzel, H., et al.: Seasonal  
2165 variability of the surface ocean carbon cycle: A synthesis. *Global Biogeochemical Cycles*, 37, e2023GB007798.  
2166 <https://doi.org/10.1029/2023GB007798>, 2023  
2167  
2168 Rustogi, P., Landschützer, P., Brune, S. et al.: The impact of seasonality on the annual air-sea carbon flux and its  
2169 interannual variability. *Clim. Atmos. Sci.*, 6, 66, <https://doi.org/10.1038/s41612-023-00378-3>, 2023.  
2170  
2171 Sabine, C. L., Key, R. M., Johnson, K. M., Millero, F. J., Poisson, A., Sarmiento, J. L., Wallace, D. W. R., and  
2172 Winn, C. D.: Anthropogenic CO<sub>2</sub> inventory of the Indian Ocean, *Global Biogeochemical Cycles*, 13, 179–198,  
2173 <https://doi.org/10.1029/1998GB900022>, 1999.  
2174  
2175 Sabine, C. L., Feely, R. A., Gruber, N., Key, R. M., Lee, K., Bullister, J. L., Wanninkhof, R., Wong, C. S.,  
2176 Wallace, D. W. R., Tilbrook, B., Millero, F. J., Peng, T.-H., Kozyr, A., Ono, T., and Rios, A. F.: The Oceanic  
2177 Sink for Anthropogenic CO<sub>2</sub>, *Science*, 305, 367–371, <https://doi.org/10.1126/science.1097403>, 2004.  
2178  
2179 Sasse, T. P., McNeil, B. I., Matear, R. J., and Lenton, A.: Quantifying the influence of CO<sub>2</sub> seasonality on future  
2180 aragonite undersaturation onset, *Biogeosciences*, 12, 6017–6031, <https://doi.org/10.5194/bg-12-6017-2015>,  
2181 2015.  
2182  
2183 Schlitzer, R.: Ocean Data View, Ocean Data View, <http://odv.awi.de> (last access: 13 March 2019), 2018.  
2184  
2185 Schmidtko, S., Stramma, L., and Visbeck, M.: Decline in global oceanic oxygen content during the past five  
2186 decades, *Nature*, 542, 335–339, <https://doi.org/10.1038/nature21399>, 2017.  
2187  
2188

2189 Seifert, M., Nissen, C., Rost, B., Vogt, M., Völker, C., and Hauck, J.: Interaction matters: Bottom-up driver  
2190 interdependencies alter the projected response of phytoplankton communities to climate change. *Global Change*  
2191 *Biology*, 00, 1– 25. <https://doi.org/10.1111/gcb.16799>, 2023.

2192

2193 Shadwick, E. H., Wynn-Edwards, C. A., Matear, R.J., Jansen, P., Schulz, E. and Sutton, A. J.: Observed  
2194 amplification of the seasonal CO<sub>2</sub> cycle at the Southern Ocean Time Series. *Front. Mar. Sci.* 10:1281854. doi:  
2195 10.3389/fmars.2023.1281854, 2023

2196

2197 Skjelvan, I., Lauvset, S. K., Johannessen, T., et al.: Decadal trends in Ocean Acidification from the Ocean  
2198 Weather Station M in the Norwegian Sea, *Journal of Marine Systems*,  
2199 <https://doi.org/10.1016/j.jmarsys.2022.103775>, 2022.

2200

2201 Smith, H. E. K., Poulton, A. J., Garley, R., Hopkins, J., Lubelczyk, L. C., Drapeau, D. T., Rauschenberg, S.,  
2202 Twining, B. S., Bates, N. R., and Balch, W. M.: The influence of environmental variability on the biogeography  
2203 of coccolithophores and diatoms in the Great Calcite Belt, *Biogeosciences*, 14, 4905–4925,  
2204 <https://doi.org/10.5194/bg-14-4905-2017>, 2017.

2205

2206 Strickland, J. D. H. and Parsons, T. R.: *A Practical Hand Book of Seawater Analysis*. Fisheries Research Board  
2207 of Canada Bulletin, 2nd Edition., 310 p. pp., 1972.

2208

2209 Sutton, A. J., Williams, N. L., and Tilbrook, B.: Constraining Southern Ocean CO<sub>2</sub> Flux Uncertainty Using  
2210 Uncrewed Surface Vehicle Observations, *Geophys. Res. Lett.*, 48, e2020GL091748,  
2211 <https://doi.org/10.1029/2020GL091748>, 2021.

2212

2213 Takahashi, T., Olafsson, J., Goddard, J. G., Chipman, D. W., and Sutherland, S. C.: Seasonal variation of CO<sub>2</sub>  
2214 and nutrients in the high-latitude surface oceans: A comparative study, *Global Biogeochem. Cycles*, 7(4), 843–  
2215 878, doi:10.1029/93GB02263, 1993.

2216

2217 Takahashi, T., Sutherland, S. C., Wanninkhof, R., Sweeney, C., Feely, R. A., Chipman, D. W., Hales, B.,  
2218 Friederich, G., Chavez, F., Sabine, C., Watson, A., Bakker, D. C. E., Schuster, U., Metzl, N., Yoshikawa-Inoue,  
2219 H., Ishii, M., Midorikawa, T., Nojiri, Y., Körtzinger, A., Steinhoff, T., Hoppema, M., Olafsson, J., Arnarson, T.  
2220 S., Tilbrook, B., Johannessen, T., Olsen, A., Bellerby, R., Wong, C. S., Delille, B., Bates, N. R., and de Baar, H.  
2221 J. W.: Climatological mean and decadal change in surface ocean pCO<sub>2</sub>, and net sea–air CO<sub>2</sub> flux over the  
2222 global oceans, *Deep-Sea Res. Pt. II*, 56, 554–577, <https://doi.org/10.1016/j.dsr2.2008.12.009>, 2009a.

2223

2224 Takahashi, T., Sutherland, S. C., Wanninkhof, R., Sweeney, C., Feely, R. A., Chipman, D. W., Hales, B.,  
2225 Friederich, G., Chavez, F., Sabine, C., Watson, A., Bakker, D. C. E., Schuster, U., Metzl, N., Yoshikawa-Inoue,  
2226 H., Ishii, M., Midorikawa, T., Nojiri, Y., Körtzinger, A., Steinhoff, T., Hoppema, M., Olafsson, J., Arnarson, T.  
2227 S., Tilbrook, B., Johannessen, T., Olsen, A., Bellerby, R., Wong, C. S., Delille, B., Bates, N. R., and de Baar, H.  
2228 J. W.: Corrigendum to “Climatological mean and decadal change in surface ocean pCO<sub>2</sub>, and net sea–air CO<sub>2</sub>  
2229 flux over the global oceans” [*Deep Sea Res. II* 56 (2009) 554–577], *Deep Sea Research Part I: Oceanographic*  
2230 *Research Papers*, 56, 11, 2075–2076, <https://doi.org/10.1016/j.dsr.2009.07.007>. 2009b.

2231

2232 Takao, S., Hirawake, T., Wright, S. W., and Suzuki, K.: Variations of net primary productivity and  
2233 phytoplankton community composition in the Indian sector of the Southern Ocean as estimated from ocean color  
2234 remote sensing data, *Biogeosciences*, 9, 3875–3890, doi:10.5194/bg-9-3875-2012, 2012.

2235

2236 Talley, L. D.: Closure of the global overturning circulation through the Indian, Pacific, and Southern Oceans:  
2237 Schematics and transports. *Oceanography*, 26(1), 80–97. <https://doi.org/10.5670/oceanog.2013.07>, 2013.

2238

2239 Tanhua, T., Hoppema, M., Jones, E. M., Stöven, T., Hauck, J., Dávila, M. G., Santana-Casiano, M., Álvarez, M.,  
2240 and Strass, V. H.: Temporal changes in ventilation and the carbonate system in the Atlantic sector of the



2241 Southern Ocean, Deep Sea Res. Part II Top. Stud. Oceanogr., 138, 26–38,  
2242 <https://doi.org/10.1016/j.dsr2.2016.10.004>, 2017.  
2243  
2244 Touratier, F., Azouzi, L. and Goyet, C.: CFC-11,  $\Delta 14\text{C}$  and  $3\text{H}$  tracers as a means to assess anthropogenic  $\text{CO}_2$   
2245 concentrations in the ocean. *Tellus B*, 59(2), 318–325, doi:10.1111/j.1600-0889.2006.00247.x, 2007.  
2246  
2247 Tréguer, P., and Le Corre, P.: Manuel d'analyse des sels nutritifs dans l'eau de mer (utilisation de  
2248 l'autoanalyseur II Technicon), 2nd ed., 110 pp., L.O.C.U.B.O., Brest, 1975.  
2249  
2250 Uppström, L. R.: The boron/chlorinity ratio of deep-sea water from the Pacific Ocean, *Deep Sea Research and*  
2251 *Oceanographic Abstracts*, 21, 161–162, [https://doi.org/10.1016/0011-7471\(74\)90074-6](https://doi.org/10.1016/0011-7471(74)90074-6), 1974.  
2252  
2253 van Heuven, S. M. A. C., Hoppema, M., Huhn, O., Slagter, H. A., and de Baar, H. J. W.: Direct observation of  
2254 increasing  $\text{CO}_2$  in the Weddell Gyre along the Prime Meridian during 1973–2008, *Deep-Sea Res. Pt. II*, 58,  
2255 2613–2635, <https://doi.org/10.1016/j.dsr2.2011.08.007>, 2011.  
2256  
2257 Vázquez-Rodríguez, M., Touratier, F., Lo Monaco, C., Waugh, D. W., Padin, X. A., Bellerby, R. G. J., Goyet,  
2258 C., Metzl, N., Ríos, A. F., and Pérez, F. F.: Anthropogenic carbon distributions in the Atlantic Ocean: data-based  
2259 estimates from the Arctic to the Antarctic, *Biogeosciences*, 6, 439–451, <https://doi.org/10.5194/bg-6-439-2009>,  
2260 2009.  
2261  
2262 Wanninkhof, R., and Trinanes, J.: The impact of changing wind speeds on gas transfer and its effect on  
2263 global air-sea  $\text{CO}_2$  fluxes, *Global Biogeochem. Cycles*, 31, doi:10.1002/2016GB005592, 2017.  
2264  
2265 Wanninkhof, R., Barbero, L., Byrne, R., Cai, W.-J., Huang, W.-J., Zhang, J.-Z., Baringer, M., and Langdon, C.:  
2266 Ocean acidification along the Gulf Coast and East Coast of the USA, *Continental Shelf Research*, 98, 54-71,  
2267 <https://doi.org/10.1016/j.csr.2015.02.008>, 2015  
2268  
2269 Weir, I., Fawcett, S., Smith, S., Walker, D., Bornman, T., and Fietz, S.: Winter biogenic silica and diatom  
2270 distributions in the Indian sector of the Southern Ocean, *Deep Sea Research Part I: Oceanographic Research*  
2271 *Papers*, Volume 166, 103421, <https://doi.org/10.1016/j.dsr.2020.103421>, 2020.  
2272  
2273 Weiss, R. F. and Price, B. A.: Nitrous oxide solubility in water and seawater. *Marine Chemistry*, 8(4), 347–359,  
2274 doi:10.1016/0304-4203(80)90024-9, 1980.  
2275  
2276 Wright, R. M., Le Quéré, C., Mayot, N., Olsen, A., and Bakker, D.: Fingerprint of climate change on Southern  
2277 Ocean carbon storage. *Global Biogeochemical Cycles*, 37, e2022GB007596. Doi: 10.1029/2022GB007596,  
2278 2023.  
2279  
2280 Xue, L., Cai, W. J., Takahashi, T. et al.: Climatic modulation of surface acidification rates through summertime  
2281 wind forcing in the Southern Ocean. *Nat. Commun.*, 9, 3240, Doi:10.1038/s41467-018-05443-7, 2018.  
2282  
2283 Yun, J., Jeong, S., Gruber, N., Gregor, L., Ho, C.-H., Piao, S., Ciais, P., Schimel, D., and Kwon, E. Y.: Enhance  
2284 seasonal amplitude of atmospheric  $\text{CO}_2$  by the changing Southern Ocean carbon sink, *Science Advances*, 8, 41,  
2285 doi: 10.1126/sciadv.abq0220, 2022.  
2286